

Structural Study of Human Voltage-Gated Potassium Channel K_v1.1

Simon Philip Davies

Submitted in accordance with the requirements for the degree of
Doctor of Philosophy

The University of Leeds

Faculty of Biological Sciences, School of Biomedical Sciences

July 2018

Intellectual property and publication statement

The candidate confirms that the work submitted is his own and that appropriate credit has been given where reference has been made to the work of others. This copy has been supplied on the understanding that it is copyright material and that no quotation from the thesis may be published without proper acknowledgement.

© 2018-19 The University of Leeds and Simon Philip Davies.

The right of Simon Philip Davies to be identified as author of this work has been asserted by him in accordance with the Copyright, Designs and Patents Act 1988.

Acknowledgements

First and foremost, I would like to give my most sincere thanks my supervisors Dr. Stephen Muench and Dr. Jonathan Lippiat for their lending me their guidance, support and wisdom throughout my project. I am also grateful for the help of Prof. Asipu Sivaprasadarao (better known as Rao), who lent me his experience and scrutiny, which improved my understanding of membrane proteins and their study.

The work detailed in this thesis would not have been possible without the aid of Pfizer Inc., which provided support in the conception and the financing of this project. I am grateful to Dr. Ian Storer and Dr. David Pryde of the former Neusentis research and development site, both of whom gave me great support. Dr. Vincent Postis and Mayuri Parmar must also be thanked for sharing their expertise with SMA and DIBMA, which greatly elevated the quality of this work.

Much of the electron microscopy work detailed in this thesis was possible thanks to Dr. Rebecca Thompson and Dr. Emma Hesketh, whose endless patience and iron will have kept the EM control room running smoothly. On that note, thanks are also in order for Rachel Johnson and Shawn Rawson for helping me with the tricky business of using Relion and navigating the Astbury Biostructure Laboratory servers.

I am also forever grateful for the help and advice of Vincent Agboh, Dave Carrier, Emily Caseley, Julie Haggelund, Eoin Leen, Amelia Lesiuk, Tim Munsey, Peter Oatley, Tony Palmer, Mark Richards, Sarah Sabir, Nita Shah, Dave Sharples, Maren Thomsen and Chris Watson, all of whom taught me a great deal. Of course, I must also give my very sincere thanks to everybody on Astbury Level 6 for their help, ideas and the occasional inspiring chat.

None of this work could have been accomplished without the friends that I have made along the way: Alex, Brendan, Cate, Craig, Emma, Glenn, Jamie, Jennifer, Joanna, Julia, Lucy, Matt, Sophie and Zak, as without their great kindness, humour and camaraderie the road would have been an awful lot harder.

Last, but certainly not least, I would like to thank my parents, Julie and Paul, as well as my grandfather, Roy, for all the love and support that they have given me throughout my time at university and making all of this possible.

Abstract

Voltage-gated ion channels are vital components to the process of signal transmission in nerve cells. They constitute an inviting target for the development of drugs which target aberrant pain signal transmission. Voltage-gated potassium channels are an essential component in signalling along neural pathways, as their role in restoring resting membrane potential in nerve cells is crucial to priming neurons for further signal transmission following membrane depolarisation.

In this thesis, work towards developing a structural understanding of interactions between the human $K_v1.1$ voltage-gated potassium channel and inhibitory molecules will be discussed. This project has involved the development of expression vectors and cell lines for expression of $K_v1.1$ in human cell cultures, as well as experimentation with methods for extracting the protein with recently developed maleic-acid polymers SMA and DIBMA, which retain the native lipid envelop surrounding the channel complex. The extracted protein has been analysed through both biochemical characterisation through mass spectrometry and circular dichroism spectroscopy, as well as structural studies conducted through both negative stain and cryo-EM, resulting a low-resolution model from negative stain.

This work lays the foundation for future investigation of the human $K_v1.1$ channel, providing tested means and methodologies for the production of proteins in human cell expression systems, extraction through non-detergent methods and their analysis via cryo-electron microscopy.

Table of contents

Intellectual property and publication statement	i
Acknowledgements	ii
Abstract.....	iv
Table of contents	v
List of figures	xi
List of tables	xvi
List of abbreviations	xviii
1 Introduction	1
1.1 Integral membrane proteins and plasma membranes	1
1.1.1 Overview	1
1.1.2 Challenges associated with membrane protein study	2
1.1.3 Methods for membrane protein extraction.....	4
1.2 Cation channel superfamily.....	8
1.2.1 Overview	8
1.2.2 Voltage-gated potassium channels.....	9
1.3 Pharmacology of K _v 1.1 and related channels	15
1.4 Application of electron microscopy	16
1.5 Aims and objectives	21
2 Materials and Methods	22
2.1 Cloning strategy and construct design.....	22

2.1.1	Expression vector design	22
2.1.2	PCR.....	32
2.1.3	DNA fragment insertion	35
2.1.4	Bacterial culture	36
2.1.5	Agarose gel electrophoresis	38
2.1.6	DNA sequencing.....	38
2.2	Protein expression.....	39
2.2.1	Adherent human embryonic kidney cell culture.....	39
2.2.2	Suspension HEK cell culture	40
2.2.3	Transient human embryonic kidney cell transfection	42
2.2.4	Development of stably transfected HEK 293S GnT1 ⁻ cell lines for K _v 1.1 expression.....	45
2.2.5	Fluorescence microscopy.....	46
2.3	Protein purification.....	46
2.3.1	HEK cell lysis	46
2.3.2	Membrane protein extraction.....	47
2.3.3	Immobilised metal affinity chromatography	48
2.3.4	Size-exclusion chromatography purification	52
2.3.5	TEV cleavage.....	52
2.4	Protein quality validation	53
2.4.1	SDS-PAGE	53
2.4.2	Protein concentration.....	53

2.4.3	Western blotting.....	54
2.4.4	SEC-MALS.....	55
2.4.5	Circular dichroism spectroscopy	56
2.4.6	Mass spectrometry	58
2.5	Structural analysis	59
2.5.1	Negative stain electron microscopy	59
2.5.2	Cryo-electron microscopy.....	60
2.6	K _v 1.1 coinubation with alpha-dendrotoxin.....	64
3	Expression of K_v constructs in HEK cell culture.....	65
3.1	Background.....	65
3.2	Cloning and constructs.....	67
3.2.1	K _v 1.1 constructs.....	67
3.2.2	K _v β2 constructs.....	71
3.3	Transient transfection of HEK cells.....	74
3.4	Stable transfection.....	77
3.4.1	Hexahisitide tagged construct, K _v 1.1-TEV-EYFP-His ₆	77
3.4.2	Decahistodine tagged construct, K _v 1.1-TEV-EYFP-His ₁₀	78
3.4.3	K _v 1.1-TEV-EYFP-His ₁₀ /KCNAB2 double transfection	79
3.5	Comparison of suspension culture media	80
3.5.1	Influence of different media types on cell growth	80
3.5.2	Influence of pluronic acid and primatone on cell growth in suspension.....	88

3.5.3	Effects of media types on protein purification	91
4	Purification and characterisation of K_v proteins	94
4.1	Background.....	94
4.2	Comparison of cell lysis methods	97
4.3	Western blotting of transfected and untransfected cells	99
4.3.1	Sample preparation	99
4.3.2	Comparison of western blotting using anti-GFP antibodies	99
4.3.3	Comparison of western blotting using anti-K _v 1.1 antibodies..	101
4.4	Extraction of membrane proteins and primary purification by IMAC	104
4.5	Comparison of cobalt and nickel IMAC resin	106
4.6	Äkta Explorer purification and size-exclusion chromatography	108
4.6.1	Äkta Explorer-based IMAC.....	108
4.6.2	Äkta Explorer-based SEC	109
4.7	Mass spectrometry	110
4.8	TEV cleavage	117
4.9	Circular dichroism.....	120
4.9.1	Spectrum and Dichroweb analysis.....	120
4.8.2	CD measurement of protein stability in temperature ramp.....	123
4.10	SEC-MALS	129
5	Structural analysis of homotetrameric K_v1.1	131
5.1	Background.....	131

5.2	Negative stain electron microscopy	132
5.2.1	Grid optimisation.....	132
5.2.2	Data collection	133
5.2.3	Data processing.....	135
5.3	Cryo-electron microscopy	139
5.3.1	Grid preparation.....	139
5.3.2	Grid Screening	139
5.3.3	Data collection and processing	140
5.4	Negative stain EM of Kv1.1 co-incubation with α -DTX	143
6	Discussion	147
6.1	Expression of Kv proteins in HEK cell culture	147
6.1.1	Construct production	147
6.1.2	Kv β 2 co-expression.....	148
6.1.3	Suspension culture of HEK cells	148
6.2	Protein purification and characterisation of Kv proteins	150
6.2.1	Methods for primary purification.....	150
6.2.2	Methods for secondary purification	151
6.2.3	Protein characterisation.....	152
6.3	Structural analysis of homotetrameric Kv1.1.....	155
6.3.1	Negative stain electron microscopy	155
6.3.2	Cryo-electron microscopy.....	155
6.3.3	α -DTX co-incubated sample.....	156

6.4	Final Comments	157
7	References.....	159
8	Appendix.....	176
8.1	Maps of plasmids used during project	176
8.1.1	pcDNA6.....	176
8.1.2	pcDNA3.1.....	177
8.1.3	pJET1.2.....	178
8.2	Mass spectrometry data	179
8.2.1	A1 band.....	179
8.2.2	B1 band.....	180
8.2.3	B2 band.....	181
8.2.4	B3 band.....	182
8.2.5	B4 band.....	183
8.2.6	B5 band.....	184

List of figures

Figure 1.1 – Cartoon representation of integral membrane proteins extraction the maleic acid polymer SMA	6
Figure 1.2 – Diagrams of the chemical structures of SMA and DIBMA polymers	7
Figure 1.3 – Cartoon representation of tetrameric K _v 1.1 homology model and schematic diagram of K _v 1.1 monomer	12
Figure 1.4 – Graphs detailing the rise year-on-year of structures determined by electron microscopy vs. other methods.....	18
Figure 1.5 – Cartoon representation of a selection of membrane proteins whose structures have recently be determined through electron microscopy	20
Figure 3.1 – Agarose gel of PCR product from KCNA1-EYFP mutagenesis	68
Figure 3.2 – Agarose gel of miniprep products from PCR	69
Figure 3.3 – Agarose gel of PCR product from primers designed to extract the human kcnab2 gene from foetal human brain cDNA.....	73
Figure 3.4 – A fluorescence microscope views of HEK293 TSA cells transiently transfected with a pcDNA6 plasmid encoding K _v 1.1-TEV-EYFP-His ₆	76

Figure 3.5 – Cell growth and viability over time in suspension culture across a series of medium types.....	82
Figure 3.6 - Work-flow diagram describing the development of cell cultures in FreeStyle 293 and EX-CELL medium for the comparison of cell growth in both medium types.....	84
Figure 3.7 – Graph detailing the number of HEK cells recorded over time in suspension culture in PEM, FreeStyle, EX-CELL and DMEM when supplemented with pluronic acid and primatone.....	90
Figure 3.8 – SDS-PAGE comparing of the purification fractions of K _v 1.1-TY10 protein derived from HEK cells suspension culture established in FreeStyle vs. EX-CELL medium on HisPur cobalt resin	92
Figure 4.1 – SDS-PAGE gel comparing tissue grinding and sonication	98
Figure 4.2 – Post-transfer SDS-PAGE of whole cell contents of untransfected HEK 293S GnTII ⁻ cells and HEK 293S GnTII ⁻ cells expressing K _v 1.1-TY10 and chemiluminescent western blot of transferred SDS-PAGE contents with polyclonal anti-GFP antibodies.....	100
Figure 4.3 – Post-transfer SDS-PAGE of whole cell contents of untransfected HEK 293S GnTII ⁻ cells and HEK 293S GnTII ⁻ cells expressing K _v 1.1-TY10 and chemiluminescent western blot of transferred SDS-PAGE contents with polyclonal anti-K _v 1.1 antibodies.....	102
Figure 4.4 – SDS-PAGE of IMAC purified K _v 1.1-TY10 extracted in DDM, SMA and DIBMA	105

Figure 4.5 – SDS-PAGE comparing the binding and elution of proteins in DDM-solubilised membranes derived from stably transfected HEK 293S GnTI ⁻ cells expressing Kv1.1-TY10 on nickel-charged sepharose and cobalt-charged HisPur resins	107
Figure 4.6 – Fluorescence of elution fractions collected from 1 ml HisTRAP column during Kv1.1-TY10 purification	109
Figure 4.7 – Graphs detailing the fluorescence recorded for each 0.15 ml fraction eluted from SEC purification on Superdex 200 column.....	110
Figure 4.8 – SDS-PAGE submitted for mass spec analysis. The FreeStyle 250 mM imidazole preparation was selected as it appeared to contain the most prominent selection of contaminants.....	112
Figure 4.9 – Schematic diagram displaying peptides detected in band B1 by mass spectrometry (blue lines) which align with sequence of Kv1.1	114
Figure 4.10 – Schematic diagram displaying peptides detected in band B1 by mass spectrometry (blue lines) which align with Kv1.3.....	115
Figure 4.11 – Sequences of Kv1.1 and Kv1.3 colour coded according to fragments identified in mass spectrometry.....	116
Figure 4.12 – SDS-PAGE of TEV cleavage incubation products	118
Figure 4.13 – SDS-PAGE and western blot detailing TEV protease digestion of Kv1.1-TY10 protein.....	119
Figure 4.14 – CD spectra of Kv1.1-TY10 in 150 mM NaCl, 50 mM Tris, 10 mM KCl pH 7.4 across 180-260 nm wavelengths.....	122

Figure 4.15 – Graph of CD spectra of fresh Kv1.1-TY10 recovered in DDM, with the profile at ramping temperatures.....	124
Figure 4.16 – Graph of CD spectra of fresh Kv1.1-TY10 recovered in SMA, with the profile at ramping temperatures.....	125
Figure 4.17 – Graph of CD spectra of fresh Kv1.1-TY10 recovered in DIBMA, with the profile at ramping temperatures.....	126
Figure 4.18 – Graph plotting the elipicity of Kv1.1-TY10 at 222 nm in DDM, SMA and DIBMA across an increasing temperature	128
Figure 4.19 – Graph of SEC-MALS data from DDM-solubilised Kv1.1-TY10	130
Figure 5.1 – Example of negative stain micrograph from Kv1.1-TY10 extracted in DDM and coated in 1% uranyl acetate and class averages produced from processing of selected particles	134
Figure 5.2 – Negative stain EM structure produced from processing of micrograph dataset of DDM-solubilised Kv1.1-TY10	136
Figure 5.3 – Cartoon representation of map generated from negative stain data of SMA-solubilised Kv1.1-TY10	138
Figure 5.4 – Representative image of micrographs taken of SMA-solubilised sample screened at the Diamond Synchrotron electron microscopy facility	141

Figure 5.5 – Classes generated with and without a reference model from autopicked cryo-EM data of SMA-solubilised sample	142
Figure 5.6 – Representative micrograph of DDM-solubilised Kv1.1-TY10 co-incubated with α -DTX	144
Figure 5.7 – Representative micrograph of diluted Kv1.1-TY10 co-incubated with dendrotoxin- α	145
Figure 8.1 – Map of pcDNA6 plasmid.	176
Figure 8.2 – Map of pcDNA3.1 plasmid.	177
Figure 8.3 – Map of pJET1.2 plasmid.	178

List of tables

Table 2.1 – Table describing fusion tags utilised during Kv1.1 and Kv β 2 construct design and production.....	24
Table 2.2 – Primers used in the modification of plasmids encoding Kv1.1-EYFP constructs	26
Table 2.3 – Primers used in the modification of plasmids encoding Kv β 2 constructs.....	30
Table 2.4 – Table detailing the mixture of primers, buffers and reagents used in the standard PCR protocol used in the course of the project.....	33
Table 2.5 – Seeding density and volume of media used one hour pre-transfection.....	43
Table 2.6 – Table describing PEI:DNA complex formulation for wells and plates of varying sizes.....	44
Table 2.7 – Table of grid types used in preparation of Kv1.1 samples for cryo-EM	62
Table 3.1 – Table of living and dead cells counted in 180 ml starter cultures 96 hrs after establishment in FreeStyle and EX-CELL media.....	85
Table 3.2 – Table of living and dead cells counted in 180 ml FreeStyle and EX-CELL cultures 72 hrs after transfer from starter cultures	86

Table 3.3 – Table of living and dead cells counted in 180 ml FreeStyle and EX-CELL cultures 120 hrs after transfer from starter cultures and 48 hrs after the addition of 5 mM sodium butyrate	87
Table 8.1 – Table of protein fragments identified through mass spectrometry in band A1.	179
Table 8.2 – Table of protein fragments identified through mass spectrometry in band B1.	180
Table 8.3 – Table of protein fragments identified through mass spectrometry in band B2.	181
Table 8.4 – Table of protein fragments identified through mass spectrometry in band B3.	182
Table 8.5 – Table of protein fragments identified through mass spectrometry in band B4.	183
Table 8.6 – Table of protein fragments identified through mass spectrometry in band B5.	184

List of abbreviations

α -DTX – alpha-dendrotoxin

ABSL – Astbury Biostructure Laboratory

Voltage-Gated Calcium Channel Subunit α -1 – Ca_v1.1

CHAPS – 3-[(3-cholamidopropyl)dimethylammonio]-1-propanesulfonate

CMV – cytomegalovirus

CTF – contrast transfer function

DDM – n-dodecyl- β -D-maltopyranoside

DIBMA – diisobutylene maleic acid

DIBMALP – diisobutylene maleic acid lipid particle

DMEM – Dulbecco's modified Eagle's/essential medium

DPBS – Dulbecco's phosphate-buffered saline

dRI – difference of refractive index

EM – electron microscopy

EYFP – enhanced yellow fluorescent protein

FBS – foetal bovine serum

F-SEC – fluorescence size exclusion chromatography

GFP – green fluorescent protein

GnTII – A-1,3-mannosyl-glycoprotein 2-b-N-acetylglucosaminyltransferase
null mutation

HEK – human embryonic kidney

His-tag – polyhistidine-tag

His₆ – hexahistidine

His₁₀ – decahistidine

IMAC – immobilised metal affinity chromatography

IP – intellectual property

KCNA1 – voltage-gated potassium channel subfamily A, member 1

KCNA3 – voltage-gated potassium channel subfamily A, member 3

K_v – voltage-gated potassium channel

K_v1.1 – voltage-gated potassium channel subfamily A, member 1

K_v1.1-TY10 – K_v1.1 with C-terminal TEV cleavage site, EYFP and
decahistidine tags

K_v1.3 – voltage-gated potassium channel subfamily A, member 3

K_vβ2 – voltage-gated potassium channel beta subunit 2

LB – lysogeny broth

LS – light scattering

MALS – multi-angle light scattering

Nanotag – nTag

PCR – polymerase chain reaction

PEI – polyethylenimine

PEM – protein expression Medium

Protein ID – protein identification

QELS – quasi-elastic light scattering

RI – refractive index

Ryanodine Receptor 1 – Ryr1

SANS – small-angle neutron scattering

SDS – sodium dodecyl sulphate

SDS-PAGE – sodium dodecyl sulphate polyacrylamide gel electrophoresis

SEC – size exclusion chromatography

SEC-MALS – size exclusion chromatography-multiangle light scattering

SMA – styrene maleic acid

SMALP – styrene maleic acid lipid particle

TBS – tris-buffered saline

TEV – tobacco etch virus

TSA – tumour-specific antigen

UV – Ultraviolet

1 Introduction

1.1 Integral membrane proteins and plasma membranes

1.1.1 Overview

Plasma membranes are a ubiquitous and essential feature of all cellular organisms; these structures are crucial to forming the boundaries of organic bodies, creating a barrier which encapsulates and holds together the machinery and pathways of the cell, while protecting them from perturbations in the external environment. Plasma membranes are formed from a collection of amphipathic, lipid-based molecules, most often phospholipids though occasionally glycolipids, which arrange into a bilayer. The hydrophilic phosphate or sugar groups are orientated outward, facing into the surrounding aqueous environment, with the hydrophobic lipid groups of both layers arranged in parallel, facing tail-to-tail (Maibaum et al. 2004).

Cellular membranes are not simple, impenetrable walls, however; they are complex, intricate systems in their own right. The plasma membranes of all cells are composed of a rich assortment of phospholipids, integral membrane proteins and sugar groups, all of which work in coordination for a variety of tasks (Van Meer et al. 2008). In animals, sphingolipids, such as sphingomyelin and sphingomyolin, have been known to form lipid raft structures, which help to compartmentalise the membrane (Kinoshita et al. 2018).

Membranes have a selective permeability to allow essential nutrients and signals from the outside world into the cell. Many of the processes which occur

at and across cell membranes are conducted by integral membrane proteins which are embedded in the lipid bilayer.

1.1.2 Challenges associated with membrane protein study

1.1.2.1 Membrane protein expression

Identifying and developing systems for expressing proteins is the first step in production of materials for structural study. Host systems must be able to produce correctly folded, functional samples in quantities of the order of milligrams for structural characterisation (for example, X-ray crystallography and NMR) (Kim, Y. et al. 2008). This requires expression machinery which is able to recognise motifs in the peptide sequence and chaperone the nascent protein so that it can fold to form a functional final product. The expression machinery must also be able to handle a high volume of transcripts and translated peptide chains to avoid the generation of misfolded protein, both for the sake of efficiency, as well as to avoid fatally over-encumbering waste disposal pathways (Klepsch et al. 2011).

Historically, many soluble proteins from bacterial, archaea and eukaryotes have been expressed for study using well-characterised model Gram-negative bacterium *Escherichia coli* for fast and reliable generation of samples, thanks to its ease of manipulation and fast doubling time (Postis, V. G. et al. 2013). Thanks to modified plasmid vectors, *E. coli* cells have been used extensively to express proteins from across the tree of life (Choi et al. 2006).

The study of eukaryotic integral membrane proteins, however, is often beset by more problems than their soluble counterparts. One of the chief issues being incompatibilities between the machinery required for native membrane proteins targeting and folding with bacterial expression systems in transgenic expression. Expression of eukaryotic proteins is exceptionally challenging in bacterial systems due to fundamental differences in the structure and composition of both cell membranes and expression machinery (Kota and Ljungdahl 2005, Postis, V. G. et al. 2013).

Membrane proteins bring their own unique challenges in generating proteins that are both stable, folded and functional for research. Firstly, targeting and insertion of mammalian membrane proteins into lipid bilayers is often governed by a complex interaction between stop-transfer membrane-anchor targeting motifs near the N-terminus of protein primary sequence and internal translation and chaperon machinery such as Signal Recognition Particle, Hsc70/Hsp70 or Asna-1/TRC40 at the endoplasmic reticulum of the cell (Rabu and High 2007, Janda et al. 2010). Disruption to any of the elements involved in this process can result in misfolding of the proteins (Popot, J L and Engelman 2000).

Overexpression of membrane proteins can also be hazardous for the host cell. Overexpression of membrane proteins can overwhelm protein folding machinery within the cell, leading to build up of toxic aggregates. The presence of excessive number of channel proteins or pumps can cause lethal disruptions to the normal balance of nutrients, salts and/or pH of the cytosol by allowing aberrant exchange of molecules or ions with the extracellular

environment. Therefore, expressing channels/transporters that are constitutively active may require inhibitors to prevent killing of the host cell.

Additionally, cell membranes are effectively 2-dimensional spaces, as opposed to the 3-dimensional spaces of the cytosol. This gives membrane proteins significantly less space to diffuse and travel, as well as making overpopulation and overcrowding hazardous to the functioning of the membrane. Many membrane structures which influence membrane-associated proteins, such as curvature and the formation of rafts, can be dependent on the presence of specific of membrane proteins.

1.1.3 Methods for membrane protein extraction

1.1.3.1 Detergents

The most common approach for the extraction of membrane proteins is to emulsify the lipid bilayer using detergents, such as n-dodecyl- β -D-maltopyranoside (DDM) (Vanaken et al. 1986). Detergent molecules are a popular choice for dissolving lipid bilayers in order to liberate embedded proteins as they have very similar characteristics to lipids; both being amphipathic molecules with polar head groups connected to longer, hydrophobic tails (Gohon and Popot, J.-L. 2003). As such, they similarly form micelle structures which are able to substitute the membrane around an integral membrane protein, effectively forming a 'belt' which can stably house the protein.

The traditional model for membrane disruption by detergent, commonly referred to as the Three-Stage Model, states that lipid bilayers are disrupted

by the insertion of detergents into the monolayers of the membrane. In the first stage, the introduction of further molecules into the membrane results in increased packing of the molecules and increasing the turbidity of molecules in the membrane. In the second stage, the addition of detergent leads to an increase in the curvature of the membrane, leading to curvature stress which causes the membrane to bulge. Finally, in the third stage, as the ratio of detergent to native lipid increases further, the membrane bulge completely decouples from the opposing monolayer, rapidly sealing off and leaving the membrane as a miscelle (Lichtenberg et al. 2013).

Detergents are broadly classified into 4 primary groups: ionic detergents (e.g. sodium dodecyl sulphate [SDS]), non-ionic detergents (e.g. DDM), zwitterionic detergents (e.g. 3-[(3-cholamidopropyl)dimethylammonio]-1-propanesulfonate [CHAPS]) and bile salt detergents (Lund et al. 1989, Seddon et al. 2004). Each detergent type has its own strengths and weaknesses, with non-ionic and bile salt detergents being relatively mild and ionic detergents generally being harsh, often disrupting the protein's local environment and fold by changing the local electrical charges (Lund et al. 1989).

1.1.3.2 Maleic acid polymers

While detergents are popular and easy to use, with multiple well-established protocols for their use, they are not optimal for the extraction of membrane proteins. Detergent molecules substitute for natural lipids in the micelle, removing natively associated molecules, such as cholesterol, which can be essential for protein folding and function. In such cases, detergent-free

methods which preserve natively associated lipid molecules around the protein.

Styrene maleic acid polymers have reached prominence in recent years for their capacity to quickly and consistently form lipid nanodiscs, which are capable of encapsulating integral membrane proteins in preserved segment of bilayer (Postis, V. et al. 2015) (Figure 1.1). The extracted membrane segment, encapsulated by SMA, is referred to as an SMA lipid particle (SMALP).

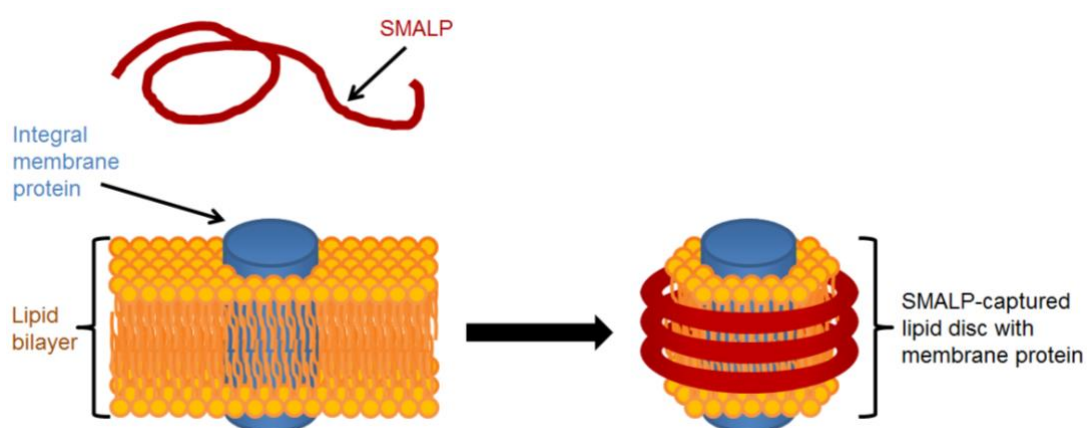


Figure 1.1 – *Cartoon representation of integral membrane proteins extraction the maleic acid polymer SMA.*

SMA has displayed success in extracting ABC transporters and bacterial potassium channel proteins for membranes, with the former displaying activity comparable to that of the native environment once extracted, displaying their capacity for retaining native fold and functionality (Gulati et al. 2014, Dörr et al. 2014). Such properties make SMA a very enticing target for study, as this

in theory allows proteins to be studied in states much closer to the native state than is afforded by traditional detergent-based methods.

Diisobutylene maleic acid (DIBMA), a polymer similar to SMA, has recently been reported as being able to form similar nanodisc structures of cellular lipid bilayers, simultaneously encapsulating membrane proteins (Oluwole et al. 2017b) (Figure 1.2). DIBMA and DIBMA lipid particles (DIBMALPs) containing membrane proteins have several advantages over SMA, such as reduced absorbance in the far-UV segment of the spectrum, reduced effects on lipid acyl chain ordering and lower susceptibility to aggregation in the presence of divalent cations (Oluwole et al. 2017a).

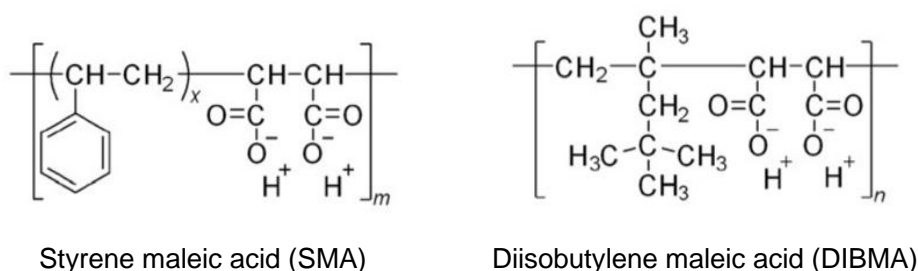


Figure 1.2 – Diagrams of the chemical structures of SMA and DIBMA polymers. Figure adapted from (Oluwole et al. 2017a).

Research of DIBMALPs is currently in its infancy; as of the time of writing, no materials have yet been published on the structure of any protein extracted in DIBMA, nor has any data been published characterising or probing the stability of proteins in DIBMA-based nanodiscs. DIBMA is of particular interest

at present thanks to its lack of intellectual property (IP) restrictions which currently apply to SMA, allowing for more flexibility in its discussion and application.

1.2 Cation channel superfamily

1.2.1 Overview

The formation and maintenance of concentration gradients across lipid membranes is a common feature of cellular organisms. Gradients of cations are used in a wide range of physiological activities, such as the storage of energy as electrochemical potential to drive oxidative phosphorylation of ADP in the case of ATP synthesis and transduction of signals along and between neuronal cells (Ostroumov et al. 1979, Dimroth et al. 2000).

The formation of such concentration inequities requires the cooperative function of a series of ion pump and channel proteins, which promote an ordered uptake and secretion of a series of ions to generate and dissipate electrochemical gradients (Gouaux and Mackinnon 2005).

In resting neurons, K^+ are maintained at an intracellular concentration of 155 mM, compared to concentrations of 4 mM in the extracellular environment (Hille 2001). The net effect of the electrochemical gradients of each of these ion types creates a resting potential across the membrane of -70 mV (Hille 2001).

The cation channel superfamily constitutes a large and varied group of integral membrane proteins which facilitate the passive transport of ions across lipid bilayers, conducting them down their electrochemical gradients. Members of

the cation channel superfamily share a number of common architectural features which are conserved across all three domains of life (Hille 2001). Their functions are essential to a wide variety of cellular processes, ranging from signalling and transport to maintaining homeostasis of essential cell nutrients.

1.2.2 Voltage-gated potassium channels

Voltage-gated potassium channels (K_v channels) are a vital component of many signalling systems, playing a crucial role in mediating electrochemical signalling through neuronal and smooth muscle cells. K_v channels sense the difference in charge across the plasma membrane, coupling the state of the cell's membrane potential to the channel's conformational state. K_v channels, when activated, act as an ion conduit, allowing K^+ to flow out of the cell from the intracellular environment, driven by the electrochemical gradient.

K_v channels are activated in response to membrane depolarisation (Figure 1.3); when the activation potential of the channel is reached, the channel shifts its conformation which allows greater conductance of potassium ions across the lipid bilayer, allowing intracellular K^+ ions to diffuse out of the cell down their electrochemical gradient. The outward flow of positive charge along with the potassium ions causes a shift in membrane potential back towards a negative value and the resting potential of the cell (typically approximately -70 mV) is re-established (Lewis et al. 2011). Once the membrane potential of the cell has returned to its resting state, the K_v channel is deactivated (Hille 2001).

K^+ channels are the largest family of ion channels in the human genome, with over 70 genes in total (González et al. 2012, Humphries and Dart, C. 2015).

The K_v1 channel (KCNA) subfamily of voltage-gated potassium channels proteins are often referred to as *Shaker*-type channels. This nomenclature is derived from early *in vivo* studies of a homologous K_v channel gene in *Drosophila melanogaster*, which was dubbed Shaker after the shaking leg phenotype observed as a result of mutations in the gene (Tempel et al. 1987). All K_v channels are members of the larger voltage-gated ion channel superfamily, which includes all other potassium channel families, as well as Na⁺ and Ca²⁺ ion channel families and some H⁺ ion channels (Hille 2001).

All K_v channels share a number of unique structural elements – early insights into the structure of the pore-forming domain of potassium channels came in the form of a 3.2 Å X-ray crystal structure of the prokaryotic KcsA channel derived from *Streptomyces lividans* (Doyle et al. 1998). KcsA is a pH-sensitive potassium channel constructed from a symmetrical, tetrameric arrangement of integral membrane proteins, dubbed ‘α subunits’. While KcsA provided much information on the general architecture of potassium channel pores and the structural basis of their selectivity for K⁺ ions, it did not provide any information on the mechanism of voltage-gating in larger K_v channel α subunits.

Each K_v1 α subunit features a soluble T1 domain at its N-terminal, followed by a series of 6 transmembrane helices, dubbed S1-S6, in order from N-terminal to C-terminal. K_v channel α subunits are able to form both homotetramers, as well as heterotetramers with other proteins in the same family, such as the K_v1.1, K_v1.2 and K_v1.4 proteins of the K_v1 family (Figure 1.3) (Jan, L. Y. and Jan, Y. N. 2012)

All voltage-gated cation channels, including Na^+ and Ca^{2+} , feature a highly conserved ~20 amino acid-long region, often dubbed the 'P-loop', which constitutes the selectivity filter of the channel. Conservation of the P-loop among all potassium ion channels is not limited to its amino acid sequence; the structure of the selectivity filter observed in mammalian K_v channel selectivity filters are virtually identical to the selectivity filter found in the distantly related bacterial K^+ channel KcsA (Long et al. 2007).

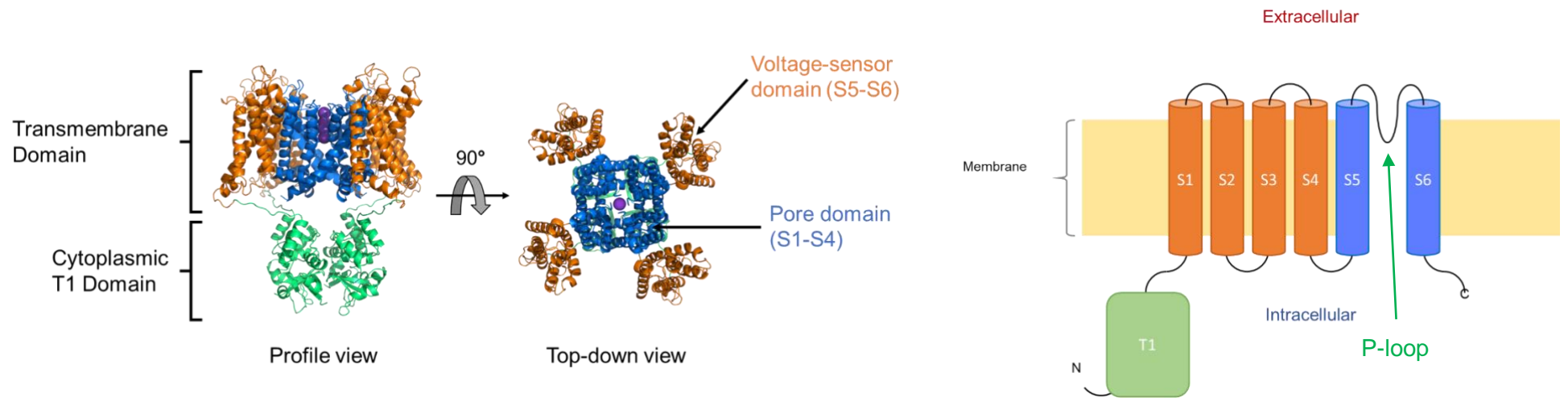


Figure 1.3 – Cartoon representation of tetrameric *K_v1.1* homology model (a) and schematic diagram of *K_v1.1* monomer (b). The homology model featured in (a) was generated using the online Phyre2 server, with the structure of the *Rattus norvegicus* chimera *K_v1.2-2.1* (PDB ID: 4JTC) used as the template for generating the homology model (Kelley et al. 2015, Banerjee et al. 2013).

In K_v channels, the P-loop is located in the linker between helices S5 and S6 (Figure 1.3). The backbone carbonyl groups face inward at the extracellular opening of channel, forming a series of 4 binding sites that coordinate K^+ ions in a cubic geometry (Doyle et al. 1998). The diameter of each binding site is too small to accommodate ions larger than K^+ , such as Ca^{2+} . Smaller ions, such as Na^+ , are excluded as their smaller size makes them unable to coordinate with all carbonyls at each ion-binding position, due to the octahedral geometry required for binding Na^+ ions (Hille 2001).

The use of backbone carbonyl groups in ion transport is crucial to the efficiency of the process. Carbonyl groups are sufficiently electronegative to dehydrate and bind K^+ , while also holding the ions weakly enough to keep the energetic cost of binding and release relatively low (Zhou, Y. et al. 2001). This system of selection is highly energy efficient; K^+ ions are able to cross the membrane, allowing transport to occur at rates comparable to free diffusion.

Gating of K_v channels is achieved through the movement of a voltage-sensor domain, which is formed from a helix-turn-helix motif comprising the C-terminal portion of the S3 TM helix, the subsequent linker region and the following S4 TM helix (Stühmer et al. 1989, Frech et al. 1989, Long et al. 2005). The voltage-sensor domain acts as a mobile paddle, which shifts in response to changes in voltage across the membrane (Long et al. 2007). It is the motion of this domain that couples the state of the cell's membrane potential with the activity of the channel.

Movement of the paddle in response to a positive membrane potential shifts the protein into a conformation which favours potassium conductance. This

sensitivity to voltage is conferred by a series of charged residues along the S4 helix (Figure 1.3), which face into the hydrophobic core of the plasma membrane (Bezanilla, F 2000). The structure of the voltage-sensor domain is highly conserved across multiple voltage-sensitive ion channel families. In contrast to the core sequence of the P-loop, however, the amino acid sequence of the voltage-sensor domain is considerably less well conserved, (Long et al. 2007).

Drosophila Shaker K_v channels feature in-built inactivation domains located at their N-termini, which act in a 'ball-and-chain' fashion, binding to the intracellular opening of the channel for rapid inactivation of ion conduction; this form of regulation is referred to as N-type inactivation. The involvement of the α subunit N-terminal was confirmed by both proteolytic digestion and deletion of the first 22 amino acids of the protein (Armstrong and Bezanilla, Francisco 1973, Hoshi et al. 1990, Zagotta et al. 1990). Many mammalian K_v channels, including $K_v1.1$, do not possess an N-terminal inactivation domain, however (Hille 2001).

Accessory proteins, known as β subunits, KCNAB, or $K_v\beta 2$, often modulate the activities of potassium channels. β subunits are closely related to the aldo-keto reductase subfamily of NADPH-dependent oxidoreductases, possessing NADPH-binding sites (Gulbis, Jacqueline M et al. 1999). β subunits co-assemble with *Shaker*-type channels during translation and folding at the endoplasmic reticulum to form an octomeric complex, composed of the tetrameric pore formed from four α subunit and four β subunits (Gulbis, J M et al. 2000). Each $K_v\beta$ protein is associated with the T1 domain of an α subunit. The subunits then remain closely associated with cytoplasmic T1 domain of

the channel's α subunits (Gulbis, J M et al. 2000). Three β subunits are known to associate with K_v1 family channels: KCNAB1 ($K_v\beta1$), KCNAB2 ($K_v\beta2$) and KCNAB3 ($K_v\beta3$); for example, the $K_v\beta2$ subunit is known to co-localise and associate readily with $K_v1.1$ subunits (Rhodes et al. 1996).

1.3 Pharmacology of $K_v1.1$ and related channels

Shaker-type K^+ channels are involved in a large number of biological processes and diseases and many have been extensively studied as therapeutic targets. The identification and development of inhibitors for inappropriately active channels has become a large and active field of research. The $K_v1.3$ channel, for example, has been studied, as excessive activation of this channel is known to cause unbalanced calcium signalling in human effector T cells, leading to excessive activation and autoimmune disease (Beeton et al. 2006).

Deletion or suppression of $K_v1.1$ (KCNA1) has been demonstrated to cause increased sensitivity to pain stimuli in studies conducted with mice, with $K_v1.1$ null mutations also reduced the effectiveness of morphine and other opiates in relieving neuropathic pain (Galeotti et al. 1997, Clark and Tempel 1998). It has been suggested that absence of $K_v1.1$ may reduce the action potential required to activate sensory neurons, causing nerve cells to become hyperexcitable, potentially explaining the reduced effectiveness of anaesthetics in null mutants (Ishikawa et al. 1999).

Localised application of the local ester-type anaesthetic butamben, a topical anaesthetic typically associated with rapid, but short-term suppression of pain, to the spinal column via epidural has been found to produce long-lasting relief for chronic pain with few side-effects (Beekwilder et al. 2003). An interaction

between butamben and Kv1.1 has been demonstrated, with inhibition of Kv1.1 activity also reported. It is not clear however if reductions in analgesic responses are caused by inhibition of Kv1.1 by butamben, or through its interaction with other components involved in signal transmission in the dorsal root ganglion (Beekwilder et al. 2003).

There are currently no known ligands which have been proven to bind and inhibit Kv1.1 with specificity over related voltage-gated channel activity. While some experimental evidence suggests that Kv1.1 is involved in the transmission of neuropathic pain, the details of its role in this process has also not been established with any certainty. Indeed, a recent study has suggested that the voltage-gated sodium channel Nav1.8, which has also been linked to neuropathic pain, is also inhibited by butamben (Garrison et al. 2014, Thériault and Chahine 2014). The development of structural insights of Kv1.1 inhibition may provide clues as to the significance of its role in pain management.

1.4 Application of electron microscopy

Electron microscopy (EM) possesses a number of advantages over the more traditionally popular technique of X-ray crystallography. First and foremost, EM require significantly smaller quantities of sample, in theory requiring only micrograms, rather than milligrams. This can remove significant hurdles to the determination of the structure, such as limitations in sample acquisition, low expression or less efficient purification, are less of an issue owing to the ability to positively select particles of specific shapes in electron micrographs.

The analysis of proteins via EM is not limited by the ability of target molecules to form highly ordered crystals, rather its focus on individual particles in

suspension theoretically allows proteins to be observed in states more similar to their conformations in their conditions in free solutions.

In recent years, EM has risen to become an essential tool in the investigation and analysis of biomolecular structures. While historically limited to large complexes or highly symmetrical structures, recent advances in technology have significantly improved the competitiveness of EM in the field. In recent years, the proportion of structures which have been determined by cryo-electron microscopy (cryo-EM) has been steadily increasing as a proportion of published protein structures (Earl et al. 2017) (Protein Data Bank in Europe 2018) (Figure 1.4).

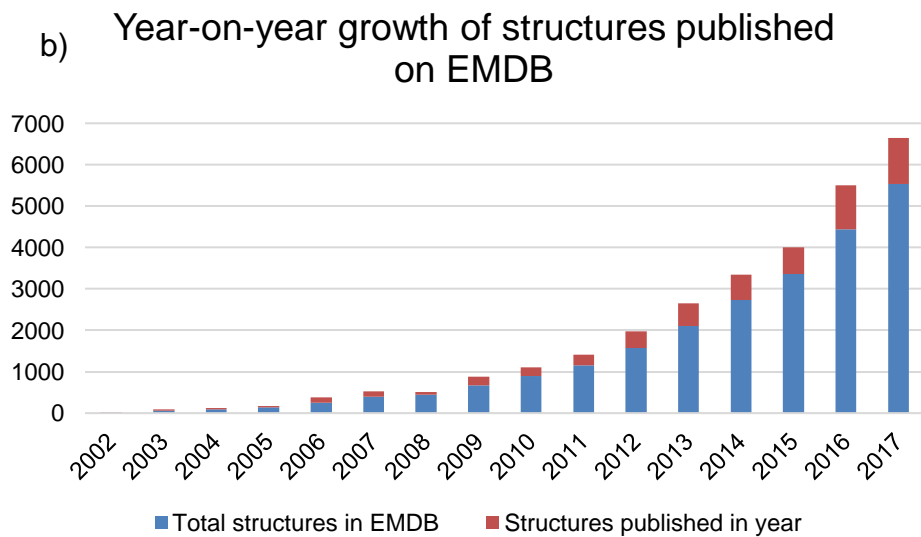
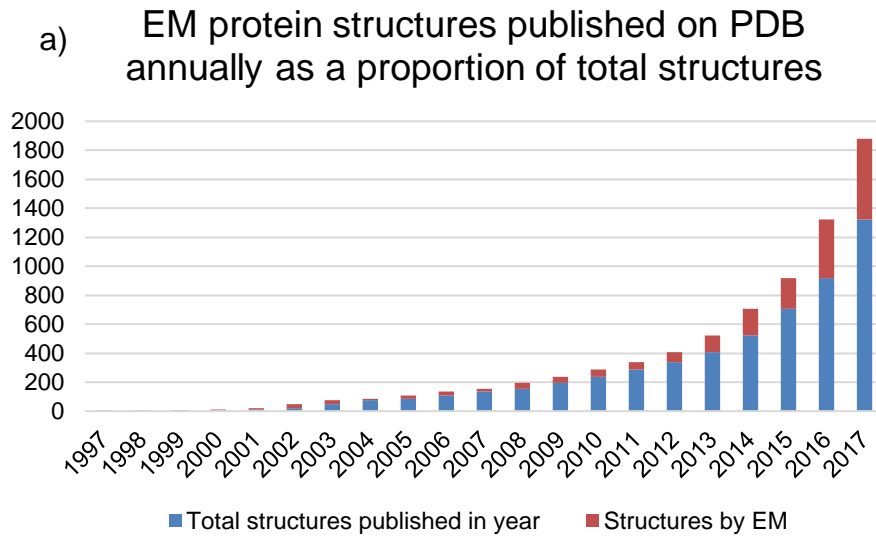


Figure 1.4 – Graphs detailing the rise year-on-year of structures determined by electron microscopy vs. other methods (Protein Data Bank 2018, Protein Data Bank in Europe 2018).

The recent development of direct electron detectors (DEDs) have improved the signal to noise ratio and contrast of micrograph images, allowing structures attained by EM to reach atomic resolutions (Bai, X. chen et al. 2015). Additionally, they allow movies to be captured at significantly higher framerates, reducing exposure times and, in turn, reducing radiation damage of samples. The higher number of recorded movie frames also permits improved motion correction of micrographs, allowing more precise averaging of microscope views, decreasing image blur and increasing particle resolution (Thompson, R. F. et al. 2016, Bai, X. chen et al. 2015).

Membrane proteins have not been exempt from this renaissance in EM technology. In recent years, a number of high-profile membrane proteins have had their structures determined to atomic resolution through cryo-EM, including Ryanodine Receptor 1 (Ryr1), Piezo1, Gamma Secretase and Voltage-Gated Calcium Channel α -1 (Ca_v1.1) (Yan, Zhen et al. 2015, Ge et al. 2015, Lu, P. et al. 2014, Wu, J. et al. 2015). (Figure 1.5).

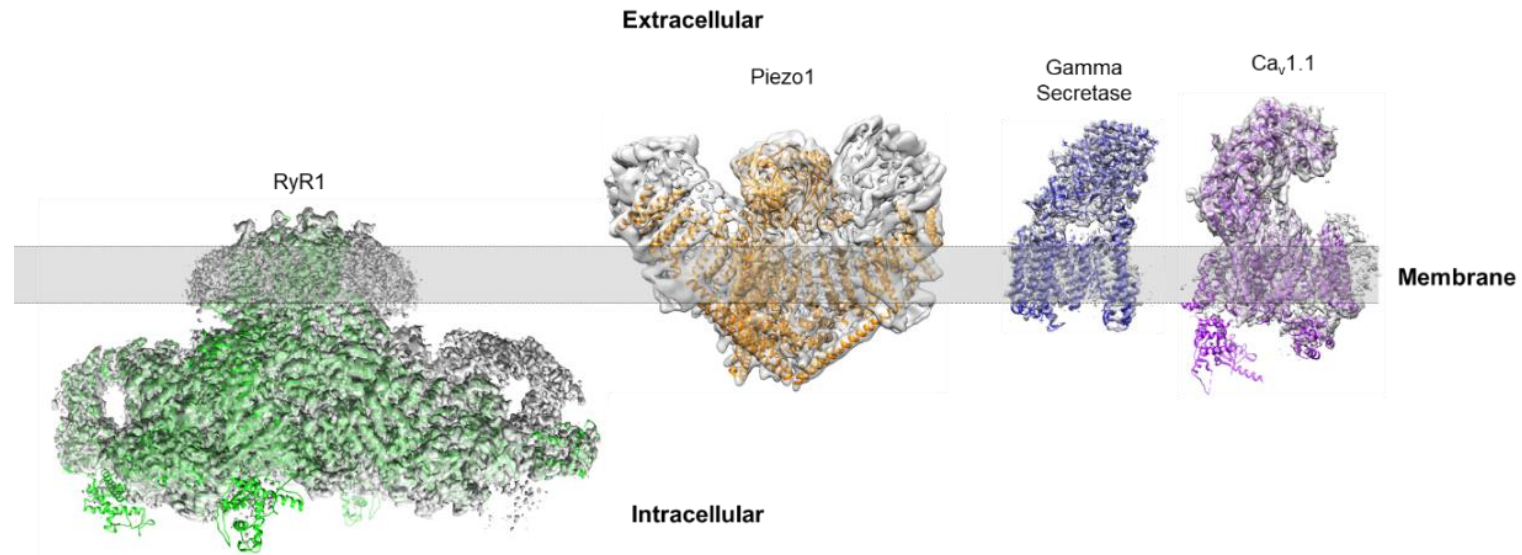


Figure 1.5 – Cartoon representation of a selection of membrane proteins whose structures have recently be determined through electron microscopy (Yan, Zhen et al. 2015, Ge et al. 2015, Lu, P. et al. 2014, Wu, J. et al. 2015).

1.5 Aims and objectives

This project was conceived with the aim of expressing and purifying the human variant of Kv1.1 for structural study, followed by investigation of the structural basis of its interactions with known inhibitors. This information could then be applied to the development of rationally designed drug molecules targeting Kv1.1, whose inhibition could then be exploited for pain relief.

The above aim was planned to be achieved through obtaining the following objectives:

- Design and construct plasmid to encode and express Kv1.1 with tags to assist purification and analysis
- Develop mammal cell-based host systems for overexpressing the Kv1.1 ion channel complex
- Purify the Kv1.1 complex using C-terminal tags to avoid disrupting residues at the N-terminal involved in membrane targeting
- Investigate extraction by SMA and DIBMA nanodisc scaffolds and compare their effectiveness with traditional detergents
- Determine the structure of the complete Kv1.1 channel alone and in complex with the regulatory Kvβ2 subunit through cryo-EM
- Investigate the effects of various inhibitory molecules on the electrophysiological characteristics of the Kv1.1 pore
- Establish the binding sites of inhibitor molecules at the Kv1.1 channel

2 Materials and Methods

2.1 Cloning strategy and construct design

2.1.1 Expression vector design

2.1.1.1 Use and advantages of pcDNA plasmids

The cloning and expression of KCNA1 and KCNAB2 was mediated by pcDNA6 and pcDNA3.1 plasmids, respectively (see Appendix 8.1 for details), which possess a number of features making them appropriate for the needs of the project. Firstly, these plasmids are suitable for transformation into bacterial hosts for amplification and storage. To compliment this, pcDNA6 and pcDNA 3.1 both carry an ampicillin resistance gene, allowing transformed bacteria to be selected through the application of appropriate antibiotics (ampicillin, carbenicillin, etc.). pcDNA plasmids also possess a human cytomegalovirus (CMV) immediate-early promoter upstream of the plasmid polyclonal site, which enables inserted genes to be expressed in mammalian systems, such as HEK (human embryonic kidney) 293 cells.

pcDNA plasmids carry additional genes encoding for resistance to antibiotics that target mammal cells. pcDNA6 and pcDNA3.1 carry resistance gene for blasticidin and neomycin, respectively allowing antibiotics to be used to select for transfected HEK 293 cells. This feature aids the development of stably transfected cell lineages through elimination of non-transfected cells. Additionally, as both plasmids contain resistance genes for different antibiotics, they can be selected for via separate antibiotics. Each gene inserted into these plasmids were accompanied by upstream Kozak consensus sequences to facilitate gene transcription in eukaryotic cells.

2.1.1.2 Fusion tags

A number of tags were selected for inclusion in Kv1.1 and Kv β 2 fusion constructs. The addition of tags was used to modify the properties of the expressed proteins, allowing, approaches to expression and purification not available while working with native proteins. The fusion tags used during in constructs development are listed below in Table 2.1.

2.1.1.3 Design of Kv1.1 constructs and cloning vectors

Cloning and expression of the *KCNA1* gene was mediated through the pcDNA6 plasmid. pcDNA6 plasmids encoding three Kv1.1 constructs were provided by Dr. Jon Lippiat of the University of Leeds School of Biomedical Sciences at the beginning of the project:

- **KCNA1** – Native Kv1.1
- **KCNA1-EYFP** – Kv1.1 + C-terminal enhanced yellow fluorescence protein tag
- **KCNA1-V5-His₆** – Kv1.1 + C-terminal V5 antibody epitope and hexahistidine tag

These constructs formed the basis of further constructs, through modification of plasmids via site-directed mutagenesis. Kv1.1 constructs featuring additional and alternative tags were designed to allow multiple methods for purification to be tested. Tags were restricted to the C-terminal of the protein in order to reduce the risk of disruption of insertion of the N-terminal region of the protein into the cell membrane. Tobacco etch virus (TEV) protease

cleavage sites with the sequence ENLYFQS were also included upstream of some tags in some constructs to allow their removal following purification.

Tag	Function	Amino acid sequence
EYFP	Indicator of protein expression through fluorescence chromatography. Target for anti-green fluorescent protein (GFP) antibodies in western blotting. Potential epitope for purification using anti-GFP antibody resin.	VSKGEELFTGVVPILVELDGDVNGHKFS VSGEGEGDATYGKLTCLKFICTTGKLPVP WPTLVTTTFGYGLQCFARYPDHMKQHDFE KSAMPEGYVQERTIFFKDDGNYKTRAEV KFEGDTLVNRIELKGIKIDFKEDGNILGHK LEYNYNSHNVYIMADKQKNGIKVNFKIR HNIEDGSVQLADHYQQNTPIGDGPVLLP DNHYLSYQSALS KDPNEKRDMVLLLEFV TAAGITLGMDELYK
V5	Antibody epitope for purification on anti-V5 antibody resin and antibody target in western blotting.	GKPIPNPLLGLDST
c-Myc	Antibody epitope for purification on anti-Myc antibody resin.	EQKLISEEDL
Hexa/deca-histidine tag (His _{6/10})	Nickel-cobalt-binding group used in immobilised metal affinity chromatography; extension to His ₁₀ increases metal affinity. Target for anti-polyhistidine antibodies in western blotting.	HHHHHH [HHHH]
FLAG	Antibody epitope for purification on anti-FLAG antibody resin.	DYKDDDDK

Table 2.1 – Fusion tags utilised during Kv1.1 and Kvβ2 construct design and production. The function and amino acid sequences of each tag had been included in the table to provide context for their use.

The following constructs were planned for development during the course of the project:

- Kv1.1-EYFP-His₆
- Kv1.1-TEV-EYFP-His₆
- Kv1.1-TEV-EYFP-His₁₀ (Kv1.1-TY10)
- Kv1.1-TEV-EYFP-His₁₀-FLAG

To this end, a series of primers were designed in order to modify the base Kv1.1-EYFP construct encoded in pcDNA6 in order to introduce new elements and remove unwanted ones (See Table 2.2).

Tags	Forward primer	Reverse primer	Melting temp (°C)
EYFP-His ₆	CATCATCACCATCACCATTGAGTTTAAACC	CTTGACAGCTCGTCCATGCC	58.1
TEV-EYFP-His ₆	CTTCCAGAGCGTGAGCAAGGGCGAGGAG	TACAGGTTCTCGAATTC AACATCGGTCAGTAGC	58.5
TEV-EYFP-His ₁₀	CACCATCACCACCATCATCACCATCACCATTGAGTT TAAACCCGCTGATC	GGATCACTCTCGGCATGGACGAGCTGTACAAG	63.8
TEV-EYFP-His ₁₀ -FLAG	GATGATGACAAGTGAGTTTAAACCCGCTGATCAGCC TCGACTGTGC	GTCCTTGTAGTCA TGGTGATGGT GATGATGGTGATG ATGGTGCTTGTACA	62.7

Table 2.2 – Primers used in the modification of plasmids encoding Kv1.1-EYFP constructs. The elements encoding for various elements have been colour coded, with EYFP in yellow, Polyhistidine in green, TEV in red and FLAG in blue. The melting temperature refers to the temperature the elements which anneal to the unmodified plasmid (in capitals) denature.

The KCNA-EYFP-His₆ construct was developed by modifying the plasmid encoding the KCNA1-EYFP construct. This was achieved through insertion and deletion through PCR (see section 2.1.2 for details on PCR method) (Lee, J. et al. 2010). using a forward primer to clone outward from the His₆ segment of the pcDNA6 plasmids and a reverse primer above designed to anneal and clone outward from 3' end of the gene encoding K_v1.1-EYFP, while excluding the stop codon.

```
>KCNA1Gb_His_forward  
5'-catcatcaccatcaccattgagtttaaacc-3'  
>KCNA1Gb_His_reverse  
5'-cttgtacagctcgtccatgcc-3'
```

The above primers excluded both the stop codon and linker between the *KCNA1-EYFP* gene and the His₆ encoding segment. This would produce a new gene with a polyhistidine tag fused onto the C-terminal end of the product. Sequencing of the resulting plasmid was carried out to check that the PCR program had produced the desired mutations. Once the plasmid encoding the KCNA1-EYFP-His₆ fusion construct was available, this plasmid was in turn used as the basis for the development of a K_v1.1-TEV-EYFP-His₆ fusion construct. Production of this plasmid was carried out through further PCR mutagenesis, using the following forward and reverse primers:

```
>KCNA1G_His_TEV_forward  
cttccagagcgtgagcaagggcgaggag  
>KCNA1G_His_TEV_reverse  
tacaggttctcgaattcaacatcggtcagtagc
```

The K_v1.1-TEV-EYFP-His₆ plasmid was further modified to produce a K_v1.1-TY10 construct. This was undertaken using the following forward and reverse primers, which were designed to add four additional histidine codons to the C-terminal of the fusion protein, with the additional histidine codons highlighted in green:

```
>KCNAB2-His10_Forward
catcatcaccatcatcacatcaccattgagtttaaacccgctgatcag
>KCNAB2-His10_Reverse
gtgcttgtagcagctcgtccatgccgagagtgatccc
```

2.1.1.4 Design of K_vβ2 constructs and cloning vectors

K_vβ2 expression and cloning was mediated through the use of pcDNA3.1 plasmids. pcDNA3.1 was selected as the vector for *KCNAB2* as it features a neomycin resistance gene in place of blasticidin resistance gene. This allowed for selection of cell lines co-transfected with both pcDNA6 and pcDNA3.1. As K_vβ2 is a soluble protein, fusion tagging of the N-terminal was considered to be less of a risk to protein folding and stability, as intracellular soluble proteins typically possess fewer signal peptides compared to membrane proteins and secretory proteins.

The *KCNAB2* gene was sourced from foetal human brain cDNA library. Designs for K_vβ2 constructs included eliminating the stop codon at the 3' end of *KCNAB2*, allowing transcription to run through the full length of the gene into downstream hexahistidine and c-Myc tags encoded by the pcDNA3.1 plasmid, terminating with an included stop codon. as well as the addition of a fluorescent mCherry tag to allow K_vβ2 to be detected separately from EYFP-

tagged Kv1.1 in doubly transfected cell lines. Primers were designed to facilitate these goals (Table 2.3).

Tags	Forward primer	Reverse primer	Melting temp (°C)
Foetal cDNA	GCCGGAATTCACCATGTATCCAGAATCAACGAC GGGCTC	GCGGTCTAGATTAGGATCTGTAGTCCTTTTTGC TGTAGGGTTTATTG	64.6
cMyc-His ₆	CCCGCGGTTGAACAAAACTCATCTCAGAAGAG GATCTGAATATGC	CCCTCTAGAGGATCTGTAGTCCTTTTTGCTGTA GGGTTTATTGCC	66.4
His ₆ -mCherry	GTCTAGAGTTTCAAAGGTGAAGAAGATAATAT GGCTATTATTAAAG	GACCGGTTTTATATAATTCATCCATACCACCAG TTGAATGTCTACC	59.2

Table 2.3 – Primers used in the modification of plasmids encoding K_vβ2 constructs.

A pcDNA plasmid encoding native KCNAB2 protein was generated through PCR cloning from a human cDNA library derived from foetal human brain cells. Primers for the cloning of human *KCNAB2* were designed based on the sequence of the *Homo sapiens* variant with NCBI reference code NM_003636.3:

>KCNAB2_forward_primer

GCCGGAATTCACCATGTATCCAGAATCAACGACGGGCTC

EcoRI

>KCNAB2_reverse_primer

GCGGTCTAGATTAGGATCTGTAGTCCTTTTTGCTGTAGGGTTTATTG

XbaI

The primers above were designed to allow restriction digestion and ligation into the pcDNA3.1 plasmid. The elements highlighted in red in the primer sequences denote these restriction sites (EcoRI in the forward primer, XbaI in the reverse primer). The PCR product was then subjected to restriction digestion by EcoRI and XbaI and ligated into a pcDNA3.1 plasmid cut with the same restriction enzymes and the *KCNAB2* gene was ligated into the cut pcDNA3.1 plasmid. Modification of the plasmid was checked through sequencing.

A further *KCNAB2* construct was generated featuring a 3' region encoding for a C-terminal c-Myc-His₆ tag through PCR mutagenesis. This was undertaken using forward and reverse primers designed to remove the stop codon at the end of the *KCNAB2* gene, allowing the c-Myc and His₆ tags downstream of

the polyclonal site to be transcribed with the gene. The primers used had the following sequences:

>KCNAB2-Stop_Forward

cccgcggttgaacaaaaactcatctcagaagaggatctgaatatgc

>KCNAB2-Stop_Reverse

ccctctagaggatctgtagtcctttttgctgtagggtttattgccc

2.1.2 PCR

2.1.2.1 Site-directed mutagenesis

Site-directed mutagenesis was utilised during the course of the project to modify the nucleic acid sequence of plasmids. This allowed the amino acid sequences of final expressed proteins to be adjusted to include or exclude linking segments or to add or remove fusion tags. Site-direct mutagenesis was performed using custom forward and reverse primers designed to hybridise to loci within plasmids where modifications were desired. Modifications were designed to introduce new nucleotide sequences, exclude sections of the template to delete unwanted segments, or modify sequences.

Polymerase chain reactions were carried out using Q5 polymerase (New England Bioscience). Reactions were carried out in both 25 μ l and 50 μ l volumes, depending on the need for product DNA. 0.5 μ M forward and reverse primers were applied, along with appropriately dilute 5 \times Q5 polymerase reaction buffer (New England Bioscience) and 200 μ M dNTPs. The volumes of each component used in reaction mixtures is detailed in Table 2.4. 0.5 μ g

of template plasmid DNA was added and the volume of the reaction mixtures increased to the addition of nuclease-free triple-distilled water.

	Forward primer (10 μM)	Reverse primer (10 μM)	Q5 reaction buffer	dNTPs (10 mM)
25 μl vol.	1.25 μ l	1.25 μ l	5 μ l	0.5 μ l
50 μl vol.	2.5 μ l	2.5 μ l	10 μ l	1 μ l

Table 2.4 – Table detailing the mixture of primers, buffers and reagents used in the standard PCR protocol used in the course of the project.

Touchdown PCR was then used to generate and amplify the mutagenized plasmid. This was conducted using a Dyad DNA Engine thermal cycler (Bio-Rad). The programme involved an initial 1 min melt at 98°C before the thermal cycle. Each subsequent cycle was programmed to begin with a 30 sec melting step at 98°C, followed by a 30 sec annealing step, which varied between each cycle, followed by a final extension step at 72°C for 20 sec. The annealing step was programmed to begin at 5 °C above the primers' melting temperature in the first cycle, reducing in 0.5°C increments for 19 cycles to 5°C below the primers' melting temperature. This was followed by 10 further cycles with an annealing at 5°C below the primers' melting temperature for a final total of 30 cycles (see Table 2.1 for the melting temperatures of primers

used). The programme then concluded with a final extension at 72°C for 3 min, before reducing to holding temperature of 10°C for recovery.

Following PCR amplification, reaction mixtures were treated with DpnI restriction enzyme, which has a short recognition site, GATC, and only recognises methylated DNA. DpnI treatment digested and eliminated methylated template plasmid derived from bacterial cultures, leaving only the PCR product. These reaction mixtures were then loaded and run on 1% agarose gels (see section 2.1.5), with any bands corresponding to the predicted weight of the desired PCR product recovered through gel extraction using a QIAquick gel extraction kit (Qiagen) following the manufacturer's instructions.

The process of site-directed mutagenesis was used extensively during the project in order to modify plasmids and generate new K_v1.1 fusion construct genes. For example, site-direct mutagenesis was used in order to insert 4 additional histidine codons (CAC, CAG) onto the hexahistidine tag of the K_v1.1-TEV-EYFP-His₆ construct in order to produce an extended dexahistidine tag, producing the K_v1.1-TY10 construct (see Table 2.1).

2.1.2.2 Cloning from cDNA library

Human *KCNAB2* was cloned from a cDNA library derived from foetal brain tissue using PCR, with primers designed to hybridise with the 5' and 3' ends of the sequence encoding the protein. The primers (discussed in section 2.1.1) were designed to introduce an EcoRI restriction site at the 5' end of the gene, along with a 3' XbaI restriction site.

2.1.3 DNA fragment insertion

2.1.3.1 Overhang restriction and ligation

Extraction of segments of DNA and insertion into new vectors was sometimes handled through cutting of strands using specific restriction enzymes. Many restriction enzymes target specific palindromic sequences, creating single-stranded overhangs which are able to hybridise with complementary sequences. DNA which has been cut with the same restriction enzymes will be able to hybridise, allowing the sequence to be ligated together. This can be exploited to excise segments flanked by restriction sites out of one DNA strand and insert it into a new vector which has been cut with the same restriction enzymes.

DNA restrictions carried out during the course of this project were cut using enzymes supplied by New England Biosciences. 1 unit of enzyme is determined by the manufacturer as the amount of enzyme required to digest 1 µg of Phage λ DNA in 1 hour at 37°C in a total reaction volume of 50 µl, with enzymes supplied at a concentration of 2 units/µl. Digestions were carried out by mixing 0.5 µl of restriction enzyme in supplier storage buffer for every µl of DNA in the reaction volume. CutSmart Buffer (New England Bioscience) was added to the reaction mixture at a ratio of 1:9, if compatible with the desired enzyme. If the restriction enzymes used were not compatible with CutSmart, NEBuffers 1.1, 2.1 or 3.1 were applied as appropriate instead.

Reactions were placed into 37 °C heating blocks for 1 hr incubation. DNA from the reaction was then visualised via agarose gel electrophoresis (See section 2.1.5 for details).

2.1.3.2 CloneJET PCR cloning and blunt ligation

PCR cloning and insertion into pJET1.2 was used in the extraction and amplification of the human *KCNAB2* gene from foetal human brain cDNA (see Appendix 8.1 for details of plasmid). This method was used in order to reduce the number of steps required to generate a vector hosting the gene. Inserting the gene into pJET1.2 vector was selected as it would avoid an additional restriction digest step involved in sticky end-based ligation. Following insertion, it would also provide a series of restriction sites both upstream and downstream of the gene without potentially cutting any segments out of the polyclonal site.

2.1.4 Bacterial culture

2.1.4.1 Heat shock transformation

Transformation of plasmids into bacterial hosts was used in order to clone and maintain populations of plasmid DNA. Transformations were conducted using XL1-Blue supercompetent *E. coli* cells (Aligent Technologies). This was carried out through incubation of 25 µl of competent cell stocks (containing ~ 2.5×10^6 cells) on ice with 10 ng of plasmid DNA for 1 hr. Cells were then transferred to a 42°C heating block for 45 sec, then returned to ice and incubated for a further 2 min. Transformed cells were then taken forward to culturing on lysogeny broth (LB) agar plates.

2.1.4.2 LB agar culture

LB agar was produced from commercial powder (Sigma-Aldrich) and melted in doubly distilled water through heating to 120°C. Molten agar was split into

50 ml aliquots and allowed to cool to ~50°C. To select for transformed cells, 50 µl of 100 mg/ml ampicillin solution was added to each agar aliquot for a final working solution of 100 µg/ml. 25 ml of molten agar was then poured into sterile 60 mm plastic petri dishes and allowed to cool until solid.

Transformed XL1-Blue cells were transferred to agar plates and spread across the gel surface using a glass spreader under aseptic conditions. Inoculated plates were then placed into 37°C incubators and allowed to grow overnight. Following incubation, plates were retrieved and used in the inoculation of liquid LB cultures. Between uses, plates were sealed using parafilm wax; this was done to reduce infection and drying of the agar while in storage, extending the lifetime of the plates.

2.1.4.3 Liquid LB culture

Liquid LB was produced from commercial powder (Sigma-Aldrich). As with LB agar cultures, 100 mg/ml ampicillin solution was diluted ×1000 into Liquid LB to select for cells transformed with plasmid. Small-scale liquid cultures were established in 30 ml universal tubes containing 4 ml of Liquid LB. Discrete colonies identified on LB agar plates were collected using a wire loop and transferred to the 4 ml Liquid LB under aseptic conditions. Universal tubes containing inoculated medium were then placed into incubation at 37°C overnight on a 200 rpm shaker platform. Incubated media was collected following overnight incubation and cells were pelleted through centrifugation at 4,800 × g. The supernatant was then deposited through decanting and the pelleted cells placed into storage at -20°C for miniprep plasmid recovery at a later date.

Larger scale 500 ml Liquid LB culture volumes were also established in order to provide larger quantities of DNA for polyethylenimine (PEI)-based HEK 293 cell transfection carried out at later stages of work. These larger scale cultures were established through the inoculation of 500 ml Liquid LB with 0.5 ml of inoculated media from small scale cultures following overnight incubation. Cells were collected, pelleted and stored in the same manner as small-scale cultures.

2.1.5 Agarose gel electrophoresis

1% (w/v) agarose gels were made by mixing 500 mg agarose powder with 50 ml TAE buffer. The powder was dissolved at high temperature through microwaving the mixture. Once the powder was melted, 1 μ l ethidium bromide was added to the mixture and the molten gel poured into a mould with the appropriate comb added for the number of wells needed.

Once cooled and solidified, the comb was gently removed and the gel was placed into a gel running system and submerged under a shallow pool of TAE buffer. Samples mixed with appropriately diluted gel DNA dye, purple (New England Bioscience) were then loaded into the wells, along with an appropriate DNA ladder for measuring the mass of species on the gel. 80 V was then applied across the gel for 60 min, with the gel loading wells placed adjacent to the negative anode.

2.1.6 DNA sequencing

Sanger sequencing of plasmid DNA was conducted externally by submission of samples to Source Bioscience and Beckman-Coulter (now GeneWiz).

Plasmids were sequenced using T7 forward and BGHR/BGHR2 reverse primers provided by the sequencing companies. Sequencing data was aligned with plasmid sequences using Clustal Omega, then evaluated and adjusted using Jalview 2 and SerialCloner 2.6.1 (Waterhouse et al. 2009, Sievers et al. 2011).

2.2 Protein expression

2.2.1 Adherent human embryonic kidney cell culture

Expression plasmids encoding Kv1.1 and Kv β 2 constructs were initially conducted in HEK 293 (Human Embryonic Kidney) TSA (tumour-specific antigen) cells. Stocks of HEK 293 TSA cells were maintained as adherent cultures in T25 tissue culture flasks. Cells were grown in Dulbecco's modified Eagle's/essential medium (DMEM) with high glucose + GlutaMAX™ supplement (Gibco; Life Technologies), mixed with 10% foetal bovine serum (FBS). Cell cultures were grown at an ambient temperature of 37°C with 5% concentration of atmospheric CO₂.

Culture flasks were maintained until either the confluence of adhered cells reached ~80% or the pH indicator of the medium indicated significant acidification of the environment. Cells in these flasks were preserved through subculturing; this involved the removal of old media through aspiration, followed by washing of cells with 2 flask volumes of Dulbecco's phosphate-buffered saline (DPBS). Cells were then treated with 0.05% trypsin-EDTA (Gibco; Life Technologies); 200 μ l for T25 flasks or 600 μ l for T75 flasks. Cells were then incubated for 10-15 min at 37%. Following this, cells were dislodged by gentle aspiration of DMEM supplemented with 10% FBS to inhibit trypsin

enzymes and prevent damage to the cell by excessive proteolysis of membrane proteins. Resuspended cells were then transferred to a 15 ml falcon tube and pelleted through centrifugation at 200 x g for 3-5 min. The pelleted cells were then resuspended into a culture volume of DMEM, before being split and transferred a new flask and diluted $\times 10$ in DMEM. Finally, the cells were placed back into incubation at 37°C.

The size of the flask used varied in accordance with the total volume of the culture; T25 flasks were used for smaller-scale 5 ml cultures, T75 flasks were used for medium-scale 12 ml cultures and T175 flasks were used for large-scale 30 ml cultures.

2.2.2 Suspension HEK cell culture

Culture of HEK cells in suspension was conducted using a protocol suggested by Dr. Paul Miller at Ludwig institute of Cancer, University of Oxford. HEK cells were transferred from adherent culture to suspension through trypsin treatment, followed by gentle detachment from flask surfaces by aspiration of medium. Dislodged cells were then deposited into 250 ml Erlenmeyer flasks containing 80 ml of FreeStyle (ThermoFisher Scientific) medium. Flasks were then placed into shaking incubators with an ambient temperature of 37°C, 8% atmospheric concentration CO₂ with platform shaking rate of 120 rpm.

For comparison of culture medium on cell growth rates, cultures were established from stably transfected Kv1.1-TY10-expressing HEK293S GnTI⁻ cells gathered from adherent culture via trypsinisation at 80% confluence. Establishment cultures were prepared in two 250 ml plastic Erlenmeyer flasks. Cells were seeded into 90 ml of medium, with several of media types (DMEM,

FreeStyle 293, Protein Expression Medium [PEM; ThermoFisher] and EX-CELL [Sigma-Aldrich]) tested to compare their relative ability to sustain cell population growth. Media was supplemented with 100-fold diluted NEAA amino acid stock (Gibco), 100-fold dilute L-glutamine (Gibco), 100 mg/ml penicillin/streptomycin and 1% (v/v) foetal bovine serum (FBS) and topped up to a volume of 90 ml with either medium.

The growth rates of cells were monitored daily using a Countess automated haemocytometer (Invitrogen). Once the density of cells had reached between 2 and 3×10^6 cells per ml, cultures were split into two 40 ml volumes and diluted 1:3 into 120 ml PEM for a final volume of 160 ml in 500 ml tissue culture grade Erlenmeyer flasks. Cells were then placed back into incubation under the same conditions as previously and incubated until the cell density again approached 3×10^6 cells per ml. Once this density was reach, 5 mM sodium butyrate was added to the cell medium to boost protein expression (Kruh 1981). Cells were then collected through pelleting out of the medium by centrifugation at $200 \times g$.

In parallel to this, as there was no previous in-house experience with suspension HEK cell culture, experimentation was conducted with a series of media types was to identify the most effective type for maintain viable cells at a high rate of growth. For this, adherent HEK cells were seeded into 80 ml FreeStyle 293, PEM, EX-CELL and Gibco DMEM (Thermo Fisher) in 250 ml tissue culture grade Erlenmeyer flasks and their growth (living cell count) and viability (% living cells/total cell count) were recorded every 24 hrs.

2.2.3 Transient human embryonic kidney cell transfection

2.2.3.1 FuGENE-mediated cell transfection

Transfection of HEK cells via FuGENE HD transfection reagent (Promega) was carried for transfection of small-scale T25 flask cultures. 5 µl of FuGENE HD reagent was mixed into 100 µl of OptiMEM (Gibco; Life Technologies). 2 µg of plasmid DNA was then added and the mixture was allowed to incubate for 20 min at room temperature. The incubated solution was mixed into flasks containing freshly seeded HEK cells at ~25% confluence. 24 hrs after the addition of the transfection reagent, 5 mM sodium butyrate was applied to the transfected cell to boost protein expression. After a further 24 hrs, the transfected cells were collected through removal of media via aspiration, followed by 2 x wash with DPBS. Cells were then gently dislodged through 15 min incubation in DPBS at 37°C and pelleted through centrifugation at 200 x g and the supernatant discarded via decanting.

2.2.3.2 PEI-mediated transfection

Cells were seeded in Gibco DMEM + 10% foetal bovine serum (FBS) and 1% penicillin-streptomycin at a confluence of 25% (for seeding density see Table 2) one day prior to transfection. Cells were then allowed to adhere overnight at 37°C and 5% ambient atmospheric concentration of CO₂ prior to transfection, the flask media was removed via aspiration and replaced with DMEM + 5% FBS and 1% penicillin-streptomycin (Table 2.5) and the flask/plate returned to 37°C, 5% atmospheric CO₂ for 1 hr.

Flask/Plate	Volume of DMEM + 5% FBS media applied 1 hr prior to transformation
96 well	100µl
24 well	400µl
6 well	2ml
35 mm	2ml
T25	2ml
T75	6ml

Table 2.5 – Volume of media used in adherent HEK 293 cells one hour pre-transfection.

DNA-PEI complexes were prepared in advance through mixing at a ratio of 5:2, DNA:PEI. The volumes of DNA (400 µg/ml) and PEI (1 mg/ml) used in flasks of different volumes is detailed in Table 2.5. PEI was added to the desired plasmid DNA and mixed by swirling with a pipette tip and the mixture was allowed to incubate at room temperature for 10 minutes. DMEM + 5% FBS and 1% penicillin/streptomycin was then added to the DNA-PEI complex (see Table 2.6 for amount) and mixed by aspiration. The whole solution was subsequently added to the flask/plate and mixed by gentle rocking.

	96 well	24 well	6 well	35 mm	T25	T75
DNA, 400 µg/ml (µl)	0.83	5.20	25	20.8	65	195
PEI, 1 mg/ml (µl)	0.33	2.08	10	8.33	26	77.5
DMEM + 5% FBS (µl)	3.33	20.79	100	83.3	260	777.5
Total volume (µl)	4.49	28.07	135	112.5	351	1050

Table 2.6 – Table describing PEI:DNA complex formulation for wells and plates of varying sizes.

Flasks/plates were then returned to the incubator and left at 37°C with 5% CO₂ for 24 hours. The media was then removed via aspiration and replaced with DMEM + 10% FBS and 1% penicillin/streptomycin (in the same volume as detailed in Table 2.6). 5 mM sodium butyrate was then applied to increase protein expression. The flasks/plates were to incubator and left at 37°C with 5% CO₂ overnight; the cells were harvested 48 hrs after transfection.

2.2.4 Development of stably transfected HEK 293S GnTI⁻ cell lines for Kv1.1 expression

Stably transfected HEK 293S cell lineages were established to reduce the need to generate the large volumes of plasmid required for PEI-based transfection, requiring large investments in time and resources, or expensive FuGENE-based methods. Stably transfected cell lineages were also better suited to larger scale cell cultures, as scales beyond T75 flasks would require generating volumes of plasmid DNA difficult to realistically achieve.

HEK 293S GnTI⁻ cells were selected as host for stable transfection, as their adaptability to larger-scale suspension culture would allow scaling of expression cultures to larger volumes in the event that smaller-scale expression and purification trials proved encouraging.

Stably transfected cells were generated through transfection of cells in a T25 using the FuGENE HD reagent method detailed above (see section 2.2.3). Once cells had developed to ~80% confluence, the medium was removed through aspiration and the cells washed twice with 5 ml DPBS. Cells were then treated with 200 μ l of 0.05% Trypsin-EDTA (Gibco) and incubated at 37°C for approximately 10 min. After this, cells were then dislodged with 5 ml DMEM:F12 media and pelleted gently through centrifugation at 200 \times g for ~10 min. The supernatant was then removed through decanting and the cells resuspended in 5 ml of fresh DMEM:F12 medium. Plates were placed into a 37°C incubator with a 5% ambient atmospheric CO₂ concentration for culturing.

2.2.5 Fluorescence microscopy

Observation of fluorescence linked to EYFP tags attached to Kv1.1 constructs was used to quickly assess expression of transfected cells. Fluorescence was observed using a Nikon Eclipse TE2000-U inverted microscope in conjuncture with a Nikon C-SHG1 Super High-Pressure Mercury Lamp Power Supply. The lamp output light was filtered with an excitation filter, allowing only light around the wavelength of 475 nm (± 5 nm), which corresponds to a major excitation wavelength of EGFP and a minor excitation wavelength of EYFP, to pass through. Emission wavelengths were observed through a green light filter. Photographs of the microscope viewing field were taken using a Si-3000 digital camera (CETI).

2.3 Protein purification

2.3.1 HEK cell lysis

2.3.1.1 Tissue grinding cell homogenisation

Cells were resuspended in 1 ml of lysis buffer (50 mM Tris pH 7.6, 300 mM NaCl and Roche cOmplete EDTA-free protease inhibitor cocktail tablet [1 tablet dissolved per 50 ml of buffer]) and transferred into a 35 ml Potter-Elvehjem tissue grinder mortar. Cells were disrupted on ice with 25 gentle motions of the tissue grinder pestle. Lysate was then recovered via aspiration.

2.3.1.2 Sonication

HEK293 cells were then resuspended in 500 μ l lysis buffer (50 mM Tris pH 7.5, 300 mM NaCl and Roche cOmplete protease inhibitor cocktail tablet) and transferred to a microcentrifuge tube and placed on ice. Sonication was

conducted using a Vibra-Cell VCX 130 processor (Sonics & Materials). The sonicator probe was inserted into the tube, with attention paid to ensure that the tip of the probe had been lowered beneath the lysis buffer surface and out of contact with the walls of the tube. The probe was steadied by a stand-and-clamp to ensure that it remained stationary after set-up. Sonication of HEK cells was carried out at amplitude 40. Sonication was applied as a series 4 × 5 sec bursts, separated by 3 × 25 sec cool-down periods on ice.

2.3.1.3 Direct dissolve in detergent

Pelleted HEK293 cells were dissolved directly in lysis buffer (50 mM Tris pH 7.5, 300 mM NaCl and Roche cOmplete protease inhibitor cocktail tablet) supplemented with 1% (w/v) DDM. The cell/lysis buffer mixture was placed on a rolling platform for gentle agitation for 2 hrs in a refrigerated cold room 4 °C.

2.3.2 Membrane protein extraction

2.3.2.1 Solubilisation in detergent

Following cell lysis, raw lysate fractions were separated via centrifugation for 60 min at 17,000 × g. The soluble fraction supernatant was separated from the pelleted insoluble fraction through aspiration. The insoluble fraction was then resuspended in lysis buffer (see section 4.6.1) with 0.1% detergent based on standard lab protocols used by the Muench Group and allowed to dissolve for 2 hrs on a rolling platform at 4°C. Initially, detergent solubilisation by SDS and DDM were compared to identify which of the two would provide the greatest yields for early protein purification trials. The detergent-solubilised

lysate was then centrifuged again to remove any remaining insoluble debris and the supernatant was collected for purification trials.

2.3.2.2 Solubilisation in amphipathic maleic acid polymers

Solubilisation of membrane proteins in SMA and DIBMA was undertaken through whole-cell dissolving of HEK cells. 2.5% (w/v) SMA or DIBMA polymer were dissolved in 300 mM NaCl, 10 mM KCl, 50 mM Tris and Roche cOmplete EDTA-free protease inhibitor cocktail tablet at pH 7.4; this solution was then applied to pelleted cells in a 1:1 ratio of cell weight to buffer volume. The cells were dissolved for 1 hr at room temperature on a rotating platform or overnight at 4°C (the timescale was extended for lower temperature solubilisation as the lipids of the membrane are less fluid at lower temperatures). Following solubilisation, the mixture was gently homogenised on using a Potter-Elvehjem tissue grinder mortar to break up any large fragments remaining in solution.

2.3.3 Immobilised metal affinity chromatography

2.3.3.1 Batch purification

Initial trials were conducted using cobalt-charged TALON metal affinity resin (GE healthcare). These early trials were conducted using the batch purification method, which allowed purification trials to be conducted faster than using the column method. Later purification trials utilised HisPur cobalt resin (Thermo Fisher Scientific), as it was found to be as effective as TALON resin while being significantly less expensive.

Batch purifications were set up by gently resuspending the metal affinity resin (HisPur or TALON) through gentle agitation on rolling platform. 50 μ l of resin was then transferred into a 1.5 ml microcentrifuge tube and washed with 900 μ l triple-distilled water and the tube centrifuged at 800 \times g for 2 min in benchtop microfuge. The supernatant was carefully removed via aspiration and the pelleted resin was washed two additional times with 1 ml of triple-distilled water to remove any remaining storage buffer.

Following washing, the resin was mixed with detergent dissolved insoluble cell lysate (25 μ l of pre-incubation detergent-solubilised lysate was retained for SDS-PAGE analysis). The resin and cell lysate were then mixed with 150 μ l equilibration buffer (\times 1 Tris-buffered saline [TBS], 3 mM imidazole, 0.1% DDM) and was then incubated on a rolling platform at 4°C for 1 hr. The mixture was subsequently pelleted in a benchtop microfuge at 800 rpm for 2 min and the supernatant removed through aspiration, with 25 μ l of the supernatant retained for SDS-PAGE analysis. The resin was then washed twice with 500 μ l equilibration buffer, followed by two further washes in 500 μ l wash buffer (\times 1 TBS, 30 mM imidazole, 0.05% DDM); the supernatant from the first wash buffer rinse was retained for SDS-PAGE analysis. Finally, 120 μ l of elution buffer (\times 1 TBS, 300 mM imidazole, 0.05% DDM) was applied to the resin and allowed to incubate on rolling platform at 4°C for 5 min. The resin was then pelleted through a final centrifugation at 800 \times g and the supernatant recovered via aspiration. Both the elution fraction and pelleted resin were retained for SDS-PAGE.

2.3.3.2 Gravity column

IMAC purification via gravity column was conducted using HisPur cobalt resin. Columns were prepared by transferring 2 × desired column volume of 1:1 HisPur resin slurry into a 5 ml or 15 ml disposable plastic column, depending on the volume of resin used, with a porous filter to allow passage of fluids while holding the resin in place. IMAC purifications were performed at 4°C in a temperature-controlled environment, with all buffers chilled to 4°C in advance. The resin was allowed to settle before the 20% ethanol holding buffer was drained away under gravity.

The resin was then primed with 2 × column volumes of Equilibration Buffer (150 mM NaCl, 10 mM KCl, 50 mM Tris, 10 mM imidazole pH 7.6 + Roche cOmplete EDTA-free protease inhibitor, 0.1% DDM), which was allowed to drain immediately off of the column. The lysis solution containing the protein was then applied to the column and allowed to incubate for 10-15 min. The lysis mix was then drained away via gravity and collected for visualisation via SDS-PAGE later. The column was then washed with 2 further column volumes of Equilibration Buffer, which were allowed to drain away immediately under gravity.

The column was then washed with 12 × column volumes of Wash Buffer (150 mM NaCl, 10 mM KCl, 50 mM Tris, 30 mM imidazole pH 7.6 + Roche cOmplete EDTA-free protease inhibitor, 0.1% DDM). The higher imidazole content of the wash buffer was used to wash away weakly interacting contaminants which would associate with the resin. The Wash Buffer was allowed to incubate for 15 minutes before being eluted and retained for SDS-

PAGE. This was followed by a 12 × column volume wash with Elution Buffer 1 (150 mM NaCl, 10 mM KCl, 50 mM Tris, 100 mM imidazole pH 7.6 + Roche cOmplete EDTA-free protease inhibitor, 0.05% DDM) and allowed to incubate for 15 minutes, before being eluted and stored for SDS-PAGE. Finally, 12 × column volumes of Elution Buffer 2 (150 mM NaCl, 10 mM KCl, 50 mM Tris, 250 mM imidazole pH 7.6 + Roche cOmplete EDTA-free protease inhibitor, 0.05% DDM) was applied to the resin and allowed to incubate for 15 minutes before elution and storage for SDS-PAGE.

It should be noted that for purification of DDM-solubilised protein, the Equilibration, Wash, Elution 1 and Elution 2 buffers were supplemented with 0.1% (w/v), 0.05% (w/v), 0.02% (w/v) and 0.02% (w/v) DDM respectively in order to gradually reduce detergent concentration to values close as possible to the CMC of DDM in solution with NaCl (~0.012% [w/v]) to reduce interference by the detergent during later steps (Generon Ltd n.d.).

2.3.3.3 HisTRAP column

IMAC purification on a 1 ml HisTRAP HP column (GE Healthcare) charged with cobalt ions was conducted on an Äkta Explorer pump system (GE Healthcare). Purification was conducted in a temperature controlled cabinet maintained at a constant temperature of 4°C. Prior to sample injection, the system was washed with 10 column volumes of IMAC Buffer A (150 mM NaCl, 10 mM Tris pH 7.6, 10 mM KCl, 0.02% DDM). Once injected, the column was washed with 5 ml of IMAC Buffer A. After the initial 5ml wash with IMAC Buffer A, IMAC Buffer B (150 mM NaCl, 10 mM Tris pH 7.6, 10 mM KCl, 300 mM imidazole, 0.02% DDM) was gradually exchanged into the mash mixture at a

rate of 5% per ml. Elution fractions from the Äkta were then collected in batches of 150 µl.

2.3.4 Size-exclusion chromatography purification

Size-exclusion chromatography (SEC) was employed as a secondary purification step following IMAC. Purification was conducted in a temperature-controlled cabinet maintained at a constant temperature of 4°C SEC purification was conducted using an Äkta Explorer pump system, with sample applied to Superdex 200 column (GE Healthcare). Samples were injected into the system through 50 µl or 100 µl sample loop, with the loop size chosen appropriate for the bed volume of resin used.

2.3.5 TEV cleavage

TEV cleavage was conducted using the ProTEV enzyme kit (ProMega). Reactions were conducted by following the protocol specified by the manufacturer: 20 µl of K_v1.1-TY10 at an estimated concentration of 0.5 mg/ml was mixed with 5 µl of ×20 ProTEV buffer supplied by the manufacturer, 1 µl of 100 mM DDT and 10 units of ProTEV Plus enzyme. The reaction mixture was diluted with sterilised ddH₂O to a volume of 100 µl and split into five 20 µl aliquots. Four of the reaction mixture aliquots were placed into incubation at 30 °C for 1, 2, 4 & 6 hours to compare the effectiveness of digestion.

2.4 Protein quality validation

2.4.1 SDS-PAGE

SDS-PAGE was carried out in order to isolate and identify protein species within samples of cell lysate and purification fractions. Samples were prepared through mixing with appropriate volumes of NuPAGE® LDS sample buffer (×4) and sample reducing buffer (×10) (Life Technologies). Samples were then incubated at 70°C for 10 min on a heating block. Once incubated, samples were loaded onto a pre-cast Novex® 4-10% Bis-TRIS gel, suspended in 400 ml NuPAGE® MOPS SDS running buffer. Gels were then run at 165 V for 35-40 min and were recovered from gel moulds and stained through 15 min incubation in QuickBlue gel stain on a rocking platform. Following staining, gels were incubated overnight in triple-distilled water to allow excess stain to diffuse away, improving contrast between stained proteins and the clear background.

2.4.2 Protein concentration

The concentration of recovered proteins was predominantly determined through UV absorbance recorded using a DS-11+ spectrophotometer (Denovix). Concentrations were recorded using the 'A280' application on the device, with 1 µl buffer used as a blank to provide a base of the readings. 1 µl of sample was then applied and the protein concentration and absorption at 280 nm and 260 nm, with the concentration calculated based on the extinction coefficient of $K_{v1.1-TY10}$ of $74000 \text{ M}^{-1}\text{cm}^{-1}$ predicted by the online analysis tool ProtParam (Gasteiger et al. 2005). Each recording was taken in triplicate.

2.4.3 Western blotting

SDS-PAGE gels for western blotting were generated using the methods detailed in section 2.4.1, however unstained gels were used for each blot. Gels were prepared for western blotting by trimming away the wells and exit channel of each gel, followed by soaking for ~5 min in Towbin buffer (25 mM Tris, 192 mM glycine, 20% [v/v] methanol, pH 8.3). In parallel to this, six 6 cm × 8 cm pieces of blotting paper and one 6 cm × 8 cm nitrocellulose membrane were also soaked in Towbin buffer for ~10 min. Stacks of three buffer-soaked pieces of blotting paper were then built, with the soaked nitrocellulose placed on top of the stack. The Towbin buffer-soaked gel was placed on top of the membrane and the remaining three pieces of soaked blotting paper were placed over the membrane to form completed stacks. A roller was used to gently remove any air bubbles trapped between the different sheets of stacks.

Blotting stacks were placed into a Bio-Rad Trans-Blot Turbo Transfer System transfer cassette. The cassette was loaded into the Transfer System hub unit and the blot transfer conducted with a 1 amp, 25-volt maximum program run for 30 min. Once the transfer program was concluded, the cassette was removed and the nitrocellulose membrane was retrieved from the stack. Gels were also recovered at this point and stained as described in section 2.4.1 to check the effectiveness of each transfer.

Nitrocellulose membranes were then placed into a 150 ml sterile metal cap tube and washed for 1 hr on a rolling platform with a 30 ml tris buffered saline-tween 20 (TBST) solution + 10% (v/v) blocking agent from a BM Chemiluminescence Western Blotting Kit (Roche; Sigma-Aldrich). The

blocking solution was then discarded by decanting and a 10 ml TBST solution featuring diluted primary antibody and 1% (v/v) blocking agent was applied to the membrane. The membrane was allowed to incubate on a rolling platform overnight at 4°C.

Following incubation, the primary antibody solution was discarded by decanting and the membrane washed thrice with 20 ml TBST. Washing was carried out for 15 min on a rolling platform at room temperature. Secondary anti-mouse/rabbit antibody (Roche; Sigma-Aldrich) diluted 10000-fold into TBST + 1% (v/v) blocking agent was then applied to the membrane and incubated for 1-2 hrs on a rolling platform at room temperature. Remaining secondary antibody was then removed via decanting and the membrane washed thrice once again with 20 ml TBST following the same approach as the previous wash.

The binding of the primary and secondary antibodies was then visualised through chemiluminescence using the application of 5 ml of solution A and 50 µl of solution B supplied with the BM chemiluminescence western blotting kit. Fluorescence on the nitrocellulose membrane was recorded in a G:Box imaging cabinet, with photos recorded using the *Intelli-Chemi* function included in GeneSnap software (SynGene).

2.4.4 SEC-MALS

Size-exclusion chromatography/multi-angle static light scattering (SEC-MALS) was conducted under the supervision of Dr Maren Thompsen. Multi-angle static light scattering (MALS) was conducted using a DAWN 8+ light scattering detector (Wyatt Technology) and Optilab T-rEV refractive index

detector (Wyatt Technology). These instruments record light scattering (LS)/quasi-elastic light scattering (QELS) and refractive index (RI), respectively. Fresh buffer without protein was used as a reference for the RI in the absence of protein, allowing the difference of refractive index (dRI) to be calculated.

SEC-MALS was performed in conjunction with fluorescence size exclusion chromatography (F-SEC) on a Superdex 200 5/150 column (GE Healthcare) using a SIL-20AC injector and LC-20AD pump. Buffers for SEC were degassed before application to the column.

UV/visible light absorption of SEC elution fractions was recorded using an SPD-M20A photodiode array detector (Shimadzu), with EYFP fluorescence recorded using an RF-20A fluorescence detector (Shimadzu). Elution fractions from SEC were collected using an FRC-10A fraction collector (Shimadzu). Data output from the process was visualised and manipulated using the ASTRA programme suite (Wyatt Technology). All assays were conducted at room temperature.

2.4.5 Circular dichroism spectroscopy

2.4.5.1 Measurement of protein secondary structure

Circular dichroism (CD) spectroscopy is a method of non-destructively probing the folded state of molecules by measuring the absorbance of different wavelengths of light in the visible and infrared electromagnetic waves. Alpha-helices and beta-sheets have distinctive absorbance profiles; thus, CD

spectroscopy can be employed to determine the folding and secondary structure constitution of proteins.

CD measurements were performed on a Chirascan Plus spectropolarimeter (Applied Photophysics). Additionally, a rotating 6 cell changer carousel and Peltier temperature control unit were included in the setup, allowing multiple samples to be investigated in parallel and the temperature of cells controlled, respectively. 1 mm glass cuvettes were loaded with 200 μ l of sample at concentrations of 0.2 mg/ml. The spectropolarimeter was programmed to measure absorbance at wavelengths 180-260 nm at intervals of 1 nm. Measurement of absorbance from 200 μ l of buffer without protein was conducted in parallel to allow subtraction of background signal.

Data were analysed using the online tool Dichroweb (Lobley et al. 2002, Whitmore, Lee and Wallace 2004, 2008).

2.4.5.2 Measurement of protein denaturation through temperature ramp

Temperature ramps can be employed in parallel with real time CD spectrographic analysis to give insights into the stability of proteins by observing the temperature at which absorbance at various wavelengths change.

Temperature ramping of Kv1.1 samples was conducted using the same protocol as measurement at static temperatures. However, the temperature of the sample cuvette was increased by 1 $^{\circ}$ C over the course of two minutes between each reading, beginning at 25 $^{\circ}$ C and concluding at 99 $^{\circ}$ C. The CD ChiraScan software was programmed to record only once the temperature of

the vessel had been stable at the target temperature for at least 30 seconds. Measurements of absorbance between 180 and 260 nm at each temperature mark.

2.4.6 Mass spectrometry

Mass spectrometry was conducted by Dr. James Ault in the University of Leeds Faculty of Biological Sciences Mass Spectrometry Facility. The gel was run using pre-cast NuPAGE Novex 4-12% Bis-Tris at 165 V for 30 min; 10 µl of each sample was loaded into each lane (including laurel DS and reducing buffer). The gel was stained with Instant Blue stain for 15 min in a sterile plastic container to reduce keratin contamination. SDS-PAGE gels (conducted using method discussed in section 2.4.1) with the desired protein were provided to Dr Ault and gel lanes were excised by Dr. Rachel George of the Mass Spectrometry Facility. Gels supplied to the facility for analysis were stained using InstantBlue comassie stain (Expedeon), in accordance with the request of facility operators to avoid interference in signals.

Protein identification (Protein ID) via mass spectrometry was carried out through the in-house Synapt HDMS system (Waters). Output data from protein ID was analysed using an online-enabled UltiMate 3000 HPLC system (Dionex) in combination with ProteinLynx Global Server software.

2.5 Structural analysis

2.5.1 Negative stain electron microscopy

2.5.1.1 Grid preparation

Negative stain grids were produced using 10 nm carbon-coated copper grids (Agar Scientific). A surface charge was applied to grids through glow discharge using a PELCO easiGlow™ Glow Discharge Cleaning System; grids were placed into the glow discharge chamber carbon-side-up on a parafilm-coated glass slide, with the discharge typically lasting 30 seconds. Glow discharge was used to ensure that the grid surface was made hydrophilic, attracting water-based solutions to the grid and that protein molecules are attracted to the surface of the grid.

Protein solutions were applied to grids in 3 µl droplets onto the carbon coated side of the grid. Protein solutions were left on the surface of the grid for 1 min, then removed by blotting. This was followed by the application of 3 µl of 1% uranyl acetate onto the grid, which was allowed to settle for 1 min, before being removed by blotting; this was followed by a further 1 min application of 1% uranyl acetate, which was removed by blotting. The grid was then air dried under a lamp. Minor variations in stain depth was achieved by varying staining times. Uranyl acetate was produced and supplied by Astbury Biostructure Laboratory (ABSL) support staff.

2.5.1.2 Data collection

Data was typically collected on the in-house T12 electron microscope (FEI; now ThermoFisher Scientific), operating at 120 kV using a LaB6 filament.

Images were recorded using a Gatan CCD camera; originally a 2k × 2k camera, which was later replaced by a Gatan 4k × 4K CCD camera. Images were recorded at a typical magnification of 30,000×. Lower screen magnifications were used in initial screening to search for aggregation and to search for areas with staining depths which provided optimal contrast for particle identification.

2.5.1.3 Data processing

Data from negative stain electron microscopy were analysed using the EMAN2 micrograph processing software (Tang, G. et al. 2007). Manual picking of particles was handled using the e2spt_boxer.py tool, followed by the generation of 2D classes by the e2classaverage3d.py tool. EMAN2 aligns data using correlation co-efficiencies by which each particle is compared to a reference. These references can be determined either by the user by manually picking “representative” data or automatically by EMAN2.

2.5.2 Cryo-electron microscopy

2.5.2.1 Grid preparation

Cryo-EM grids were prepared using a Vitrobot automated vitrification module (FEI). The environment of the sample application chamber was programmed to set conditions at 100% humidity at a temperature of 4°C. Grids were charged prior to sample application through glow discharge using an easiGlow discharge cleaning system (PELCO), with discharge times typically lasting 45 sec. Charged grids were then held in tweezers and placed in a specialised holding position in the sample chamber of the Vitrobot. Grids were blotted with

Whatman qualitative filter paper. The programmed blot force was 6 and starting blot time of 6 seconds, followed by flash cooling in liquid ethane. Prepared grids were then taken forward to screening on an F20 electron microscope (FEI) at a tension setting of 120 kV with micrographs recoded using a CMOS detector.

Proteins samples for cryo-EM were applied to a series of grid types during the process of optimisation and screening (see Table 2.7). Multiple diverse types of grids were used as variations in surface compositions, hole sizes and hole spacing can greatly influence the behaviour of buffers and proteins during application, freezing and visualisation. The use of a wide variety of grid types thereby allowed single samples to be tested and screened in a multitude of environments.

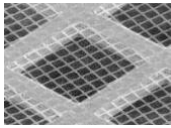
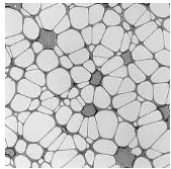
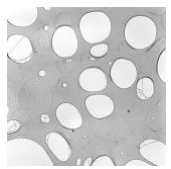
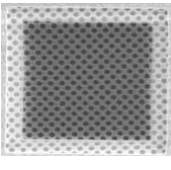
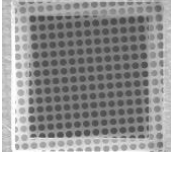
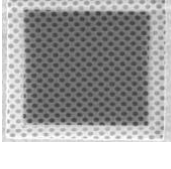
Grid type	Hole dimensions	Hole spacing	Image
Carbon	10 nm × 10 nm square	2 nm	
Lacey carbon	Variable	Variable	
Holey carbon	Variable	Variable	
Quantifoil R 1.2/1.3	1.2 μm diameter circle	1.3 μm	
Quantifoil R 2/1	2.0 μm diameter circle	1.0 μm	
Quantifoil R 2/2	2.0 μm diameter circle	2.0 μm	

Table 2.7 – Table of grid types used in preparation of $K_v1.1$ samples for cryo-EM (Quantifoil Micro Tools GmbH. 2015a; Quantifoil Micro Tools GmbH. 2015b; Agar Scientific Ltd. 2018; Electron Microscopy Sciences 2018).

Frozen grids were then transferred into plastic holding pucks under liquid nitrogen and then stored before screening in storage dewars containing liquid nitrogen before screening.

Similar to uranyl acetate staining in negative stain microscopy, it is generally preferable to keep ice as thin as necessary to stably sustain protein particles suspended in the grid holes. Producing ice with the optimal thickness often requires modifying the parameters of grid freezing machinery. To ensure good ice quality with low contrast, it is best to use buffers with low concentrations of buffering agents and additives.

2.5.2.2 Data collection

Prior to the construction and activation of the in-house Astbury Biostructure Laboratory (ABSL), cryo-EM grids were shipped to the Electron Microscope facility at the MRC Laboratory of Molecular Biology, University of Cambridge, where samples were screened and sets of micrographs taken using a Krios electron microscopes (FEI) with a K2 direct electron detector (Gatan). Once the in-house ABSL facility was brought online in June 2017, grid screening and data acquisition were moved to the on-site Krios 1 electron microscope.

2.5.2.3 Data processing

Processing of cryo-EM data was handled using the Regularised Likelihood Optimisation program (Relion) (Scheres, S. H. W. 2012). Data processing was carried out on dedicated Astbury Biostructure Laboratory workstation servers. .ser files were converted to .mrc format using a custom program

developed in-house by Dr Matt Iadanza, allowing the data to be imported into Relion for processing.

Data processing commenced with motion correction of the images using CTF (contrast transfer function) estimation. Particles in micrographs were then selected through manual picking of a selection of images.

2.6 K_v1.1 coincubation with alpha-dendrotoxin

0.4 mg/ml K_v1.1-TY10 purified via IMAC on cobalt resin was coincubated with 10 mM alpha dendrotoxin (α -DTX) in 150 mM NaCl, 50 mM Tris, 10 mM KCl pH 7.6 buffer for 30 min on ice. The mixture was then placed into a 10-250 μ l mini GeBAflex-tube for dialysis (Gene Bio-Application) and placed into a beaker with 200 ml fresh buffer and allowed to dialyse for 10 min at 4 °C. Following dialysis, the tube was transferred to second beaker for a further 10 minutes with 200 ml of fresh buffer to ensure complete removal of remaining toxin.

3 Expression of K_v constructs in HEK cell culture

3.1 Background

Voltage-gated potassium channels are predominantly expressed in electromechanically sensitive cell types, such as neurons and smooth muscle cells (Jackson 2005, Vacher et al. 2008). While extraction of protein directly from samples of neuronal cells would likely provide protein under conditions most closely resembling its natural state, securing such materials for the study of the human variant of K_v family proteins would require human tissues, which would raise serious ethical concerns. The use of HEK 293 cell culture was chosen in order to avoid these ethical issues.

The ability to transfect HEK cells in culture allowed protein to be generated using human cells through well-developed expression protocols. This also allowed genes to be modified with tags and point mutations, which would not be possible if sourced from natural tissues. While greater flexibility of gene modification is available in bacterial expression systems, they are inadequate for expressing human membrane proteins, due to the significant differences in bacterial membrane compositions and expression machinery (Wagner, S. et al. 2006).

HEK cells are compatible with both adherent and suspension culture with both approaches to cell cultivation having advantages and drawbacks. Adherent cell culture is generally simpler to establish, as the flasks do not require constant agitation, making the possibility of mechanical damage to cells much more remote. However, adherent culture flasks are less efficient, as cells are not able to take full advantage of the total volume of the flask.

Suspension culture of cells allows for much more efficient use of space, as cells are spread throughout the full volume of the flask; this makes increasing the scale of cultures less problematic, however cells grown in suspension are sensitive to more environmental factors. If conditions are not correct, cells can be prone to clumping and falling out of suspension, leading cells at the centre of clusters to starve. Excessively high rotation speeds for agitation can also destroy cells due to the increased risk of shearing.

3.2 Cloning and constructs

3.2.1 Kv1.1 constructs

Multiple Kv1.1 constructs with C-terminal tags were designed to give flexibility in purifying the protein. The generation of the constructs discussed in sections 2.1.1.3 and 2.1.1.4 was carried out using the PCR method detailed in section 2.1.2. The annealing temperatures for PCR was based on the predicted melting temperatures of the forward and reverse primers used. The native KCNA1 and KCNA1-EYFP constructs in pcDNA6 were used as the basis for the initial set of modified constructs.

3.2.1.1 Kv1.1-EYFP-His₆

The Kv1.1-EYFP-His₆ was produced from the KCNA1-EYFP construct using the primers detailed in section 2.1.1.3 to eliminate the stop codon at the terminus of the EYFP gene, allowing the gene to read through into the hexahistidine motif encoded at the pcDNA6 polyclonal site.

Following PCR, two bands were observed in an agarose gel of the post-reaction mixture. The longer of the two bands was the best match for the expected length of the product (Figure 3.1). The longer band was cut out of the gel under UV light and the DNA recovered using the Qiagen QIAEX II gel extraction kit. The linear PCR product was then treated with DpnI in order to digest any remaining methylated parent plasmid DNA and the purified PCR product was ligated using T4 polynucleotide kinase and T4 ligase. A second reaction with the ligase omitted was set up to produce a negative control. Both the ligation and negative control were carried forward into a heat shock

transformation for XL1-Blue supercompetent cells and plated on 100 µg/ml ampicillin inoculated LB agar plate; these were cultured overnight at 37°C.

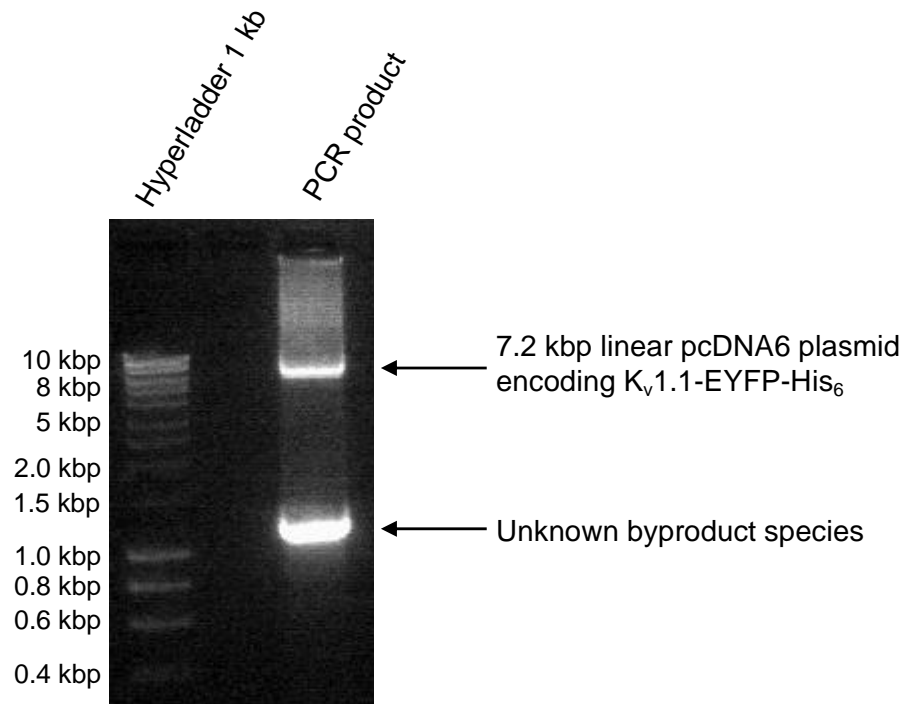


Figure 3.1 – Agarose gel of PCR product from KCNA1-EYFP mutagenesis. A band which approximately corresponds to the expected 7.2 kbp length of the PCR product can be observed in the PCR product lane. The band was purified through excision from the agarose gel, followed by gel extraction. Subsequent sequencing of the extracted band confirmed its identity to be the desired modified plasmid.

~100 transformants were observed the following day on the ligated reaction plate; a smaller number of colonies were observed on the negative control plate, though as only 9 were observed, it was determined that the majority of

the colonies on the ligation plate constituted genuine transformants. The decision was made to culture 6 colonies (A-F) from the ligated reaction plate. Colonies B, C, E and F grew sufficiently for DNA to be recovered via Qiagen miniprep. Colony PCR was then used to check for the presence of the Kv1.1 plasmid (Figure 3.2). The results of PCR mutagenesis were confirmed via Sanger sequencing.

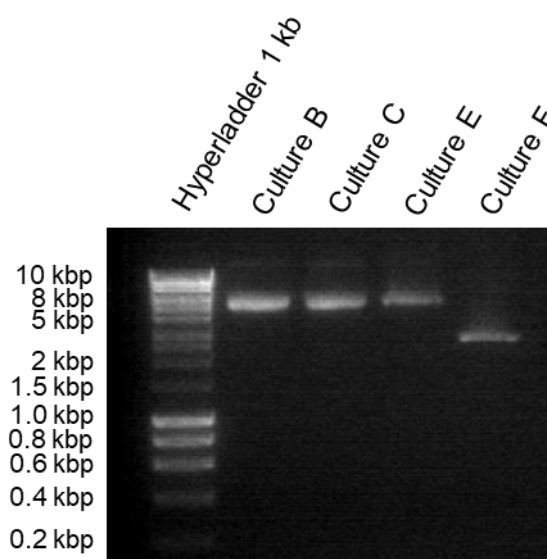


Figure 3.2 – Agarose gel of miniprep products. DNA from colonies B, C and E appeared to be the correct length, approximately matching the expected 7.2 kbp size of the plasmid. The DNA from culture F, appeared to be shorter in length, possibly as a result of incorrect priming of the template.

3.2.1.2 Kv1.1-TEV-EYFP-His₆

Following the production of a pcDNA6 plasmid encoding Kv1.1-EYFP-His₆, a further construct was devised which incorporated a TEV cleavage site into the

region between Kv1.1 and the C-terminal tags. Such a plasmid would encode a Kv1.1-TEV-EYFP-His₆ construct, which could be digested with TEV protease in order to remove the tags. Such a construct could be further purified via reverse-purification, as removal of tags following primary purification with antibody resin or IMAC-based methods could be repeated post-digestion. Removal of tags would likely be of benefit to structural analysis, also, with the elimination of domains at the end of flexible linkers resulting in more ordered samples (Eschenfeldt, W. H. et al. 2010).

Plans to modify the Kv1.1-EYFP-His₆ construct to include a TEV cut site between the Kv1.1 and EYFP genes and generate a Kv1.1-TEV-EYFP-His₆ construct were not initially successful; ligated plasmid recovered following PCR all displayed deletions at the site of ligation. One PCR product had a 3-nucleotide deletion which resulted in the loss of the internal phenylalanine of the TEV site, while preserving the downstream genes in-frame. As this construct could in theory be expressed and retain functional EYFP and polyhistidine, it was kept for possible use in the event that an extended linker would be necessary. This plasmid was dubbed 'KCNA1-PartTEV-EYFP-His₆' and a new series of primers were designed to insert the missing phenylalanine and produce a functional TEV cleavage site.

The construct was completed by introducing the missing phenylalanine residue via PCR mutagenesis using the following primers, with melting temperatures of 58.6 °C:

```
>KCNA1-FullTEV-EYFP-His_Forward
cagagcgtgagcaagggcg
>KCNA1-FullTEV-EYFP-His_Reverse
gaagtacaggttctcgaattcaacatcgg
```

The standard PCR method discussed in section 2.1.2 was applied to the KCNA1-PartTEV-EYFP-His₆ plasmid using the new primers above. Sanger sequencing of the product band for this indicated that the missing phenylalanine was inserted, completing the desired plasmid (Figure 3.5).

3.2.1.3 Kv1.1-TEV-EYFP-His₁₀

A Kv1.1-TY10 construct was produced from the above hexa-histidine-tagged counterpart through the use of primers to add a series of 4 additional histidine-encoding codons (CAT/CAC) to the C-terminal of the hexahistidine motif, upstream of the stop codon.

3.2.2 Kv β 2 constructs

3.2.2.1 Native KCNAB2

KCNAB2 cDNA was cloned from human foetal brain cDNA through PCR amplification using the primers detailed in 2.1.1.4. The forward primer included a 5' EcoRI restriction site, while the reverse primer featured a 3' XbaI restriction site to allow restriction and ligation of the cDNA into the polyclonal site of pcDNA3.1. A Kozak consensus sequence was included directly upstream of the *KCNAB2* start codon in order to boost transcription. Restriction ligation of *KCNAB2* into the polyclonal site of pcDNA3.1 was confirmed via sequencing.

The PCR product band was excised from the gel and recovered using a QIAEX II gel extraction kit (QIAGEN) and blunt ligated into the pJET1.2 cloning vector, as per the method detailed in section 2.1.1.4. Transformation into XL-1 blue bacteria and overnight culture on 100 µg/ml ampicillin plates resulted in ~200 colonies. 6 colonies were selected and grown in suspension in Liquid LB, with 100 µg/ml ampicillin. One colony failed to grow in suspension, while the remaining five grew sufficiently for plasmid DNA recovery via miniprep (Figure 3.3).

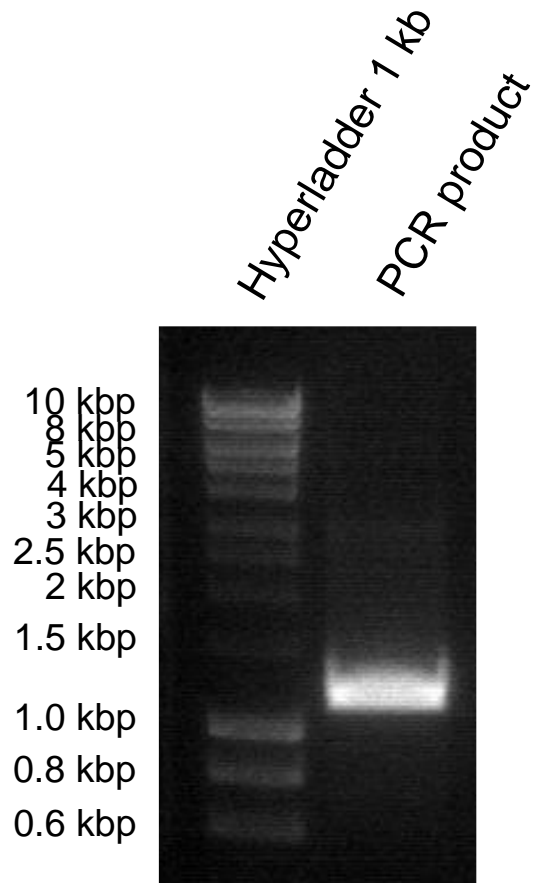


Figure 3.3 – Agarose gel of PCR product from primers designed to extract the human *kcnab2* gene from foetal human brain cDNA. The length of the expected product, based on the length of the target gene, is 1.1 kbp, which correlates with the weight of the product band observed in the PCR lane.

3.2.2.2 KCNAB2-cMyc-His₆

The pcDNA3.1 plasmid encoding native *KCNAB2* discussed in the previous section was used as the basis for the production of a tagged variant of the gene. The KCNAB2-cMyc-His₆ primers discussed in section 2.1.1.4 were used in conjunction with PCR, using the predicted melting temperatures as the basis for the annealing temperature of 61.4°C used in PCR programme (see section 2.1.2 for details), in order to clone a version of the plasmid with the native stop codon deleted, allowing the gene to read through into the cMyc and His₆ tags encoded at the 5' end of the pcDNA3.1 plasmid polyclonal site.

The PCR mixture programme discussed above was subjected to DpnI digest following the reaction. Agarose gel electrophoresis of the digested reaction mix revealed a band, which was subjected to blunt end ligation with TA ligase (New England BioScience).

3.3 Transient transfection of HEK cells

Initial expression trials of C-terminal tagged Kv1.1 constructs were aimed toward comparing the effectiveness of the FuGENE HD and PEI-based methods for mammal cell transfection (see section 2.2.3 for details). The Kv1.1-TEV-EYFP-His₆ construct was used in these trials, as the EYFP tag would allow quick visual identification of transfected cells through fluorescence microscopy.

To obtain sufficient DNA for each transfection, Kv1.1-TEV-EYFP-His₆ plasmid was recovered via maxiprep kits and repeated in triplicate. Amounts of recovered DNA were quantified using ultraviolet absorbance spectroscopy; on

each occasion, a total mass of ~1 mg of DNA was recovered, which was a sufficient quantity for PEI-mediated transient transfection of HEK cells adhered to the base of a T75 flasks.

Transfection using both FuGENE HD and PEI were tested in small-scale using HEK 293 TSA cells on 35 mm dishes, with a culture volume of 2 ml (Figure 3.4). Inspection of the plates 48 hours post-transfection on a fluorescence microscope at $\times 10$ magnification (see section 2.2.5 for details) revealed that ~30% of cells displayed signs of fluorescent protein expression without any signs of changes in morphology or retardation of growth.

While the appearance of fluorescence within the transfected cell population suggested the expression of the EYFP-tagged fusion proteins, it was not immediately clear at that stage, however, if the protein produced was correctly folded or localised to the plasma membrane, only that protein had been expressed.

Using PEI-based transfection methods necessitated continual establishment and culturing of XL1-Blue *E. coli* in order to clone plasmids for protein expression, followed by maxiprep of 5-20 g quantities of cell pellet, which proved to be more time consuming than the equivalent FuGENE-based method. As FuGENE is capable of transfection efficiencies comparable to PEI at μg quantities, requiring lower quantities of cell pellet to produce, as well as quicker miniprep methods from cell rupture and DNA collection, FuGENE-based methods were selected for all mammal cell transfection subsequent to comparison to reduce the required time investment to generate the quantities of DNA necessary for PEI-based transfection.

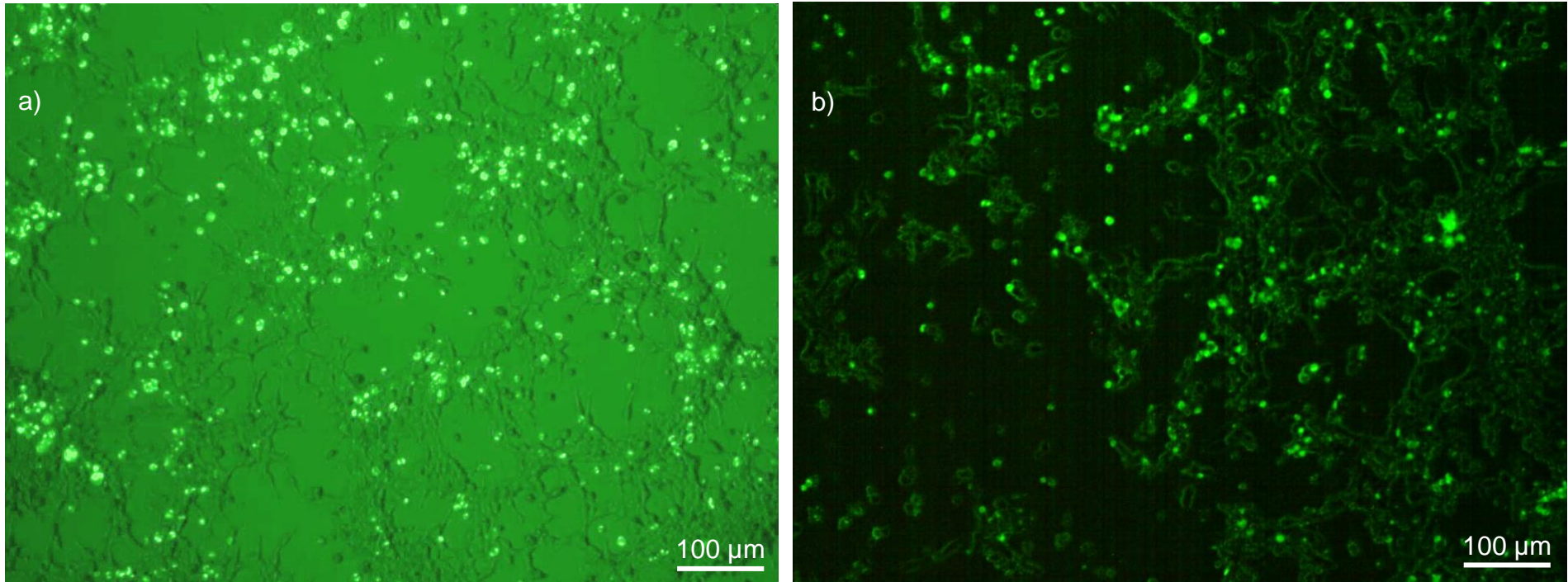


Figure 3.4 – A fluorescence microscope views of HEK293 TSA cells transiently transfected with a pcDNA6 plasmid encoding $K_v1.1$ -TEV-EYFP-His₆. In the instance of a) the cells have been transfected using the FuGENE HD reagent and in the instance of b) the cells have been transfected using PEI. The appearance of regions of green fluorescence across the cell populations in indicates that the cells had been transfected by the plasmid and had begun to express the EYFP-tagged protein in both cases.

3.4 Stable transfection

3.4.1 Hexahistidine tagged construct, Kv1.1-TEV-EYFP-His₆

Stably transfected HEK 293S GnTI⁻ cells expressing the Kv1.1-TEV-EYFP-His₆ construct were generated using the methods outlined in section 2.2.4. Cells were transfected using the FuGENE HD reagent method and seeded at 10% confluence into a T25 tissue culture flask and grown at 37°C in 5 ml of DMEM:F-12 medium. After 6 days, the media was removed via aspiration and replaced with 5 ml of fresh DMEM:F-12, with 100 ng/μl blasticidin added to apply selective pressure. Cells were cultured following the methods detailed in section 2.2.4.

Following a further 7 days incubation, cells were treated with trypsin and re-seeded at ~0.1% confluence onto a 10 cm² tissue culture dish and grown for 10 days at 37°C. Twelve individual colonies from the tissue culture dish were selected following incubation and transferred into 2 × 6-well plates. Each well was filled with 2 ml DMEM/F-12 media containing 100 ng/μl blasticidin. Cells were collected from the source plate through gentle scraping and aspiration using a 20 μl pipet tip; 2 μl drawn up into the pipette for each colony and then transferred into a plate well.

Following 14 days incubation, two fluorescent colonies were observed growing in well C2; both colonies displayed homogenous fluorescence throughout, potentially indicating them to be monoclonal.

3.4.2 Decahistodine tagged construct, Kv1.1-TEV-EYFP-His₁₀

Stably transfected HEK 293S GnTI⁻ cells expressing Kv1.1-TY10 were generated via the same method as discussed above in section 3.4.1, with cells transfected using the FuGENE HD reagent method and seeded at 10% confluence into a T25 tissue culture flask and grown at 37°C in 5 ml of DMEM:F-12 medium. After 6 days, the media was removed via aspiration and replaced with 5 ml of fresh DMEM:F-12, with 100 ng/μl blasticidin added to apply selective pressure.

Following a further 5 days incubation, cells were trypsinised and re-seeded onto a 10 cm² tissue culture dish at a confluence of ~0.1% and incubated for 10 days at 37°C with 5% atmospheric concentrations of CO₂. The dish was then placed under a light microscope and six colonies from the tissue culture dish were selected for transfer into separate wells into a tissue culture grade 6-well plate through gentle scraping and aspiration using a 20 μl pipet tip. Each well was filled with 2 ml DMEM/F-12 media containing 100 ng/μl blasticidin. The plate was placed into a 37°C incubator with a 5% ambient atmospheric CO₂ concentration for culturing.

Following 10 days incubation, four fluorescent colonies were observed growing in different wells, which were labelled colonies I-IV. Colonies I and IV displayed homogenous fluorescence, with fluorescence in colonies II and III being too dim to accurately assess their quality. Cells from colony IV were taken forward for expression of Kv1.1-TY10, with colony I cells stored as a back-up cell line.

3.4.3 K_v1.1-TEV-EYFP-His₁₀/KCNAB2 double transfection

Following the development of a stably transfected cell lines for expression of K_v1.1, a doubly transfected cell line expressing native K_vβ2 was conceived in order to express the octameric complex, which would allow the effects of the beta subunits on inhibitor binding to be included in structural studies, as well as its intrinsic regulatory effects to be assessed in characterisation trials. The K_v1.1-TY10 colony IV cell line was used as the basis for the development of this new cell lineage.

Colony IV cells were transfected via FuGENE HD with the pcDNA3.1 plasmid encoding native *KCNAB2* through the method discussed in section 2.2.4. Cells were seeded into a T25 cell culture flask at a density of 10% with 5 ml DMEM:F12 medium supplemented with 10% FBS and 1% penicillin-streptomycin.

Selective pressure applied with both 500 ng/μl G-418 (an equivalent of neomycin), as well as 100 ng/μl blasticidin. These antibiotics were selected in order to select for the pcDNA3.1 encoding the native *KCNAB2* gene, as well as pcDNA6 plasmid encoding K_v1.1-TY10, respectively. A starting concentration of 500 ng/μl was used based on antibiotic regimes used in similar stably transfected cell lineages expressing BK channel/β2 co-expression cell lines conducted by other members of the Lippiat Group.

The transfected cells failed to thrive and dislodged from the plate surface after 6 days of incubation, indicating that they had died. Transfections were repeated a further two occasions without modification of the protocol in order

to ensure that the cell death was not a result of errors in cell culture, however the cells died after 5 and 6 days in these instances, respectively.

A killing curve of single stable transfection Colony IV line cells was conducted with varying concentrations of G-418 to check if concentrations of the antibiotic were excessively high. The killing curve would allow the minimum concentration of antibiotic required for the killing of cells lacking resistance to be discerned. The killing curve was conducted in a 6-well plate seeded with 10% confluence of cells. The wells were filled to 2 ml with DMEM:F20 supplemented with 10% FBS, 1% penicillin/streptomycin and inoculated with 100 ng/μl each of blasticidin. Each separate well was inoculated with a different concentration of G-418, ranging 0, 100, 200, 300, 400 or 500 ng/μl. The growth of cells was monitored via light microscopy. Over the course of the following 7 days, cells growing in 0, 100 and 200 ng/μl concentrations of G-418 survived, while cells grown at high concentrations dislodged from the surface of the plates.

3.5 Comparison of suspension culture media

3.5.1 Influence of different media types on cell growth

Suspension cultures of stably transfected Colony VI line HEK 293S GnT1⁻ cells expressing Kv1.1-TY10 (see section 3.4.2 for details) were used in assessing the rates of HEK cell growth in suspension culture. Cell numbers in 180 ml starter cultures were monitored on a Countess cell counting machine until cell densities reached 2×10^6 cells per ml. Following this, 30 ml of cells were then taken from suspension and used to inoculate two further 150 ml cultures at 1 in 6 in 500 ml tissue culture grade conical flasks. The remaining 150 ml of both

cultures were induced through the addition of 5 mM sodium butyrate. Cells were harvested through centrifugation 48 hrs after introducing sodium butyrate, then washed twice with 25 mM DPBS. The final volume of cell paste was slightly under 5 ml.

To try and maximise the number of cells grown and resultant protein extracted different approaches were taken to check the effectiveness of other media in place of PEM as a means of increasing efficiency and reducing costs. 4 new cultures were set up from 20 ml of PEM culture grown to 2×10^6 cells per ml, then placed into 160 ml of new culture medium. FreeStyle, EX-CELL and DMEM/F-12 medium was compared against a PEM culture in parallel using Countess recordings of cell count and viability (Figures 3.5).

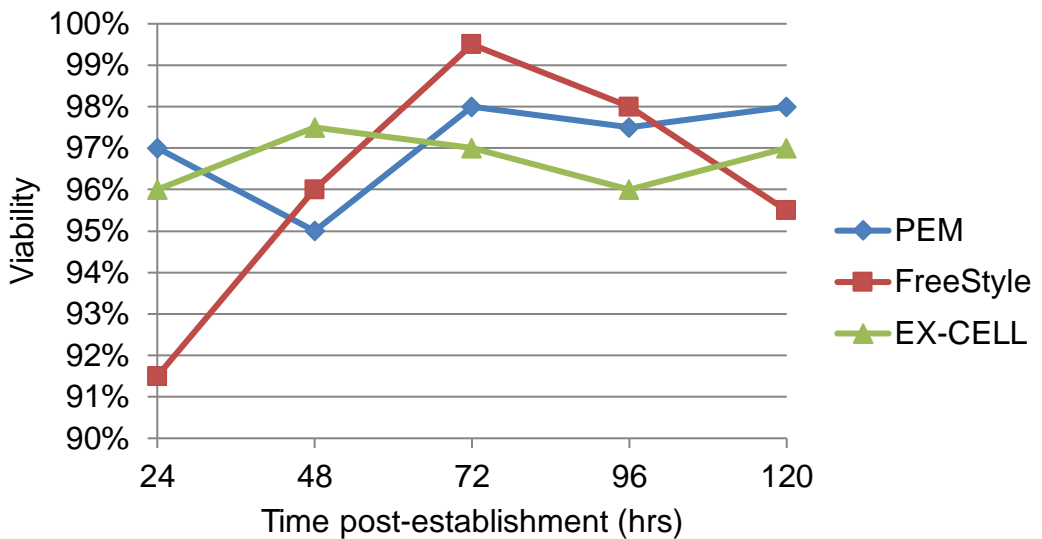
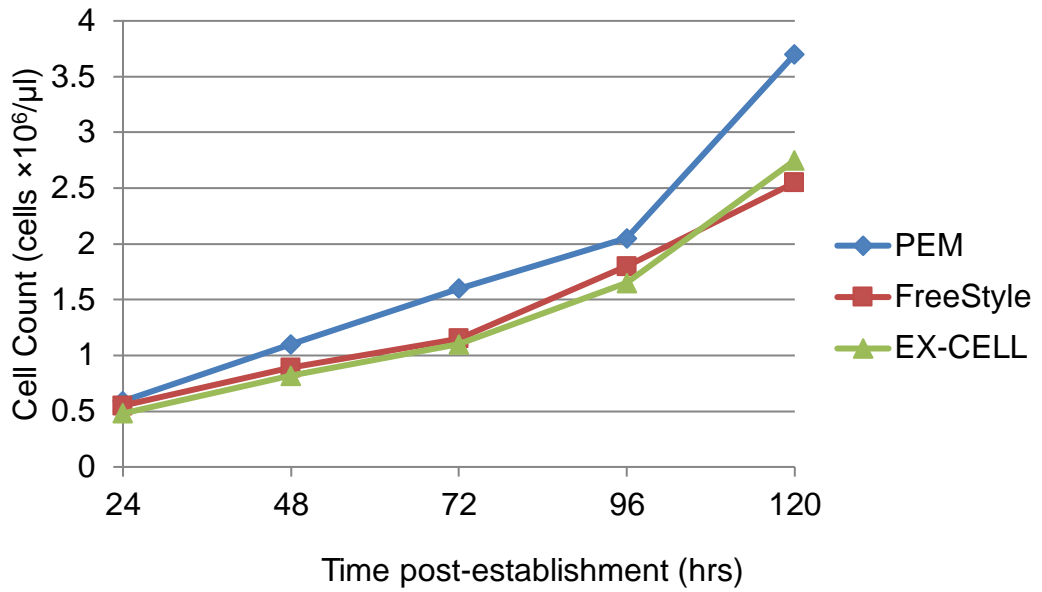


Figure 3.5 – Cell growth and viability over time in suspension culture across a series of medium types. Cell viability was calculated from the recorded number of living cells divided by the total cell count (living cell count / total number of living cells + total number of dead cells).

The results of the growth trials indicate that growth rates are highest in PEM, though FreeStyle and EX-CELL both allow for sustained growth at slightly slower rates. All three media have comparable viabilities and similar market prices; a comparison of HEK 293S GnTI^r cell growth and viability in each medium type was conducted in order to identify the most cost-effective option. DMEM/F-12 medium appears to be unsuitable for sustaining HEK 293S GnTI^r cells in suspension, however. This may be due to excessive calcium found in the medium. Further experiments with calcium-free DMEM will be required to confirm this hypothesis.

To assess the flexibility of the protocol used to grow human cells in suspension culture, the effectiveness of EX-CELL medium in establishment of suspension populations was compared directly with FreeStyle medium, which had been used in all previous trials (Figure 3.6).

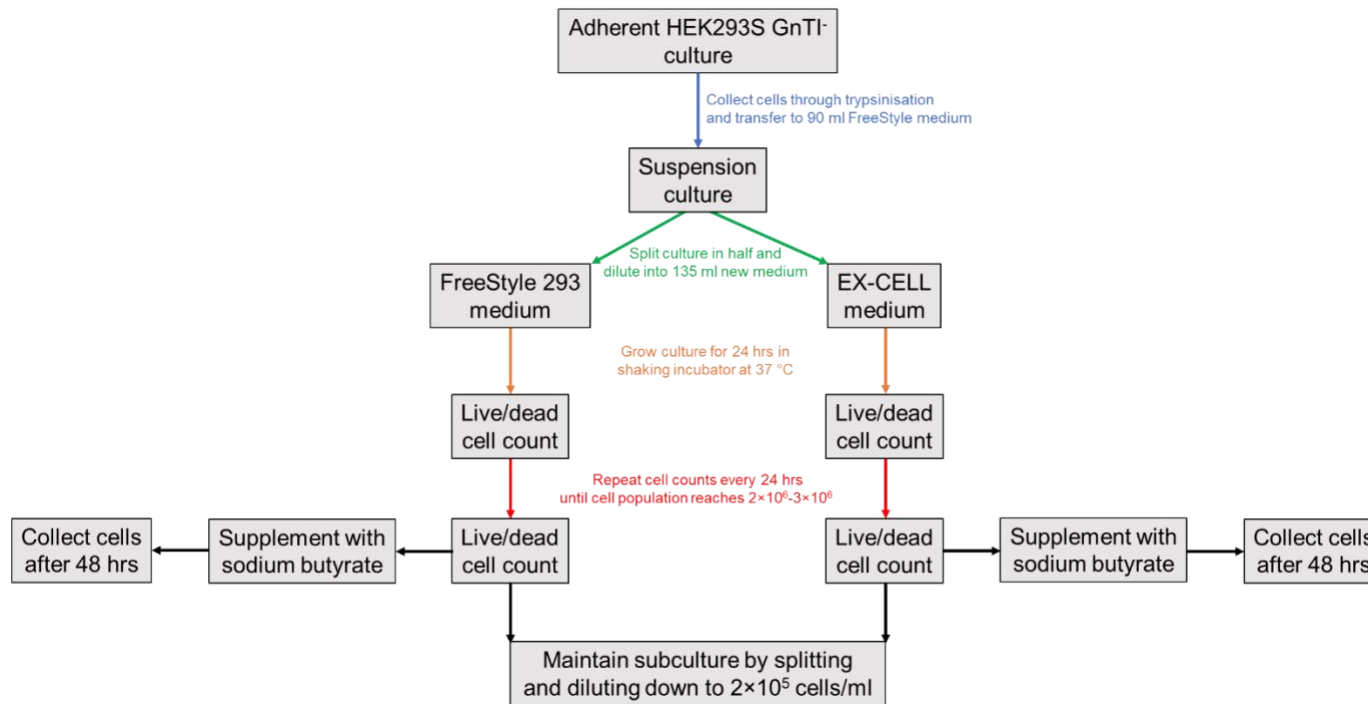


Figure 3.6 - Work-flow diagram describing the development of cell cultures in FreeStyle 293 and EX-CELL medium for the comparison of cell growth in both medium types.

Establishment cultures were allowed to acclimatise to suspension culture for 4 days in a shaking incubator at 120 rpm, with an ambient temperature of 37°C and 5% atmospheric concentrations of CO₂. At the conclusion of the 96-hour establishment period, a total cell count was taken using the Countess electronic cell counting system (Table 3.1).

	FreeStyle medium	EX-CELL medium
Live cell count (cells/ml)	1.1×10 ⁶	8.1×10 ⁵
Dead cell count (cells/ml)	2.7×10 ⁴	3.2×10 ⁴
Live cell percentage	98%	96%

Table 3.1 – Table of living and dead cells counted in 180 ml starter cultures 96 hrs after establishment in FreeStyle and EX-CELL media.

Both of the media used sustained stably transfected HEK 293S GnT1⁻ cells for 96 hrs without requiring a change of medium or addition of extra supplements. Both starter culture flasks were inoculated with an approximately equal number of cells grown in adhered culture in 30 ml DMEM-F12 in T175 flasks. Cells grown in both media displayed a similar ratio of living and dead cells, however FreeStyle medium appears to maintain a higher proportion of living cells. Cells grown in FreeStyle medium also displayed a 74% increase in the number of live cells recorded per ml.

Both FreeStyle and EX-CELL cultures were then diluted 1:1 into 500 ml plastic Erlenmeyer flasks containing 90 ml EX-CELL medium supplemented with the same additives as the establishment cultures. The flasks were returned to the incubator and grown under the same conditions as the establishment cultures. Cell counts were then taken daily until the live cell population of one of the suspension cultures approached 2×10^6 (Table 3.2). Following 3 days of further cell culture, the FreeStyle-derived cells came close enough to this boundary that the decision was taken to stimulate protein expression with the addition of 5 mM sodium butyrate.

	FreeStyle medium	EX-CELL medium
Live cell count (cells/ml)	1.8×10^6	8.6×10^5
Dead cell count (cells/ml)	5.7×10^4	7.8×10^4
Live cell percentage	97%	92%

Table 3.2 – *Table of living and dead cells counted in 180 ml FreeStyle and EX-CELL cultures 72 hrs after transfer from starter cultures.*

Both types of media continued to maintain cells in solution with high vitality, with >90% of cells counted in both types of media being live. By this stage, FreeStyle medium displayed ~110% increase in live cell numbers compared to EX-CELL medium.

To sustain cell populations post-expression, 20 ml of the FreeStyle-derived cells and 40ml of the EX-CELL derived cells were transplanted into fresh 180ml EX-CELL cultures to create new cultures with a starting density of 2×10^5 cells/ml; these were placed into incubation under the same conditions as previously discussed in section 2.2.2. Following 48 hrs additional incubation with 5 mM sodium butyrate, a final cell count was taken to observe the condition of the stimulated cells (Table 3.3).

	FreeStyle medium	EX-CELL medium
Live cell count (cells/ml)	2.3×10^6	8.9×10^5
Dead cell count	1.1×10^5	1.1×10^5
Live cell percentage	96%	89%

Table 3.3 – Table of living and dead cells counted in 180 ml FreeStyle and EX-CELL cultures 120 hrs after transfer from starter cultures and 48 hrs after the addition of 5 mM sodium butyrate.

Both cultures grew following the addition of sodium butyrate, however FreeStyle medium displayed the greater growth, with a 27.8% increase in live cell population relative to levels lacking sodium butyrate, while the number of cells in EX-CELL medium grew by only 3.5% (see Table 3.2). The overall live cell percentage in both media decreased, however EX-CELL medium

displayed the greater loss in overall population, with a loss of 3%, as opposed to 1% lost by FreeStyle medium.

3.5.2 Influence of pluronic acid and primatone on cell growth in suspension

The results discussed section 3.5.1 were still sub-optimal, as PEM, FreeStyle and EX-CELL are all substantially more expensive than DMEM, making them less economically viable than DMEM culture. In an effort to improve the vitality of cells in suspension DMEM, an additional culture was set up to investigate the effects of adding 0.2% (w/v) of the surfactant pluronic acid, which is suspected to improve mammal cell resilience to shearing, to calcium DMEM produced from commercial hydrated powder (Büssow 2015). Additionally, 2.5% (w/v) primatone was added as an anti-apoptosis agent (Schlaeger 1996). Each culture was established in 180 ml of culture, each supplemented with 100-fold diluted non-essential amino acid and glutamine. DMEM + pluronic acid was compared directly against PEM, FreeStyle and EX-CELL media, with each seeded with a starting cell density of ~ 200,000 cells/ μ l.

Cell cultures were incubated in 500 ml plastic Erlenmyer flasks at 37 °C in a shaking incubator with a shaking speed of 120 rpm with 8% atmospheric CO₂, based on a protocol developed from discussion with Dr. Paul Miller at the Structural Genetics Consortium, Oxford, UK. Grow rates were recorded through cell count readings at 24 hr intervals. 48 hrs prior to collection (at time 96 hrs) 5 mM sodium butyrate was added to each medium to stimulate additional protein production. Cells were collected via the method outlined in section 2.2.2 and protein extracted from these cultures were later used in mass spectrometry experiments (see section 4.6).

In contrast to the growth curves in section 3.5.1, FreeStyle medium supplemented with Primatone was able to support cell growth at a near-identical pace to PEM (Figure 3.7). PEM and FreeStyle media display very similar growth curves, with cell number increasing approximately 10-fold in the course of 120 hours. Growth recorded in EX-CELL is less pronounced, with the cell count increasing approximately 5-fold in the same time frame.

This may be an indication that variation in cell growth between experimental setup may obscure the true effects of varying cell medium and supplements. Despite being supplemented with both primatone and pluronic F68, the cells seeded into DMEM failed to grow – both the cell count and viability of cells in this medium dropped for the duration of the growth trial, indicating that while primatone is rich in amino acids it is not suitable as an alternative source of carbon to FBS.

Cells in DMEM decrease in number over the course of the experiment, reducing by 40% by the conclusion. Following the results discussed above, the DMEM-based culture was repeated. However the FBS content of the medium was increased to the 10% (v/v) concentration found in adherent culture, as recommended in Lin et al., 2015.

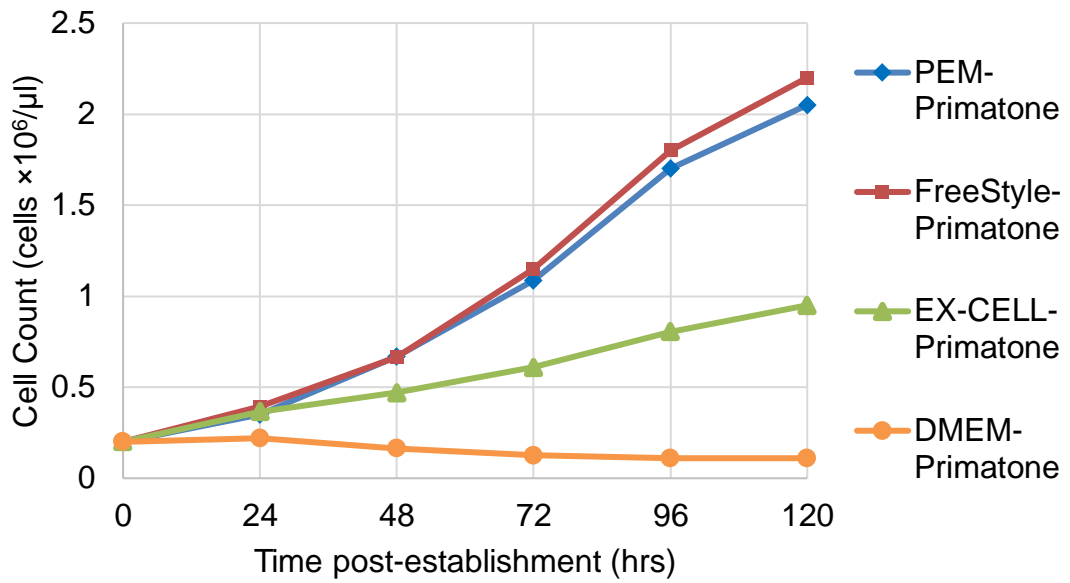


Figure 3.7 – Graph detailing the number of HEK cells recorded over time in suspension culture in PEM, FreeStyle, EX-CELL and DMEM when supplemented with pluronic acid and primatone.

3.5.3 Effects of media types on protein purification

HEK cells from suspension were collected in 50 ml falcon tubes through centrifugation at 200 × g for 10 minutes. The supernatant was then removed and the cells resuspended and washed twice with 50 ml PBS. The pellets of FreeStyle and EX-CELL establishment cells were separately pooled and weighed, with a final mass of 1.56 g and 900 mg recorded for each medium respectively. Both pellets were placed into storage at -80°C.

Pellets of HEK cells were later thawed for purification to compare the protein generated by each medium. The cell pellets were thawed on ice, then resuspended in the standard lysis buffer (300 mM NaCl, 50 mM Tris pH 7.6, 10 mM KCl, Roche EDTA-free protease inhibitor). Protein from both pellets was recovered via sonication and 1% (w/v) DDM recovery and then purified using gravity column IMAC as detailed in section 2.3.3.2. Due to the difference in the cell pellet weights produced by both media, the FreeStyle medium was incubated on a larger 180 µl bed volume of HisPur resin, compared to 100 µl for EX-CELL derived protein. The volumes of elution buffer used were changed to reflect this modification.

Following the final dialysis step, the 30 mM imidazole wash, 100 mM imidazole elution and 250 mM elution fraction was concentrated using 50 kDa cut-off membrane centrifuge tubes down to volumes of ~150 µl. For SDS-PAGE, 13 µl samples of each fraction were then mixed with 5 µl ×4 Novex LDS sample buffer and 2 µl ×10 Novex sample reducing buffer, then heated to 70°C in a metal heating block and allowed to incubate for 5 min. 9 µl of each sample were then taken forward to SDS-PAGE (Figure 3.8).

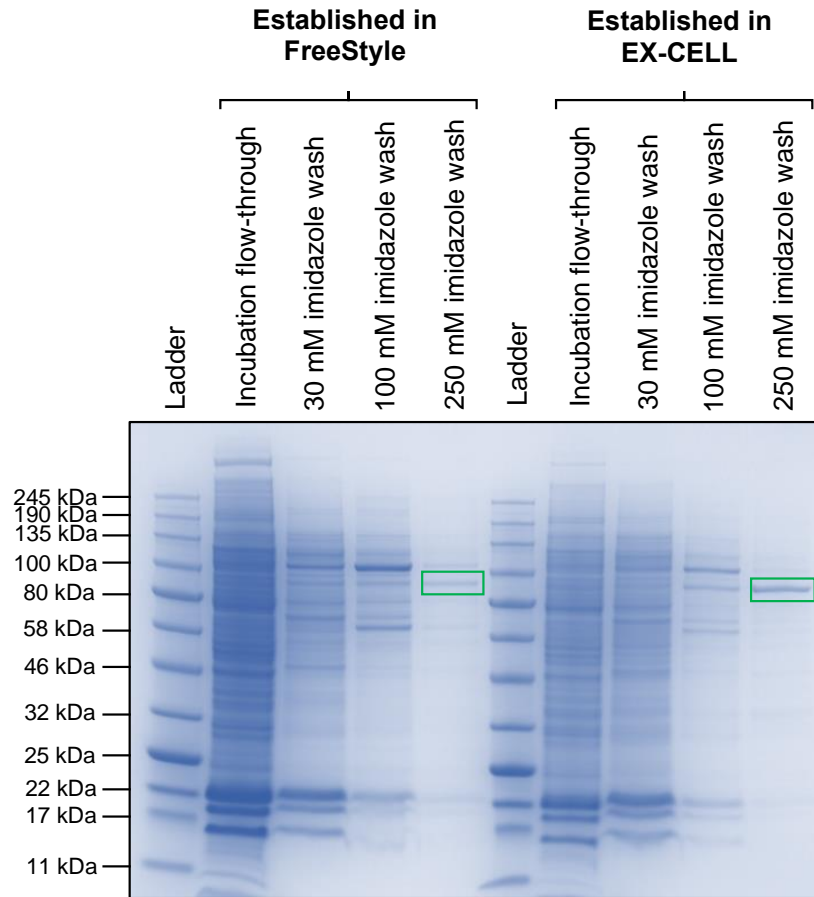


Figure 3.8 – SDS-PAGE comparing of the purification fractions of $K_v1.1$ -TY10 protein derived from HEK cells suspension culture established in FreeStyle vs. EX-CELL medium on HisPur cobalt resin. $K_v1.1$ bands are outlined in green.

The 250 mM imidazole elution fraction derived from EX-CELL medium culture was taken forward to cryo-EM (see section 5.3). Column flow-through and elution fractions show gradual increases in purity in both cases, however protein derived from FreeStyle medium display increased flow-through content compared to EX-CELL, though lower yields and higher contamination in later elution fractions. In previous purification trials on cobalt resin, the highest quantities and purity Kv1.1 was found in the 250 mM imidazole fraction. Cells established in FreeStyle appear to generate less Kv1.1 compared to cells established in EX-CELL, based on the bands observed in this gel.

4 Purification and characterisation of K_v proteins

4.1 Background

The purification of proteins is an essential step in their study and characterisation. Separating the target protein from other species is required in order to isolate its individual characteristics so that any experimental measurements are not affected by contaminants, such as RNA, DNA or other proteins. In structural studies, protein samples must be pure in order to allow the generation of repeating crystal structures in the case of X-ray crystallography, or producing homogeneous, easily-processed datasets in the case of electron microscopy (McPherson and Gavira 2014, Thompson, R. F. et al. 2016).

Purification techniques operate by separating proteins based on their physical and chemical characteristics. Proteins can be extracted through exploiting their specific interactions with binding partners, such as substrates, cofactors or antibodies. Purification through polyhistidine tagging is one of the most commonly used methods for purifying protein for analysis. Polyhistidine tagging involves adding a motif of repeated, consecutive histidine residues to the protein, usually between 6 or 12 amino acids in length, either at the N- or C-terminus, or more unusually in an unstructured linker region within the sequence (Porath 1992). These polyhistidine motifs strongly bind divalent metal ions, such as Ni^{2+} or Co^{2+} (Bornhorst and Falke 2000). Antibody-based purification methods work on a similar principal, with proteins binding to antibodies raised to specifically target elements of their amino acid sequence and/or their modified surface groups (Urh et al. 2009).

Additionally, purification by shape and size are utilised in purification by SEC, with columns with resins composed of porous beads. Small molecules are more likely to enter the convoluted, included volume of the beads making up the resin, while larger molecules will enter the excluded volume and take a more straightforward path out of the column, thus molecules tend to elute from SEC columns in order of largest to smallest. This process is also effective at separating precipitated species from folded proteins and can be combined with multi-angle light scattering (MALS) to characterise the mass and radius of species eluting from the column (Fekete et al. 2014).

Proteins removed from their native environment often suffer from issues with their structural stability. Optimising factors such as buffer composition, salinity, pH, temperature and mechanical pressure can be difficult to determine and each is able to perturb the protein structure and promote unfolding. Changes in environment and folding can adversely affect the functionality of the protein, potentially making characterisation of proteins challenging.

For membrane proteins, an additional factor to consider is finding a scaffold that can house the protein while maintaining both stability and function. Typically, this has been achieved through detergents such as DDM but these have their own limitations, for example, stripping away many of the closely associated lipids. As a result, new technologies have been developed that avoid such issues. SMA, for example, can recover membrane proteins while retaining natively associated lipids. One limitation of SMA in the industrial setting is that although it can be used by academic groups, it is currently under some amount of IP protection (Medical Research Council 2014). Therefore, new related systems such as DIBMA have been produced that act in a manner

similar to SMA without being restricted by IP. Currently, very little has been reported on the use of DIBMA for membrane proteins and part of this work was aimed at comparing DDM, DIBMA and SMA to aid future experiments in this field.

4.2 Comparison of cell lysis methods

To investigate the best route for protein extraction both the sonication and tissue grinding approaches were tested. While sonication as a method of cell disruption is often highly effective, rupturing cells into smaller fragments at a faster rate, it has been known to generate localised temperature and pressure fluctuations which can trigger unfolding of liberated proteins. Homogenisation, on the other hand, ruptures cells more gradually, often liberating less useable product, while avoiding the generation of unfolded or precipitated proteins often seen in sonication.

The effectiveness of both techniques in the preparation of Kv1.1 was compared through SDS-PAGE of the raw soluble and insoluble lysate produced from 0.5 g of HEK 293S GnT1⁻ cell pellet via both techniques (Figure 4.1). Recovery of protein from the insoluble fraction was conducted using 0.1% DDM and 0.1% SMA to compare the relative effectiveness of each detergent.

Larger quantities of protein in the soluble fraction were observed in the samples prepared using sonication compared to homogenisation, though approximately equivalent amounts of protein were observed in insoluble fractions prepared using either method (Figure 4.1). While the soluble cell lysis fraction was not the desired product for the purpose of purification, the higher yield of soluble protein in the sonicated sample was interpreted as an indicator of more complete lysis of the whole cell pellet compared to homogenisation.

Sonication was subsequently used over cell homogenisation in the majority of later cell purification trials, with the exception of extractions performed using

SMA and DIBMA, where homogenisation of cell membranes was recommended by Dr. Vincent Postis for maximal recovery of protein (see section 2.3.1).

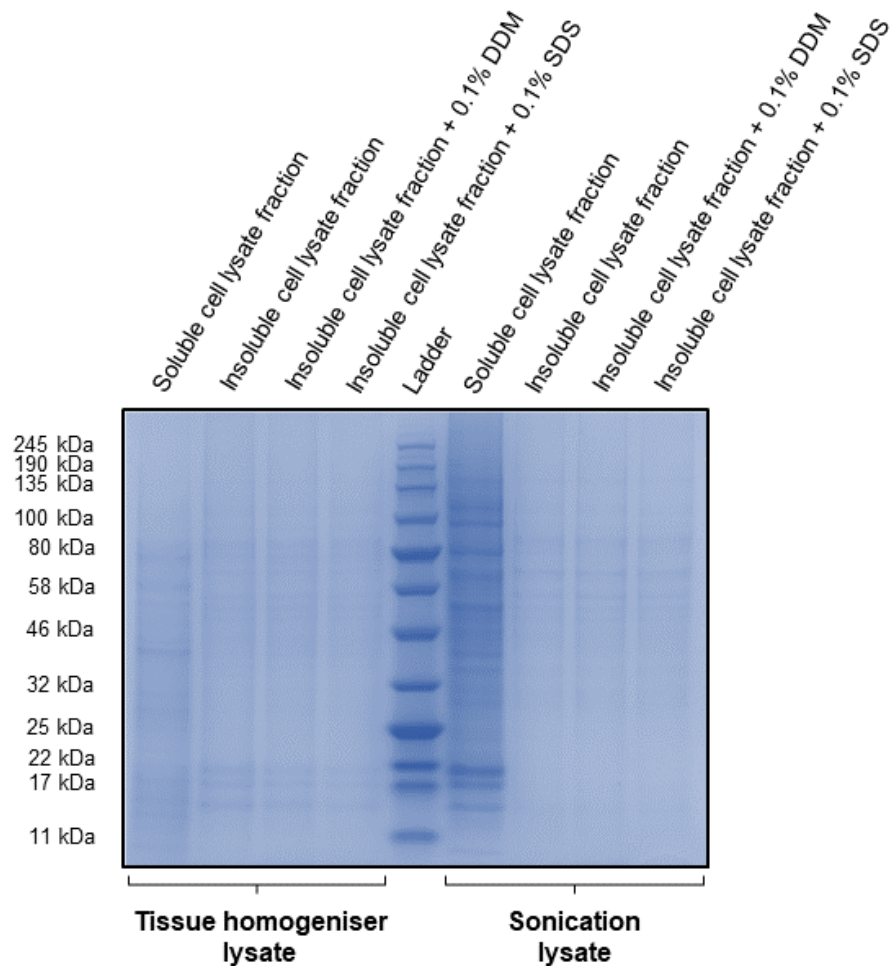


Figure 4.1 – SDS-PAGE gel comparing tissue grinding and sonication. Each lysis protocol was conducted using an equivalent weight of cell pellet. While specific bands are difficult to discern in both cases, more protein appears to be present in the soluble fraction of the sonication lysis samples, implying that the process of sonication liberates more protein than homogenisation.

4.3 Western blotting of transfected and untransfected cells

4.3.1 Sample preparation

To positively confirm that transfected HEK293S GnTII⁻ cell were able to express K_v1.1, western blots were conducted on samples of cells stably transfected with pcDNA6 encoding the K_v1.1-TY10 construct, with blotting of untransfected cells conducted in parallel as a negative control.

Both stably transfected and untransfected HEK293S GnTII⁻ were grown in suspension (as described in section 2.2.2) in DMEM medium, supplemented with 10% FBS, 2.5% primatone and 0.02% pluronic acid (as described in section 3.5). Both transfected and untransfected cell cultures were supplemented with 5 mM sodium butyrate once their cell densities reached 3×10⁶ cells per ml and collected 48 hrs afterwards.

0.5 g of cell pellet from both transfected and untransfected culture were lysed via direct dissolve in 1% DDM (see section 2.3.1.3). Direct dissolving of the cells was chosen to allow the whole contents of the cell, both in the membrane and soluble fraction to be screened.

4.3.2 Comparison of western blotting using anti-GFP antibodies

A western blot was conducted against DDM-dissolved transfected and untransfected HEK293S GnTII⁻ cells. 20 µg of protein from both lysis solutions was applied to SDS-PAGE and the material was transferred to a nitrocellulose membrane for western blotting (see section 2.4.3 for details). Rabbit polyclonal anti-GFP antibody (FL) (Santa Cruz Biotechnology) diluted 1:200

in TBST was used as the secondary antibody. Binding of the secondary antibody was visualised using the BM Chemiluminescence Western Blotting Kit, as detailed in section 2.4.3 (Figure 4.2).

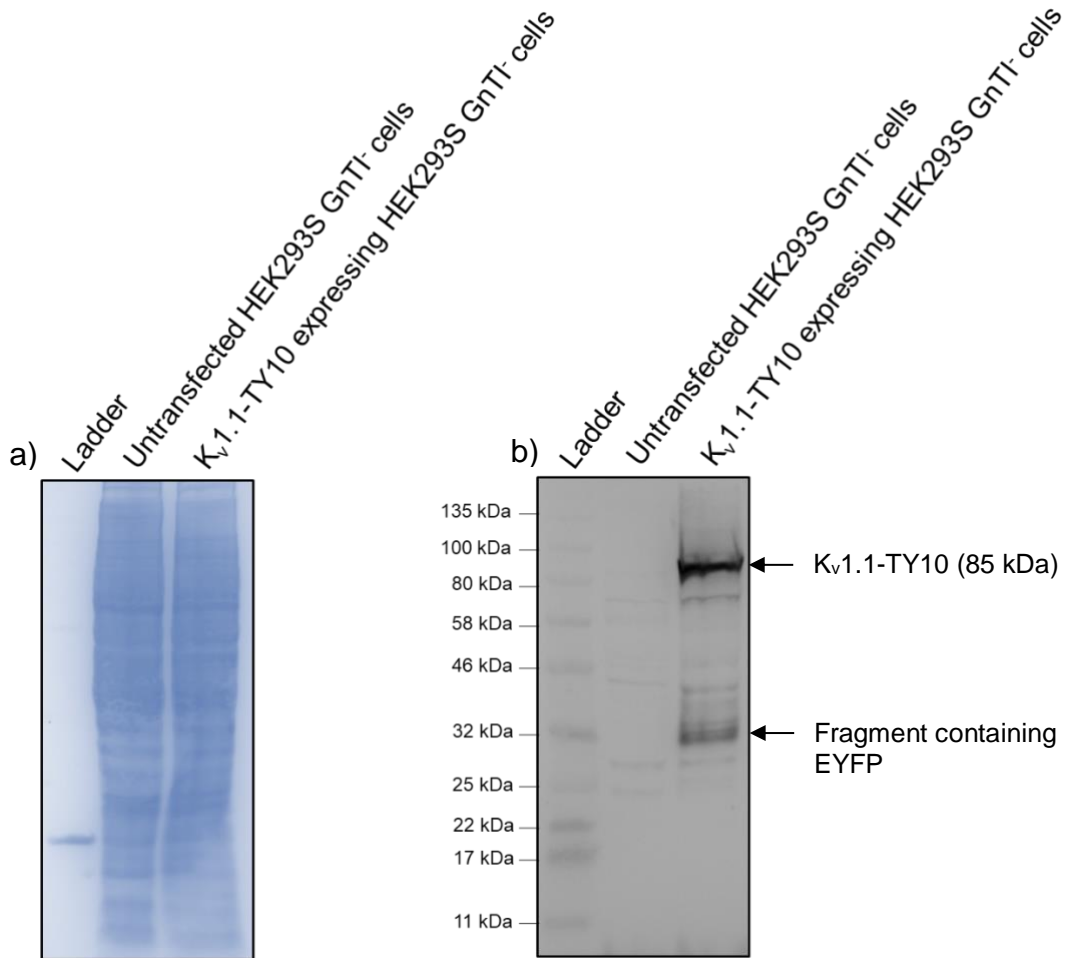


Figure 4.2 – Post-transfer SDS-PAGE of whole cell contents of untransfected HEK 293S GnT1⁻ cells and HEK 293S GnT1⁻ cells expressing Kv1.1-TY10 (a) and chemiluminescent western blot of transferred SDS-PAGE contents with polyclonal anti-GFP antibodies (b). Significantly higher signal is observed in the HEK 293S GnT1⁻ stable cell line expressing Kv1.1-TY10.

The chemifluorescence observed in the sample of transfected cell lysate was substantially stronger than that seen in the untransfected cell lysate; a strong band correlating with a mass between 80 and 100 kDa was visible in the transfected lysate, but absent from the untransfected lysate; the mass of this band match the 85 kDa mass of Kv1.1-TY10 predicted by its amino acid sequence, strongly indicating that it is expressed in the transfected cells, with the antibodies binding to the GFP-derived EYFP tag. A further, dimmer band with a mass between 25 and 32 kDa. This may correspond to a separate EYFP molecule, possibly as a product of proteolysis of Kv1.1 or cleavage of the tag.

The presence of less massive bands containing EYFP potentially indicates that there is some amount of instability of the construct. However, the less massive band correlating with EYFP appears visibly less intense than the Kv1.1-TY10 band, indicating that the full-length construct is more common than any degradation products.

4.3.3 Comparison of western blotting using anti-Kv1.1 antibodies

A further western blot was conducted against DDM-dissolved transfected and untransfected HEK293S GnTI⁻ cells using rabbit polyclonal anti-Kv1.1 antibody (A-15) (Santa Cruz Biotechnology) diluted 1:200 in TBST was used as the secondary antibody. 20 µg of protein from both lysis solutions was applied to SDS-PAGE and the material was transferred to a nitrocellulose membrane for western blotting (see section 2.4.3 for details). Binding of the

secondary antibody was visualised using the BM Chemiluminescence Western Blotting Kit, as detailed in section 2.4.3 (Figure 4.3).

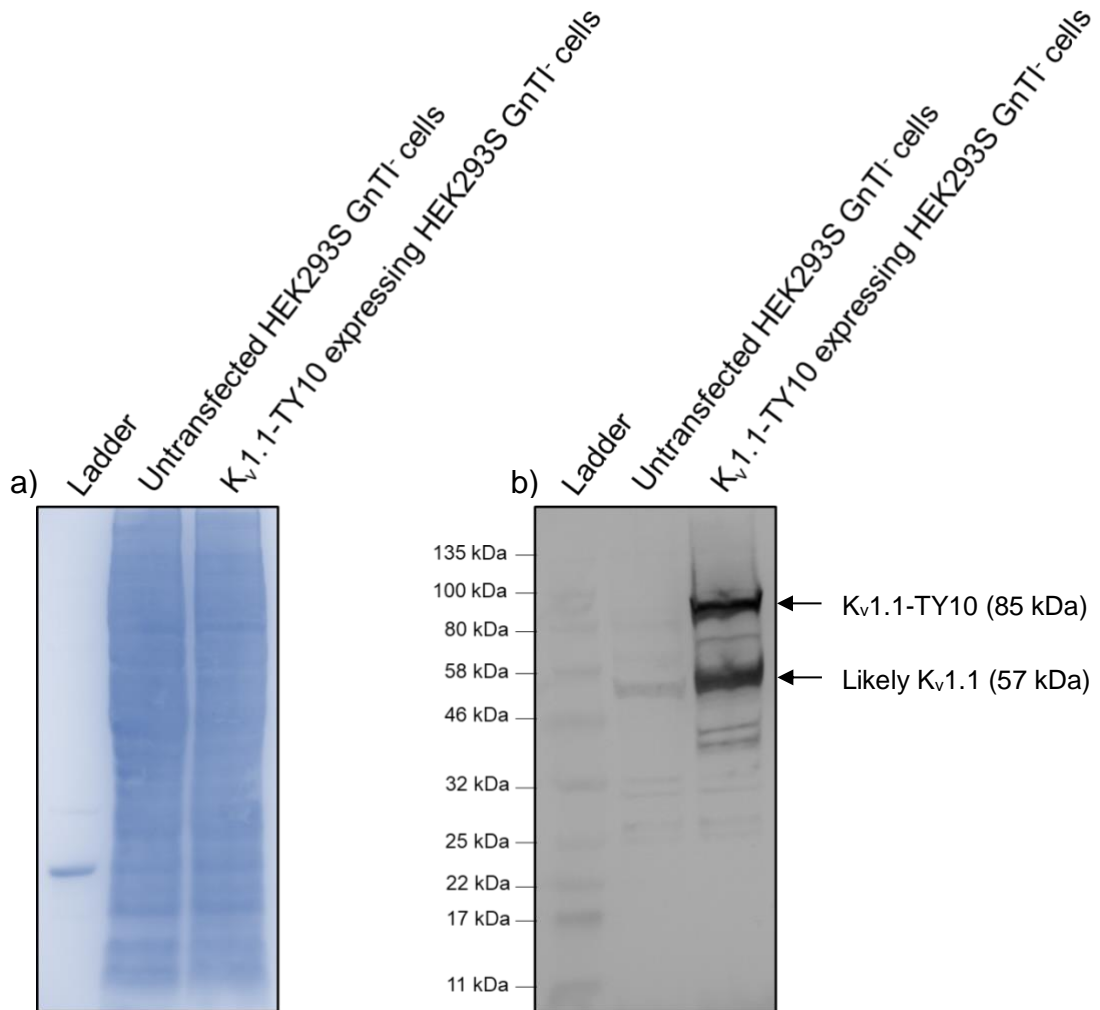


Figure 4.3 – Post-transfer SDS-PAGE of whole cell contents of untransfected HEK 293S GnTII cells and HEK 293S GnTII cells expressing K_v1.1-TY10 (a) and chemiluminescent western blot of transferred SDS-PAGE contents with polyclonal anti-K_v1.1 antibodies (b). Significantly higher signal is observed in the HEK 293S GnTII stable cell line expressing K_v1.1-TY10.

Like the western blot using anti-GFP antibodies, the chemifluorescence observed in blotting of the transfected cell lysate with anti-K_v1.1 antibodies was substantially stronger than that seen in the untransfected cell lysate, with a strong band with a molecular weight between 80 and 100 kDa being visible in the transfected lysate and absent in the untransfected lysate sample. The molecular weight of this band of this band matches the 85 kDa mass of K_v1.1-TY10 predicted by its amino acid sequence, which indicates that this band corresponds to the full-length construct.

A slightly less intense band with a mass between 46 and 58 kDa was also observed in the transfected lysate sample. To a K_v1.1 molecule missing the C-terminal tag, as the molecular weight of the band corresponds to the predicted 57 kDa mass of a K_v1.1 monomer. This observation, like the lighter band seen in the anti-GFP western blot, seems to indicate some degree of cleavage of the protein, however it is not clear if any digestion of the protein is occurring prior to or subsequent to the solubilisation of the whole cell.

It must also be noted that the ~57 kDa band has a potential equivalent in the untransfected cell lysate which is also displaying in the western blot. The band in the untransfected sample appears to be slightly less massive, though it is definitely of a similar size. This band may be the result of cross-contamination of sample, though the care was taken to avoid mixing of samples at each step. It is also possible that the band is unrelated to the transgenic expression of K_v1.1 and is an endogenously expressed protein in HEK293S GnT1⁻ cells that is coincidentally binding the polyclonal antibody. A repeat of the western blot using specific monoclonal antibodies could be performed to test this hypothesis.

4.4 Extraction of membrane proteins and primary purification by IMAC

The efficiency of protein extraction in DDM, SMA and DIBMA were compared through a combination of SDS-PAGE and UV spectroscopic measurement of protein concentrations. 800 mg of HEK 293S GnTI⁻ Kv1.1-TY10 stable line VI cell pellet were used in each instance at the outset to ensure that the final results for each extraction method were directly comparable.

Concentrations of DDM used for protein extraction was increased to 1% from the 0.1% concentration used in the previously discussed DDM/SDS comparison (see section 4.2). This modification was made in order to bring the protein preparation procedures into line with those used in earlier and contemporary research being conducted by other groups investigating cation channel structures (Nurani et al. 2008, Kintzer and Stroud 2016, Deivanayagarathy et al. 2018).

Fractions containing extracted Kv1.1 were loaded in parallel onto Novex Tris-Glycine gels. As discussed in section 3.4, protein solubilised in SMA and DIBMA eluted from cobalt resin at 100 mM imidazole, while protein extracted in DDM eluted in the 250 mM imidazole fraction (Figure 4.4).

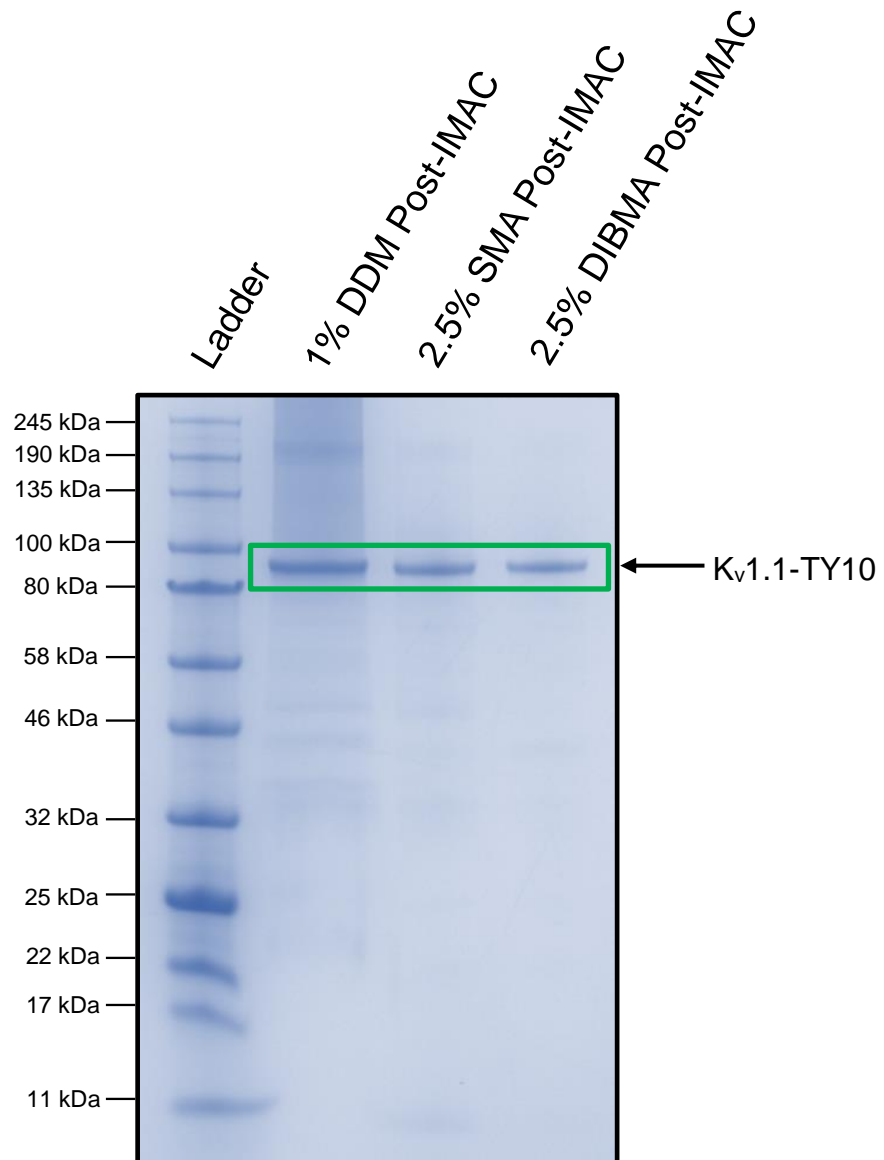


Figure 4.4 – SDS-PAGE of IMAC purified K_v1.1-TY10 extracted in DDM, SMA and DIBMA. Each method of extraction was applied to the same quantity of starting material, being 800 mg of cell pellet. Each lane contains the 250 mM imidazole elution fraction from IMAC purification.

The DDM-solubilised material displays the strongest band, with SMA and DIBMA-solubilised material displaying roughly equal quantities. Note that while some contamination is present in all 3 methods, the Kv1.1-TY10 band is significantly stronger than all other species present. This strongly suggests that extraction of protein by all 3 methods, coupled with primary purification by cobalt affinity purification via IMAC is sufficient to generate usable samples.

4.5 Comparison of cobalt and nickel IMAC resin

Comparison of Nickel and Cobalt-infused IMAC resins was conducted in order to determine which constituted the most effective option for the recovery of Kv1.1-TY10. Cells for this comparison were derived from suspension DMEM-F12 culture stimulated with 5 mM sodium butyrate for 48 hrs, with protein extracted following the protocols discussed in section 2.3.2.

To compare IMAC purification using cobalt and nickel-charged resins, two parallel experiments were conducted using 100 µl bed volume of pre-charged HisPur cobalt resin (Thermo Scientific) and sepharose resin (GE healthcare) charged with 10 column volumes of 100 mM NiSO₄. These resins were then transferred to 5 ml columns with porous filters. The detergent solubilised protein mixture was then split in half and purification of both halves carried out on either column. The dialysed protein fractions were concentrated on a 100 kDa cut-off membrane and loaded onto a pre-cast Novex 4-12% Bis-Tris gel for SDS-PAGE (Figure 4.5).

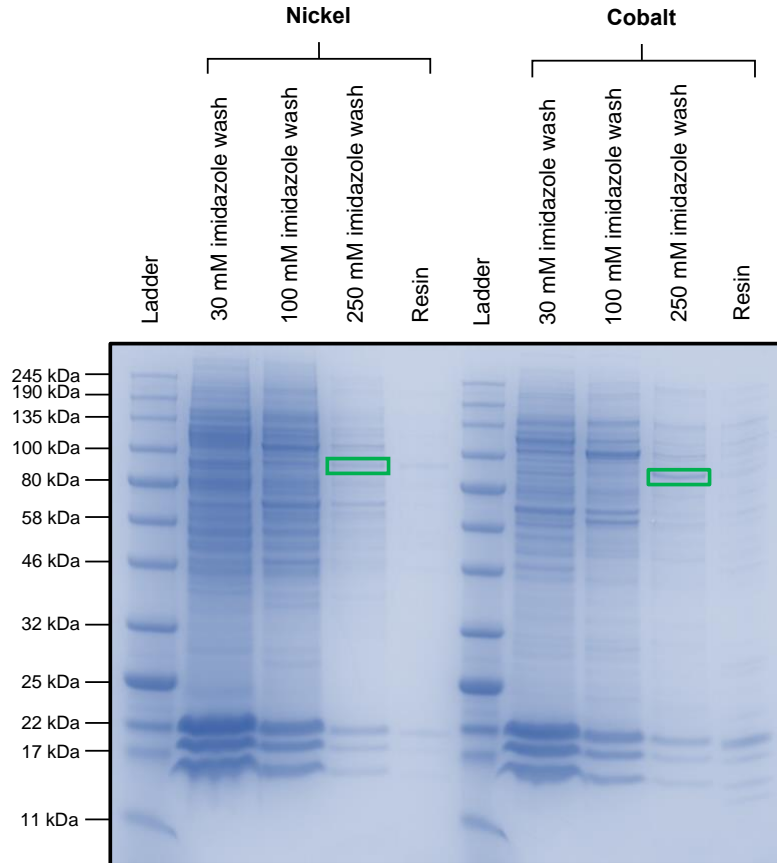


Figure 4.5 – SDS-PAGE comparing the binding and elution of proteins in DDM-solubilised membranes derived from stably transfected HEK 293S *GnT1* cells expressing *K_v1.1-TY10* on nickel-charged sepharose and cobalt-charged HisPur resins. Bands whose mass correspond to the predicted 85 kDa mass of the tagged *K_v1.1* construct have been labelled with green boxes.

The resulting gel from testing different purification resins (Figure 4.3) indicated stronger binding of *K_v1.1-TY10* by the cobalt-charged HisPur resin, corresponding to a stronger band between 80 and 100 kDa appearing in the 250 mM imidazole elution of that resin when compared to the nickel-charged sepharose.

4.6 Äkta Explorer purification and size-exclusion chromatography

4.6.1 Äkta Explorer-based IMAC

DDM-solubilised Kv1.1-TY10 was subjected to IMAC purification through the HisTRAP column method detailed in section 2.3.3.3. The A and B buffers were supplemented with 0.02% (w/v) DDM to maintain the detergent micelle surrounding the protein. Once the programmed imidazole gradient had concluded, 10 µl samples of the first 96 elutions were transferred to a 96-well microplate and analysed using a FluoSTAR OPTIMA microplate reader (BMG Biotech). The in-built GFP fluorescence intensity program was then used to measure the fluorescence of each elution fraction (Figure 4.6).

The fluorescence measured in the elution fractions revealed a distinct peak between 11.1 ml and 13.35 ml. This indicated that the EYFP-tagged protein was eluting predominantly within these fractions. Based on this, the 15 elution fractions corresponding to this peak were pooled together to form a 2.25 ml solution that was taken forward to SEC for secondary purification, as detailed in the next section.

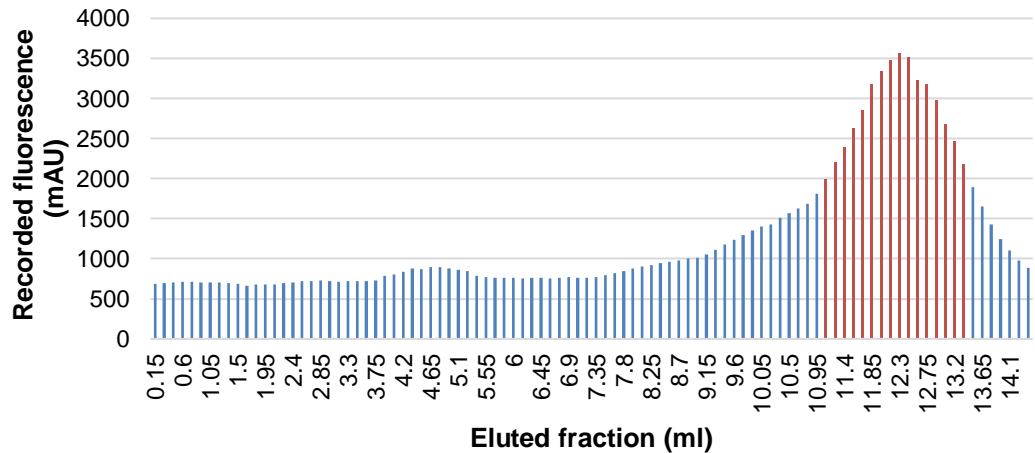


Figure 4.6 – Fluorescence of elution fractions collected from 1 ml HisTRAP column during $K_v1.1$ -TY10 purification. The peak in recorded fluorescence between 11.1 ml and 13.35 ml, highlighted in red, were interpreted to correspond to $K_v1.1$ -TY10 and retained for secondary purification via SEC.

4.6.2 Äkta Explorer-based SEC

SEC purification of the HisTRAP purified $K_v1.1$ -TY10 discussed in the previous section was conducted in accordance with the method detailed in section 2.3.4. Like the IMAC step previously, the running buffer was supplemented with 0.02% (w/v) DDM to prevent denaturation of the protein. Also, in line with the previous step, fluorescence from each elution fraction was recorded using the GFP fluorescence intensity program of the FluoSTAR OPTIMA (Figure 4.7).

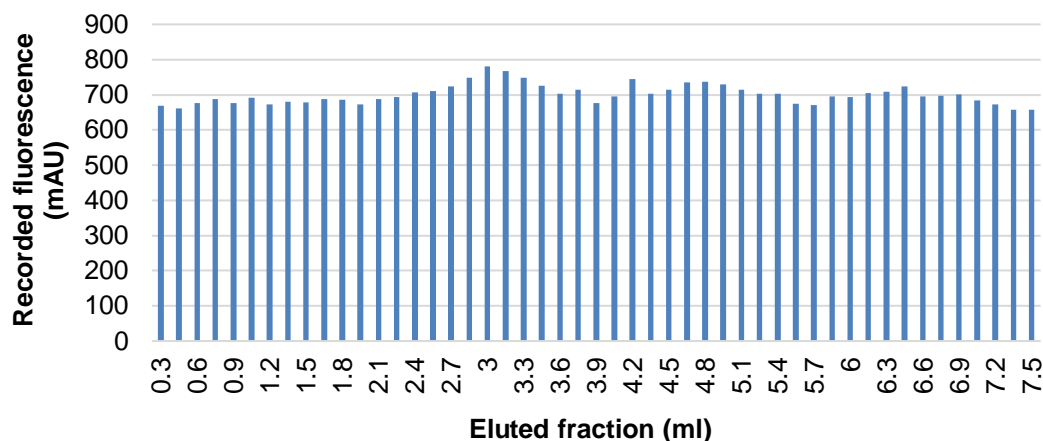


Figure 4.7 – Graphs detailing the fluorescence recorded for each 0.15 ml fraction eluted from SEC purification on Superdex 200 column.

The fluorescence observed in the elutions from this purification were weaker than the IMAC purification, as no substantial peak was observed in any elution fraction. While individual minor peaks are discernible, none extend significantly higher than the average of 695 mAU. This strongly suggests that any protein samples loaded onto the column did not elute from the column in the fractions that were screened.

The protein may have been lost during the purification process if the sample had eluted during the early washing steps prior to the collection of elution fractions. In future, it would be sensible to collect the flow-through of the initial if the protocol is ever repeated so that the sample could be analysed either by UV absorbance, fluorescence measurement or western to check for the presence of Kv1.1-TY10.

4.7 Mass spectrometry

Mass spectrometry protein identification was used to determine the identities of contaminants found in some of the lanes seen on SDS-PAGE, as well as

add further evidence to support the claim that the prominent band often observed between 80 and 100 kDa in 250 mM elution lanes is Kv1.1-TY10. SDS-PAGE was conducted with 100 mM imidazole elution from IMAC purification derived from FreeStyle 293 cultured cells and 250mM imidazole elution derived from EX-CELL cultured cells. These samples were selected as they had the most prominent bands. The gel was given to Dr. Rachel George of the Mass Spectrometry facility, who determined which bands were suitably prominent to allow collection and analysis (Figure 4.8).

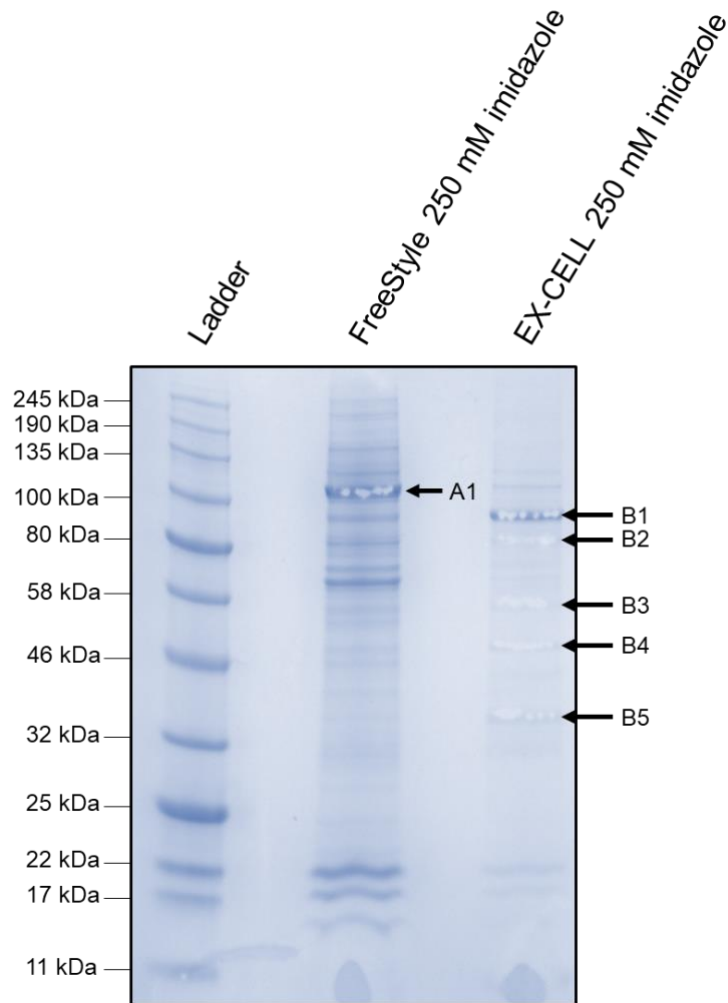


Figure 4.8 – SDS-PAGE submitted for mass spec analysis. The FreeStyle 250 mM imidazole preparation was selected as it appeared to contain the most prominent selection of contaminants. Likewise, the EX-CELL 250 mM imidazole elution fraction was also submitted as it was judged to have the most prominent band corresponding to the species suspected to be *Kv1.1*. Each collected band has been annotated using an arrow and an identifying label. Band B1 was strongly suspected to correspond to *Kv1.1-TY10*, based on its predicted mass of 85.8 kDa.

Protein identification provided insights into the identity of some of the selected bands. Analysis of band B1 provided the most evidence relating to the identity of the band corresponding to expected mass of Kv1.1-TY10 had been correctly identified, as 45 fragments returned during analysis displayed a 100% sequence identity with Kv1.1, covering 54% of the protein sequence (Figure 4.5). Protein identification also revealed 13 fragments with 100% identity with Kv1.3, corresponding to 26% coverage of Kv1.3 (Figure 4.9).

The Kv1.3 observed in the mass spec samples had 100% sequence identity with the human Kv1.3. This may suggest that the purified Kv1.1 co-purified with Kv1.3, perhaps as part of a heteromeric complex. However, only 1 fragment was unique to Kv1.3, with all other overlapping with Kv1.1 (Figure 4.10). However, it is important to note that deamination of the glutamate to a glutamine would also result in the same mass of the fragment. Therefore, it is more likely that the fragment represents a fragment of Kv1.1 with a deaminated E121 residue, rather than the Q188 residue of Kv1.3 (Figure 4.11). This conclusion is further validated by the fact that no other fragments unique to Kv1.3 were identified.

Other bands submitted for protein identification did not return reliable data, with most signals being overpowered by keratin contamination (see Appendix 8.2 for details). Some evidence was found for heat shock proteins, however, with the band immediately below Kv1.1 in the 250 mM imidazole elution fraction corresponding with low sequence identity to the protein Hsp70. Had the contaminants been identified it may have provided a means of reducing their presence through gene silencing or alternative purification approaches.



Figure 4.9 – Schematic diagram displaying peptides detected in band B1 by mass spectrometry (blue lines) which align with sequence of K_v1.1. Identified sites of post-translational modification (carbamidomethylation, deamidation and oxidation) are also highlighted.

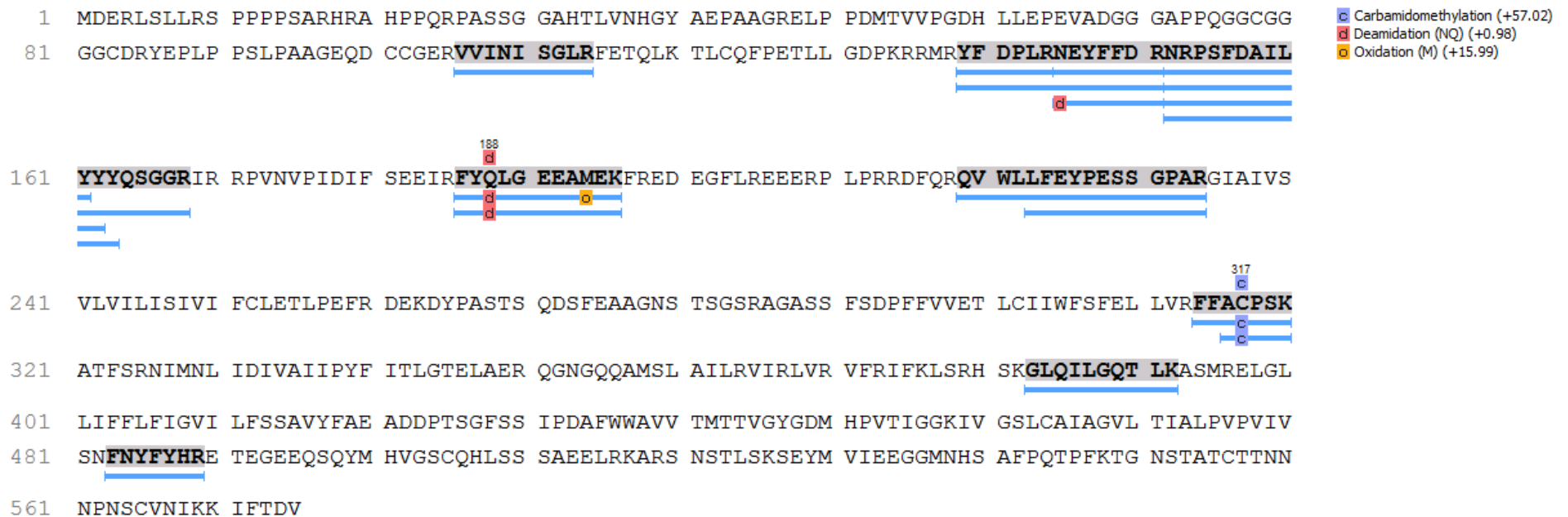


Figure 4.10 – Schematic diagram displaying peptides detected in band B1 by mass spectrometry (blue lines) which align with *K_v1.3*. Identified sites of post-translational modification (carbamidomethylation, deamidation and oxidation) are also highlighted. Note the deamination of residue 188, identified by ProteinLynx Global Server as being a deaminated glutamine.

>KCNA1

```
1  MTVMSEGENVD EASAAPGHPQ DGSYPRQADH DDHECCERVV INISGLRFET QLKTLAQFPN TLLGNPKKRM RYFDPLRNEY
81  FFDRNRPSFD AILYYYQSGG RLRRPVNVPL DMFSEEIKFY ELGEEAMEKF REDEGFIKEE ERPLPEKEYQ RQVWLLFEYP
161 ESSGPARVIA IVSVMVILIS IVIFCLETLP ELKDDKDFTG TVHRIDNTTV IYNSNIFTDP FFIVETLCII WFSFELVVR
241 FACPSKTDFE KNIMNFIDIV AIIPYFITLG TEIAEQEGNQ KGEQATSLAI LRVIRLVRVF RIFKLSRHSK GLQILGQTLK
321 ASMRELGLLI FFLFIGVILF SSAVYFAEAE EAESHFSSIP DAFWWAVVSM TTVGYGDMYP VTIGGKIVGS LCAIAGVLT
401 ALPVPVIVSN FNYFYHRETE GEEQAQLLHV SSPNLASDSD LSRSSSTMS KSEYMEIEED MNNSIAHYRQ VNIRTANCTT
481 ANQNCVNKSK LLTDV
```

>KCNA3

```
1  MDERLSLLRS PPPSARHRA HPPQRPASSG GAHTLVNHGY AEPAGREL PDMTVVPGDH LLEPEVADGG GAPPQGGCGG
81  GGCDRYEPLP PSLPAAGEQD CCGERVVINI SGLRFETQLK TLCQFPETLL GDPKRRMR YF DPLRNEYFFD RNRPSFDAIL
161 YYYQSGGRIR RPVNVPIDIF SEEIRFYQLG EEAMEK FRED EGFLREEERP LPRRDFQRQV WLLFEYPSS GPARGIAIVS
241 VLVILISIVI FCLETLPEFR DEKDYPASTS QDSFEAAGNS TSGSRAGASS FSDPFFVVET LCIIWFSFEL LVRFFACPSK
321 ATFSRNIMNL IDIVAIIPYF ITLGTelaER QGNGQQAMSL AILRVIRLVR VFRIFKLSRH SKGLQILGQT LKASMRELGL
401 LIFFLFIGVI LFSSAVYFAE ADDPTSGFSS IPDAFWAVV TMTTVGYGDM HPVTIGGKIV GSLCAIAGVL TIALPVPVIV
481 SNFNYFYHRE TEGEEQSQYM HVGSCQHLSS SAEELRKARS NSTLSKSEYM VIEEGGMNHS AFPQTPFKTG NSTATCTTNN
561 NPNSCVNIKK IFTDV
```

Figure 4.11 – Sequences of $K_v1.1$ and $K_v1.3$ colour coded according to fragments identified in mass spectrometry. Green indicates fragments which align with both proteins, yellow indicates fragments unique to KCNA1 and red indicates a glutamate residue which is misrepresented as glutamine in KCNA3 due to incorrect detection of deamination at the residue by the software (see Figure 4.8 for original output data).

4.8 TEV cleavage

Cleavage of cobalt resin IMAC purified Kv1.1-TY10 was carried out in the first instance using ProTEV Plus (Promega) following the manufacturer's instructions (see section 2.4.4) and the incubated aliquots were subjected to SDS-PAGE to check for the effectiveness of cutting between each duration of incubation. The gel revealed a disappearance in the band corresponding to Kv1.1 after only 1 hr of incubation (Figure 4.12).

In light of the above result, a further reaction was carried out to positively identify product bands from the digestion. The second reaction was conducted with the dilution by water in the manufacturer's protocol excluded. This was done to keep the sample in a small volume and allow more to be loaded for SDS-PAGE. 10 µg mass of protein from the initial protocol was retained, with the volume of ProTEV buffer and 100 mM DDT adjusted down to 0.4 µl and 0.2 µl respectively to retain the same final concentration. The sample was split into 2 × 5 µg aliquots, with 5 units ProTEV added to one, but excluded from the other as a negative control. A third 10 µl reaction mixture was also made with 5 units of ProTEV, 1 mM DDT and ×1 dilute ProTEV buffer was made as a further negative control to check the protein contents of the ProTEV enzyme alone. All 3 were then incubated at 30 °C for one hour.

All 3 mixtures were subjected to SDS-PAGE and the gel transferred onto nitrocellulose. The nitrocellulose membrane was then western blotted with anti-GFP antibody. This would allow the fragments containing EFYP generated by cleavage fragments to be identified (Figure 4.13).

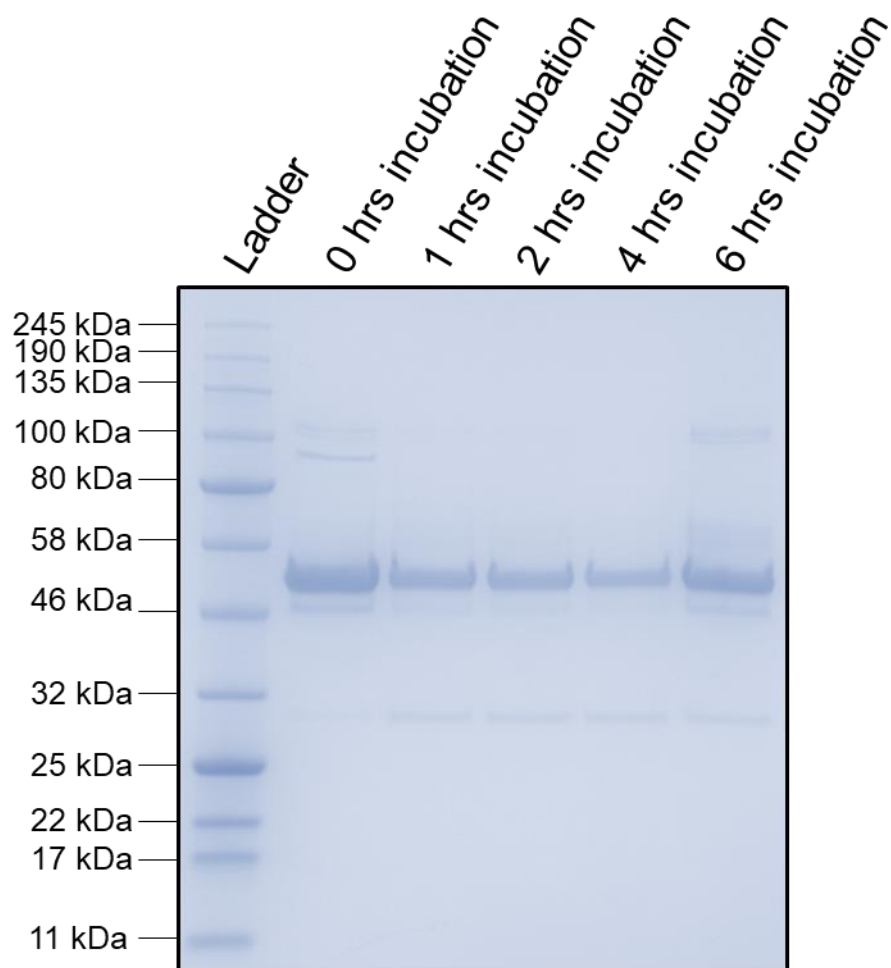


Figure 4.12 – SDS-PAGE of TEV cleavage incubation products. Each product lane features a reaction conducted for a different length of time, along with a 0 hrs incubation as a negative control.

The band observed in the 0 hrs negative control lane corresponds to the Kv1.1-TY10 protein which is the target of cleavage. This band is not seen following 1 hr of incubation, indicating digestion of the protein early during the course of incubation.

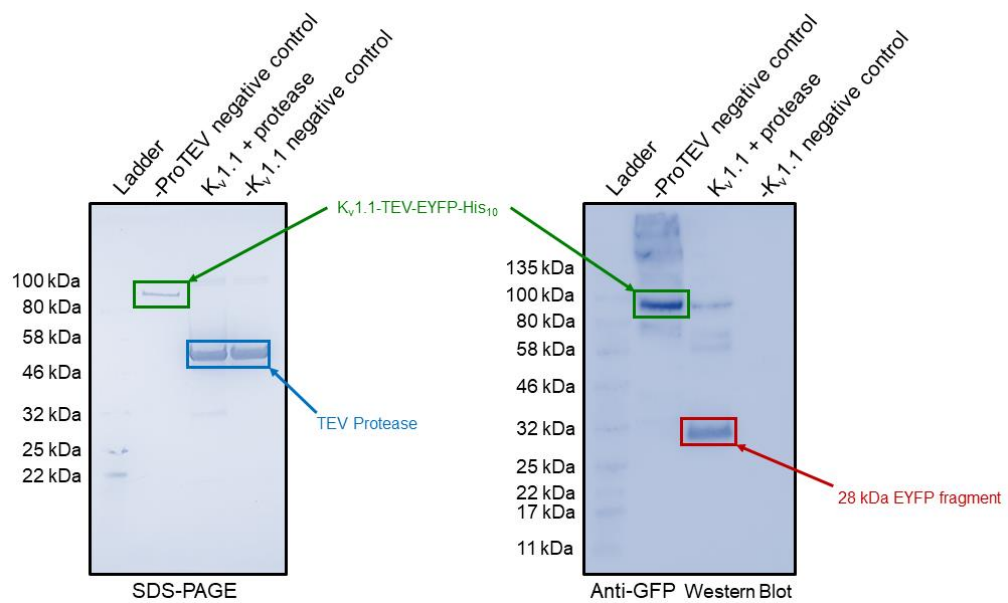


Figure 4.13 – SDS-PAGE and western blot detailing TEV protease digestion of $K_v1.1$ -TY10 protein. Bands corresponding to $K_v1.1$ -TY10 have been outlined in green, ProTEV protease has been outlined in blue and the EYFP fragment generated post-digestion has been outlined in red.

The molecular weights of the fragments were predicted by the online ProtParam tool as part of the ExPASy server, based on the amino acid sequence of the $K_v1.1$ -TY10 construct (Gasteiger et al. 2005). The predicted fragments for the N-terminal fragment containing $K_v1.1$ and the C-terminal fragment containing EYFP and His₁₀ had masses of 57.5 kDa and 28.3 kDa, respectively.

A species with a molecular weight corresponding to the predicted weight of the C-terminal cleavage product containing EYFP is visible in the western blot and is annotated in red in Figure 4.13. The absence of this species in either negative control strongly indicates cleavage of the protein at the TEV cut site.

The disappearance of Kv1.1-TY10 over time during incubation as seen in Figure 4.12, further corroborates this.

This initial result proved difficult to implement into plans for reverse purification on digested protein on IMAC, however, as the product bands appeared to be extremely faint. Attempts to reverse purify the protein produced no visible results on SDS-PAGE, nor was significant quantities of protein detectable via UV spectrometry.

Later digestion trials attempted to avert loss of protein by reducing the digestion temperature from the recommended 30°C to 4°C to avoid degradation linked to temperature. Trials were also conducted with DTT reagent excluded in case of protein loss by oxidative degradation, however neither of these modifications to the protocol increased yields of protein. Inspection of sequencing data of the pcDNA6 plasmid encoding the construct confirmed that the TEV cleavage site was intact. The lack of observed cleavage in later trials may therefore be due to obstruction of the site.

4.9 Circular dichroism

4.9.1 Spectrum and Dichroism analysis

To determine that purified Kv1.1-TY10 was correctly folded, the protein was subjected to CD spectroscopy which can give the composition of the protein. The initial buffer used in CD featured 150 mM sodium chloride. It was later realised that chloride ions are known to interfere significantly with protein studies in CD, as they are known to strongly absorb at wavelengths shorter than 195 nm (Kelly et al. 2005). While this did not impinge on the wavelengths

relating to α helical and β sheet elements, it did obscure sections of spectra which provide information on the presence of coils in the protein structure. As such, the buffer was redesigned in order to use potassium fluoride (KF) in place of sodium chloride, as fluoride ions do not have the same absorbance characteristics as chloride.

CD spectra of Kv1.1-TY10 in 0.02% DDM was recorded across a range of wavelengths from 180-260 nm at 20 °C. The protein was then split into 2 equal amounts, with one frozen gradually at -20 °C and the other flash-frozen in liquid nitrogen, then later thawed and CD analysis repeated (Figure 4.14). This would allow the effects of different methods freezing on protein folding and stability to better inform how to handle and store samples between experiments.

The spectrum that was recorded displayed a profile which was consistent with a predominantly alpha-helical protein, which was expected based on homology models of Kv1.1. These spectra were analysed using the online Dichroweb server. The data was analysed using the CONTIN programme and returned a result of ~55% alpha-helical, ~16% beta sheet and ~9% coiled, with the remaining 20% believed to be disordered. This result broadly matches the projected make-up of the construct, as Kv1.1 is ~80% alpha-helical, with the beta sheet component coming from the EYFP tag.

The troughs of in the spectra of protein samples frozen by either method are noticeably less than that seen in the unfrozen samples. This indicates that there is less secondary structure of the frozen sample than the unfrozen sample. Such a finding is not surprising as freezing of protein samples is

known to disrupt the folding of protein molecules (Wolkers et al. 2007). More absorbance is visible in protein samples frozen by liquid nitrogen compared to samples frozen by refrigeration at -20 °C, indicating that storage of samples by freezing in liquid nitrogen preserves more of the protein secondary structure.

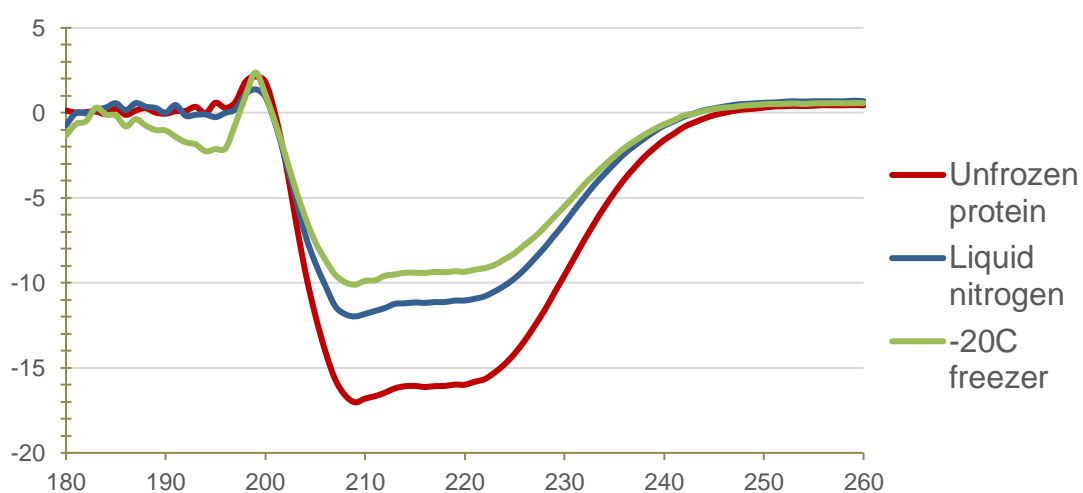


Figure 4.14 – CD spectra of Kv1.1-TY10 in 150 mM NaCl, 50 mM Tris, 10 mM KCl pH 7.4 across 180-260 nm wavelengths. This representative plot contains the troughs in the molar ellipticity at 214 nm and 222 nm, which are characteristic of alpha-helical secondary structure in analysed proteins. Later experiments replaced NaCl with NaF to avoid disruption caused though absorbance by chloride ions.

4.8.2 CD measurement of protein stability in temperature ramp

Temperature ramps were employed in conjunction with CD to investigate the inherent stability of Kv1.1, as well as the difference in its stability when extracted into DDM, SMA and DIBMA. Initial experiments with temperature ramping and CD were conducted using the in-house Chirascan Plus system at the University of Leeds, which was programmed detailed in section 2.4.6.2.

Temperature ramps were conducted using freshly purified DDM, SMA and DIBMA extracted protein (Figures 4.13, 4.14 and 4.15, respectively). At lower temperatures, DDM-extracted Kv1.1-TY10 displayed a curve typical of α helical proteins, as expected, with peaks at 214 nm and 222 nm flattening out as the temperature increased, indicating that the increase in temperature had triggered unfolding of the secondary structure.

While a consistent curve was observed for DDM-extracted protein, SMA and DIBMA displayed a less regular, jagged profile, indicating interference of the signal by the polymer. An α -helical profile could be broadly discerned in all 3 spectra, with flattening of the 222 nm and 214 nm peaks also visible, no concrete conclusions could be made.

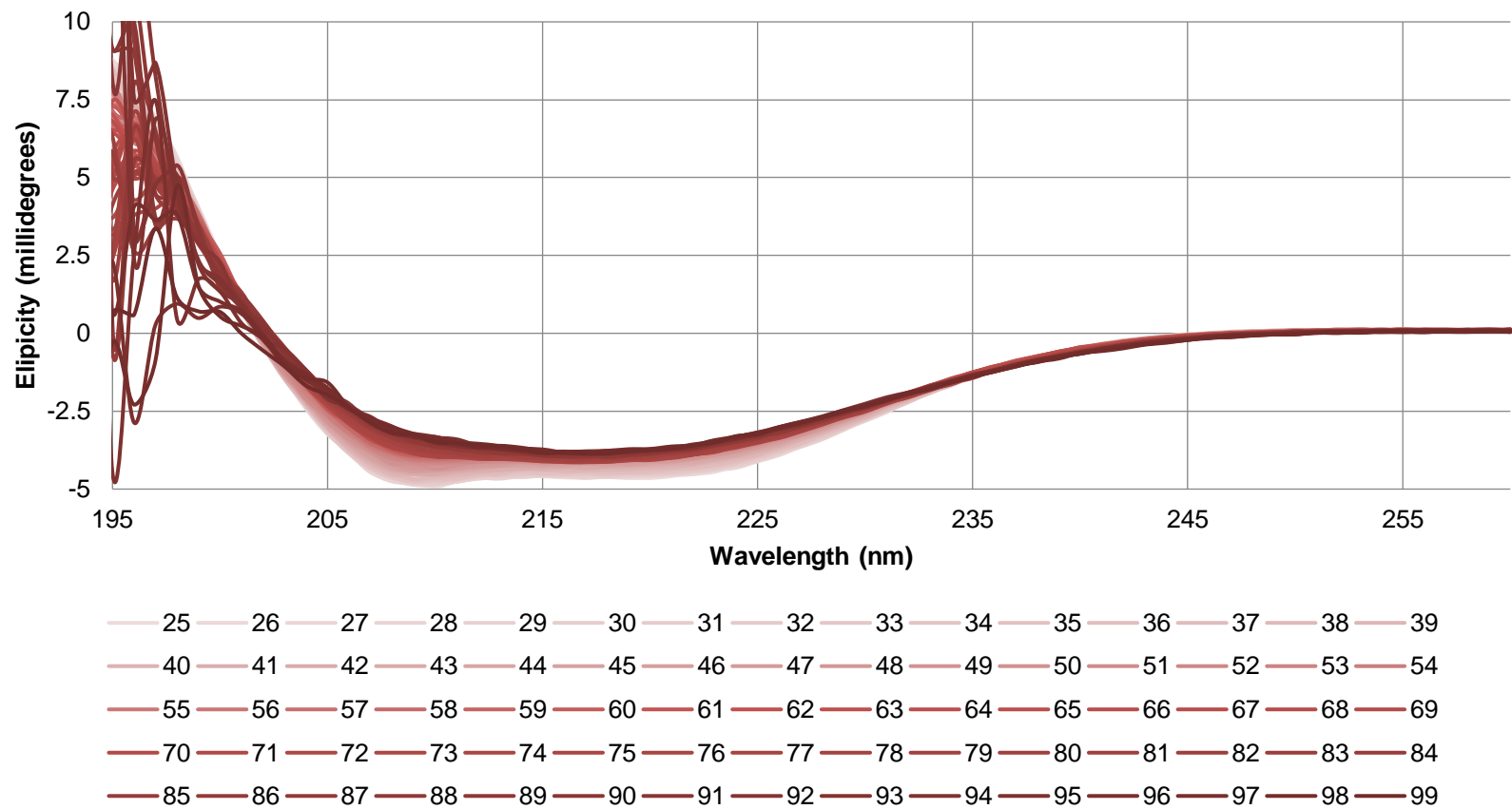


Figure 4.15 – Graph of CD spectra of fresh *K_v1.1-TY10* recovered in DDM, with the profile at ramping temperatures. Each plotted line represents the spectra of the protein at temperatures between 25°C and 99°C, coloured from light pink to maroon.

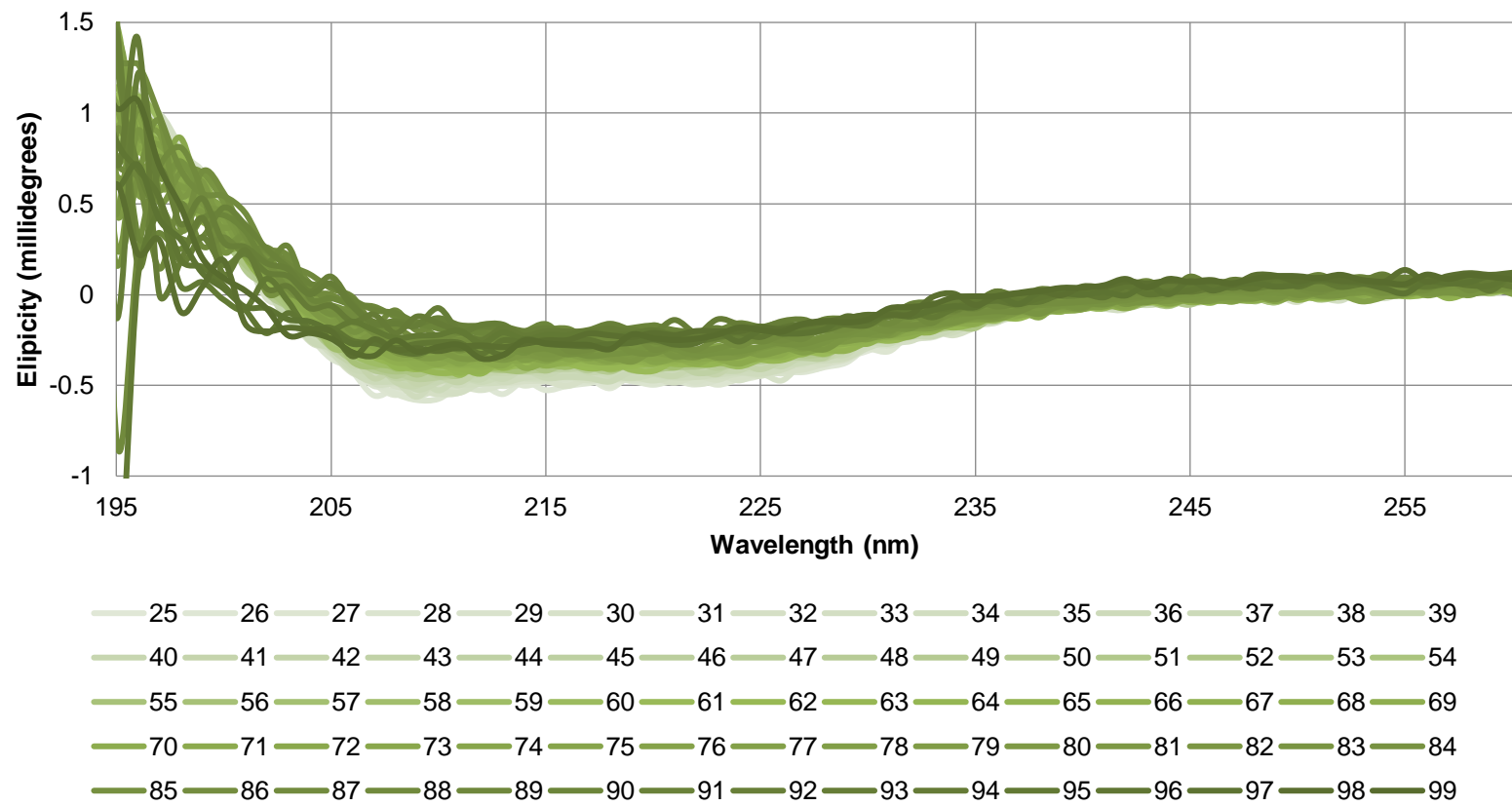


Figure 4.16 – Graph of CD spectra of fresh $K_v1.1$ -TY10 recovered in SMA, with the profile at ramping temperatures. Each plotted line represents the spectra of the protein at temperatures between 25°C and 99°C, coloured from light green to dark green.

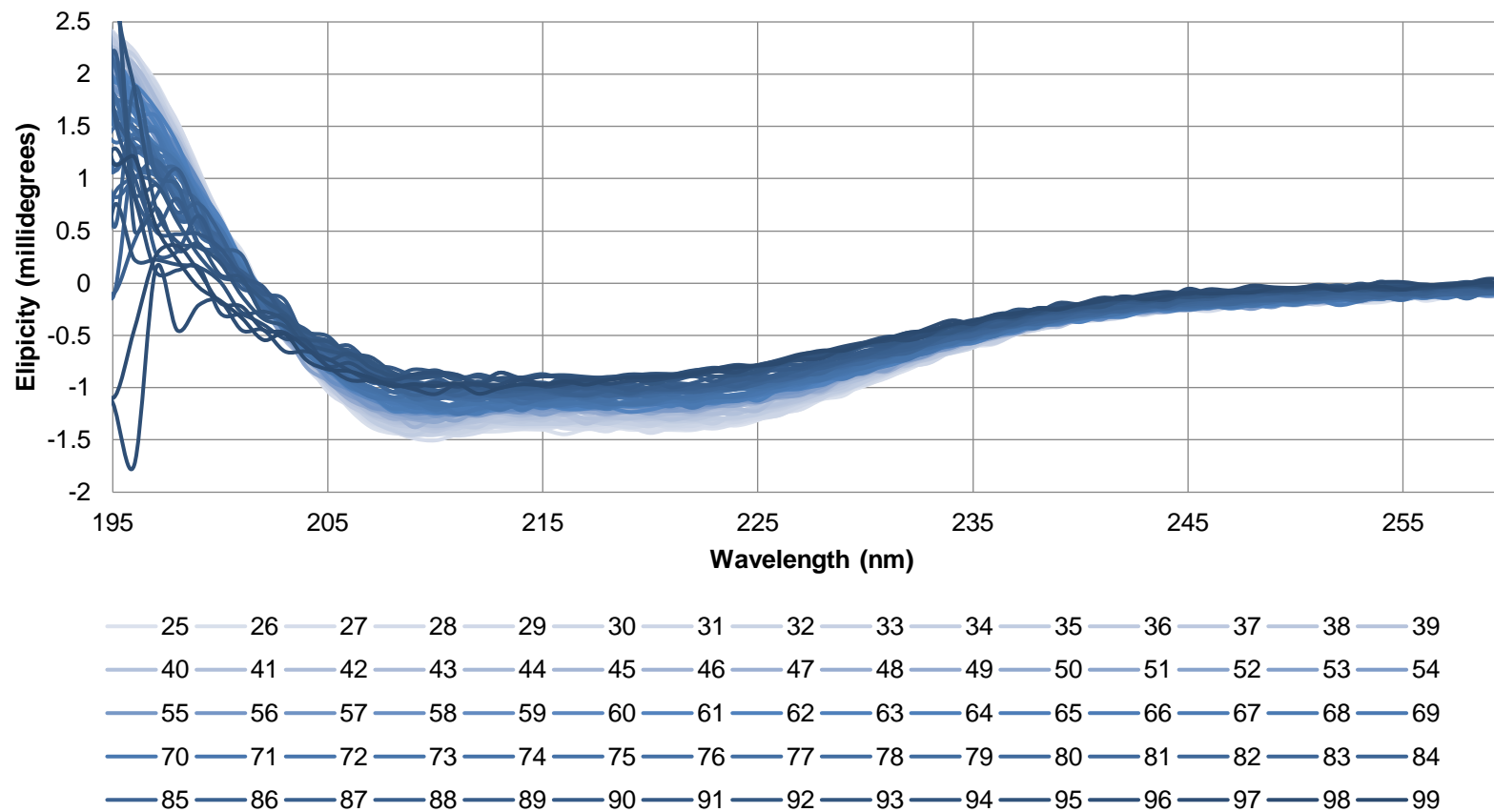


Figure 4.17 – Graph of CD spectra of fresh $K_v1.1$ -TY10 recovered in DIBMA, with the profile at ramping temperatures. Each plotted line represents the spectra of the protein at temperatures between 25°C and 99°C, coloured from light blue to dark blue.

DDM-extracted sample displayed the strongest absorption, with ellipticity reaching values approaching -5 millidegrees for 222 nm wavelength at 25 °C. Both SMA and DIBMA-extracted samples displayed less absorbance, with ellipticity reaching only -0.55 and -1.5 millidegrees, respectively. This may have been a result of interference by the polymers; the jagged-irregular appearance of the SMA and DIBMA-extracted sample data also appears to indicate some interference in the absorption which is obscuring the protein CD spectrum.

As the data for SMA and DIBMA-extracted protein displayed irregularities, the program was redesigned to take readings in triplicate at each time point rather than in singular, with a view to produce more regular, averaged readings. However, this new program proved to have a series of problems which had not initially been recognised. The time required to ramp the temperature to single incremental degrees and allow time to settle resulted in an unrealistically long cycle, as recording absorbances of 5 samples at 75 different temperature points ranging from 25°C to 99°C, with each measurement taken in triplicate, required over 72 hrs to complete. This extended time investment caused a number of issues, most prominently the unreliability of data due to the inability to account for temporally promoted degradation independent of the temperature

Faced with these shortcomings in the initial experimental design, advice was sought from collaborators in the Dafforn group at the University of Birmingham, who lent their experience in analysing membrane protein stability and the use of their JASCO J-810 Spectropolarimeter (see Graph 4.7). On their advice, the wavelength of recorded absorbance was limited only to 222

nm, firstly on the basis that recording at a limited number of wavelengths would speed up the process and significantly reduce the effects of time-based degradation on recorded absorbances. Secondly as the presence of DDM, SMA and DIBMA are all known to absorb light wavelengths between 220 nm and 180 nm, leaving 222 nm the only wavelength associated with secondary structure information that is not disrupted by their presence.

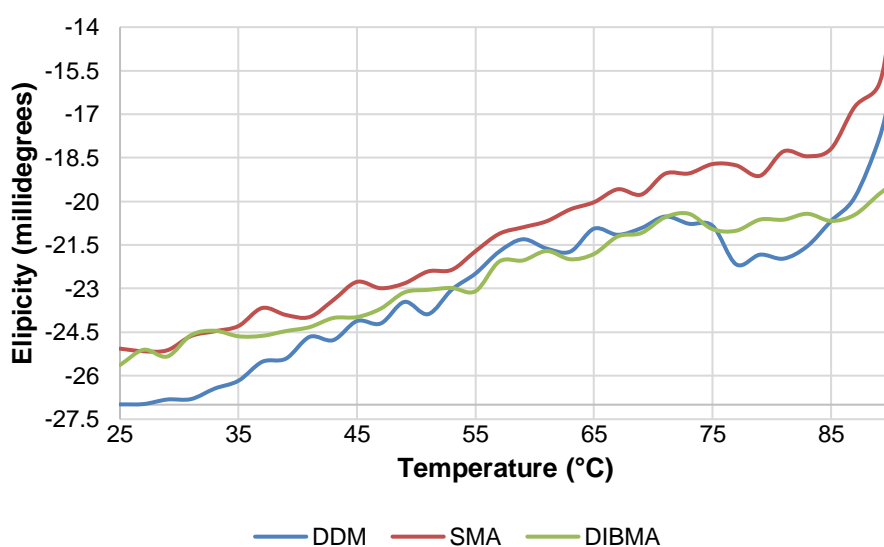


Figure 4.18 – Graph plotting the ellipticity of $K_v1.1$ -TY10 at 222 nm in DDM, SMA and DIBMA across an increasing temperature.

The ellipticity at 222 nm for protein in DDM and SMA is similar, while the DIBMA spectrum remains at a shallow incline across the entire range of temperatures.

4.10 SEC-MALS

SEC-MALS analysis of DDM-solubilised Kv1.1-TY10 was conducted as detailed in section 2.4.4. SEC was conducted over a time scale of 30 min (Figure 4.19). The first peak on the UV spectrum (elution time 8 minutes) was determined to correspond to the folded protein, as the subsequent peak at 10 minutes displayed high light scattering and UV absorption, which is typical of empty detergent micelles (Sahin and Roberts 2012).

The hydrodynamic radius determined from this data indicated a maximum radius of ~4.7 nm from peak 1, or ~16 nm for peak 2. While neither of these matches the anticipated radius of the channel complex, which in reality would be ~6 nm, it is worth noting that MALS is incapable of distinguishing between protein and detergent, meaning that the lipid belt surrounding the protein can skew the result away from the predicted values.

The molecular mass calculated from the MALS data did not match the 340 kDa mass which was predicted for a tagged tetramer. The weights are close to the predicted mass of the untagged tetramer (232 kDa). However as the tag had not been cleaved beforehand, due to the previously documented difficulties with TEV digestion, such a species is unlikely to be present. As such, the results for molecular mass calculation are also inconclusive.

Overall, SEC-MALS was unable to provide a robust description of the Kv1.1-TY10 protein, likely due to the limitations of both the MALS technique, as well as interference from detergent and the EYFP tag.

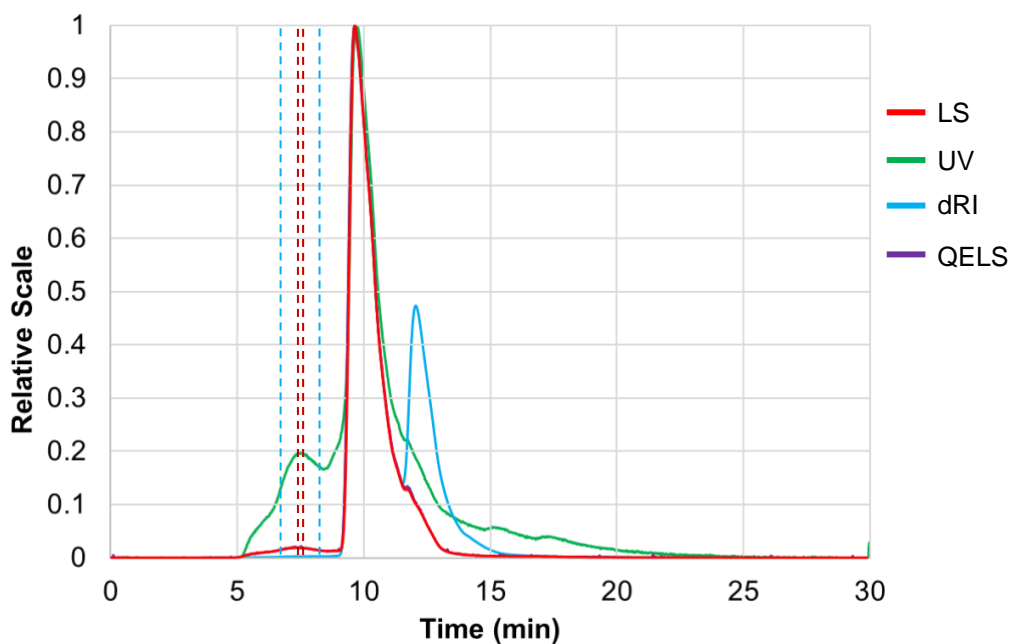


Figure 4.19 – Graph of SEC-MALS data from DDM-solubilised $K_v1.1$ -TY10. Light scattering (LS), UV absorbance, difference in refractive index (dRI) and quasi-elastic light scattering (QELS) of $K_v1.1$ -TY10 extracted in DDM are plotted as a function of time as elution fractions leave the column. LS and QELS are highly similar, with QELS being difficult to observe beneath LS. Peaks 1 and 2, as represented by red and blue dotted lines respectively around the 8 min peak, were the narrow and broad sections of the peak sections of the peak that was analysed for hydrodynamic radius and molecular mass.

5 Structural analysis of homotetrameric Kv1.1

5.1 Background

Electron microscopy is a rapid evolving field, with recent advances allowing cryo-EM to make significant strides in the development of atomic resolution structures (Rawson et al. 2016). Membrane proteins have not been excluded from this revolution, with many larger membrane protein complexes, such as PIEZO1, being determined to atomic resolution (Ge et al. 2015). With the recent construction and activation of the Astbury Biostructure Laboratory (ABSL) on-site at the Faculty of Biological Sciences, cryo-EM was a natural fit for this project in its goal to investigate the structure of Kv1.1 and its interactions with membrane scaffolds and inhibitors.

Specimens of single particles negatively stained with uranyl acetate was used for preliminary structural investigations. While negative stain electron microscopy is unable to provide the atomic resolution necessary to investigate the specific interactions between a protein and smaller drug molecules, it is possible for it to resolve flexibility in structure, as well as interactions with other molecules, such as associated proteins (subunits, toxins, etc.) and lipid nanodiscs (Burgess et al. 2004, Akkaladevi et al. 2013). Additionally, micrographs of proteins in negative stain can also allow the quality of samples, such as the presence of aggregation and the homogeneity of sample, to be inspected relatively quickly, making it an excellent technique for screening samples (Zhang, L. et al. 2013).

5.2 Negative stain electron microscopy

5.2.1 Grid optimisation

Samples of Kv1.1-TY10 purified via IMAC were taken forward to structural study via negative stain electron microscopy. The presence of both EYFP tag of Kv1.1-TY10, as well as DDM or SMA/DIBMA in prepared samples made it difficult to accurately determine concentrations of protein. This created a challenge for the production of negative stain grids, as an accurate concentration helps to determine sensible dilutions of the protein ahead of grid production. This was addressed by creating a series of dilutions for each sample, ranging $\times 10$, $\times 25$, $\times 50$ and $\times 100$ diluted, using filter sterilised dialysis buffer from the dialysis step following IMAC purification.

Each diluted sample was then applied to a negative stain grid and the density and quality of protein in each was assessed visually in EM. The quantity of protein was investigated through visual analysis of particles under negative stain. If micrographs displayed particles too densely packed to be easily differentiated, the dilution of sample was deemed to be too high. Further dilutions of up to $\times 250$ and $\times 500$ were made if grids with $\times 100$ dilute protein were found to have excessively high concentrations of protein. Protein quality was assessed on a case-by-case basis, with features such as large, irregular structures used as indicators of protein aggregation and the predominance of small, regular particles used as indicators of better-quality samples.

Grids were made using Kv1.1-TY10 extracted in DDM, SMA and DIBMA and assessed visually to gauge their individual suitability to negative stain. Both DDM and SMA extracted materials generally displayed consistently sized

particles with little sign of aggregation. As such DDM and SMA extracted sample were suitable for collection of data, as detailed in section 5.2.2. Grids featuring DIBMA extracted Kv1.1 predominantly displayed large, globular species typical of aggregated protein.

In the first instance, screening of negative stain grids was conducted on a T12 electron microscope (FEI) using a Gatan CCD camera. Grids were screened and evaluated on a number of properties, including: depth of grid staining deep enough to provide contrast, but light enough to preserve detail; particles being separated and easy to discern individually (i.e. monodispersed); finally, particles displaying consistency in size and overall shape.

5.2.2 Data collection

Data was collected on samples of IMAC-purified Kv1.1-TY10; initial data collection was conducted using DDM-solubilised samples. The views obtained from the first batch of grids, generated through 20x dilution onto the grid surface and coated with 1% uranyl acetate, displayed high density, though particles were sufficiently monodispersed to allow individual particles to be discerned (Figure 5.1a). Most of the observed particles displayed similar dimensions, with acceptable levels of staining. A dataset of 140 micrographs was collected at 30,000 x magnification for processing on a Technai T12 microscope operating at 120Kv. 2307 particles were manually selected from a subset of 90 micrographs; these particles were then sorted by their appearance into classes, with each class representing a particular view of the molecule, which were then averaged to produce a consensus image of the particular class (Figure 5.1b).

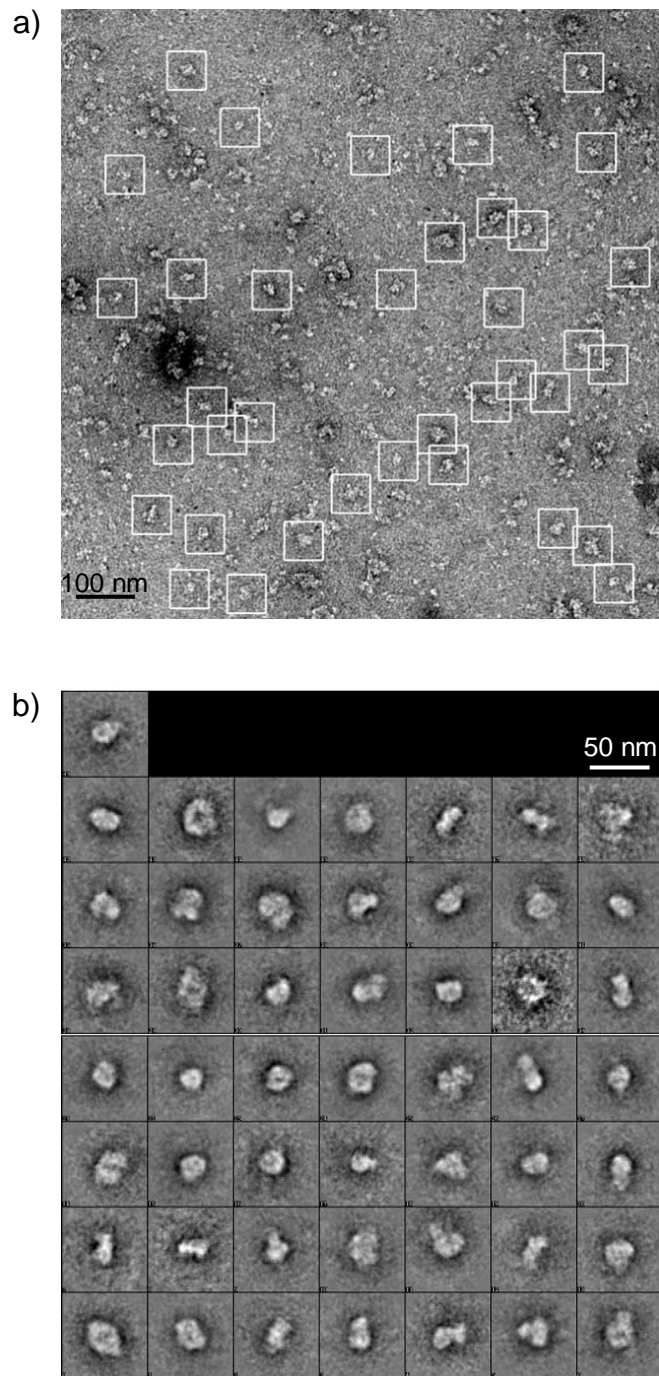


Figure 5.1 – Example of negative stain micrograph from *K_v1.1-TY10* extracted in DDM and coated in 1% uranyl acetate (a) and class averages produced from processing of selected particles (b).

Later negative stain data sets were collected on the in-house F20 microscope (FEI) using a CMOS detector. This set up permitted larger micrographs to be recorded (due to the increase in camera size), with higher magnifications possible, due to increased microscope stability. The data were processed in RELION to look for differences based on new developments in algorithms, in particular the maximum likelihood procedures that better estimates the noise in the images (Rawson et al. 2016). Although multiple negative stain data sets were collected to assess protein quality, only a few representative examples are presented here.

5.2.3 Data processing

5.2.3.1 DDM-solubilised Kv1.1-TEV-EYFP-His₁₀

An electron density map based on images of purified Kv1.1 collected using the T12 microscope was generated using the program IMAGIC to classify particles and EMAN2 to generate an initial 3D reconstruction. The resulting reconstruction was generated using the standard 3D reconstruction procedure of projection mapping and particle assignment (Tang, G. et al. 2007). 2307 manually selected particles were used for structure generation.

To generate the model both 4-fold (C4) and no symmetry (C1) were applied with the 4-fold symmetric processed data; regardless of the imposition of symmetry, the C1 data still displayed 4-fold symmetric properties (Figure 5.2). The homology model of Kv1.1 based on the Kv1.2-Kv2.1 chimera produced by Phyre2 was fitted into the EM map using the default Chimera map fitting tool. and appears to fit very well into the global shape of the structure (Pettersen et al. 2004, Kelley et al. 2015).

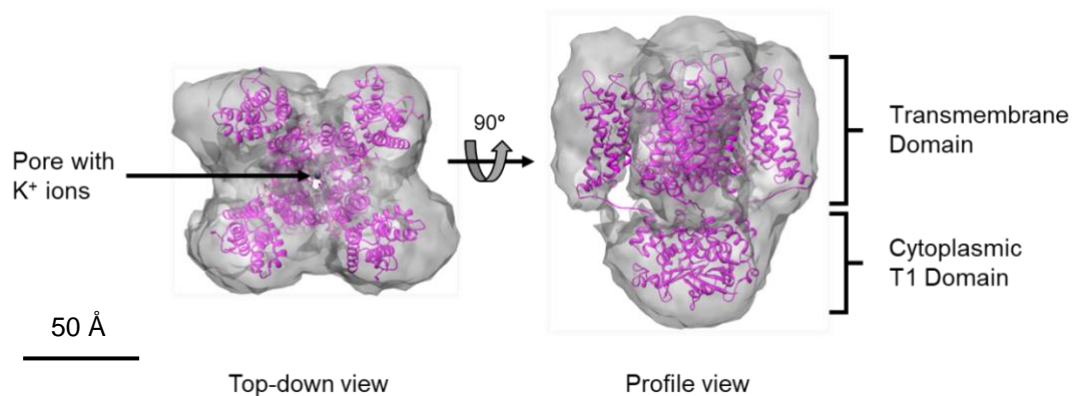


Figure 5.2 – Negative stain EM structure produced from processing of micrograph dataset of DDM-solubilised $K_v1.1$ -TY10. Electron density from data processing is represented in grey. A cartoon representation of a $K_v1.1$ homology model generated by Phyre2 from the *Rattus norvegicus* $K_v1.2$ -2.1 chimera structure, represented in pink, has been fitted into the density map (Banerjee et al. 2013, Kelley et al. 2015).

The $K_v1.1$ homology model and the electron density map seen fitted in Figure 5.2 match strongly, indicating that the particles selected in the micrographs and classes subsequently picked belong to $K_v1.1$ -TY10. No density relating to the C-terminal EYFP can be seen in the electron density, however. This is likely a result of class averaging removing flexible elements, as the linker connecting the C-terminal tags is unstructured and likely to allow the EYFP domain to move freely.

5.2.3.2 SMA-solubilised Kv1.1-TEV-EYFP-His₁₀

Negative stain analysis of samples was also used as a method to visually assess Kv1.1-TY10 samples to check for signs of aggregation or degradation. Particles for the production of a model of the channel complex in SMA were picked manually in the EMAN2 Boxer program. 9909 particles were picked across all 140 micrographs. Particles were processed to produce two separate data stacks: one comprised all 9909 particles, and a second consisting of a subset of 6786 particles which were inspected visually to have the highest detail of particles and lowest background noise. Models were generated from both sets without imposing symmetry. Unlike the model determined from DDM-solubilised sample, the models were incomplete, showing inconsistency in the sizes of different domains, with large holes in the channel.

C4 symmetry was then applied in a second processing run of both particle stacks. This adjustment resulted in structure which more accurately resembled the predicted structure of Kv1.1. The model best resembling the homology model was produced from the particle stack composed of the 6786 particles partitioned from the complete set (Figure 5.3). Although the resulting model appeared consistent with the anticipated structure of the complex, the imposition of 4-fold symmetry may have introduced bias into the resulting map.

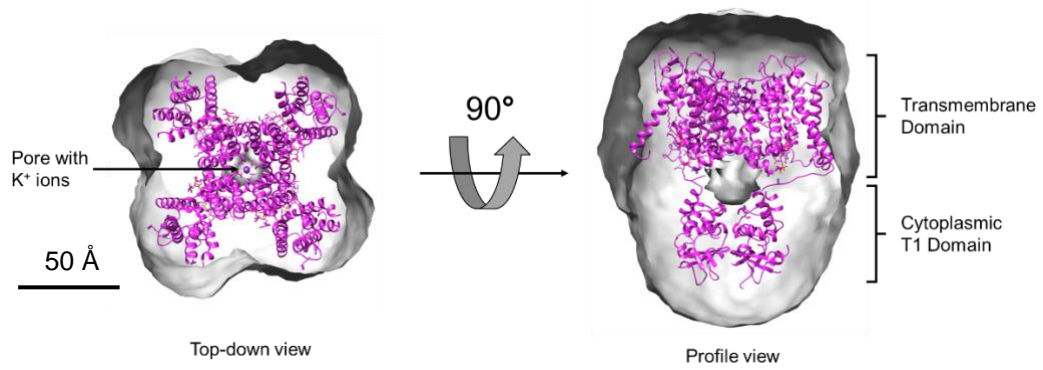


Figure 5.3 – *Cartoon representation of map generated from negative stain data of SMA-solubilised Kv1.1-TY10. A top-down view is represented on the left, with a 90° rotation to a side view on the right. A homology model generated from the sequence of Kv1.1 using the Phyre2 server has been fitted into the interior of the map to illustrate its resemblance to the predicted structure.*

5.2.3.3 DIBMA-solubilised Kv1.1-TEV-EYFP-His₁₀

A dataset of micrographs was collected from grids produced using DIBMA-solubilised samples of Kv1.1-TY10. The protein displayed signs of aggregation and unfolding, with few distinct particles visible on the grid. As a result, selection of particles for processing was difficult and ultimately too few were available to make processing of data viable.

In order for DIBMA to be used consistently for future structural studies and characterisations, the polymer must be able to extract proteins in a folded, stable state. The initial data from negative stain does not indicate this to be the case, although further optimisation and study will be required to fully discount DIBMA.

5.3 Cryo-electron microscopy

5.3.1 Grid preparation

After initial negative stain analysis, along with the low-resolution structures obtained, there was sufficient confidence in the quality and stability of DDM and SMA-extracted samples to move forwards to cryo-EM. DIBMA-extracted samples were also analysed in some instances to ensure that issues with protein stability were not a result of negative stain sample preparation practices.

In the first instance, a range of different grid types were tested (see Table 2.7 for details). Graphene oxide grids of SMA-solubilised sample were prepared using the Leica EM GP with the standard program employed by Dr. Stephen Muench. Grids were prepared in pairs at concentrations of 3 and 4-fold dilution from the IMAC-purified sample. These grids were stored in liquid nitrogen ready for later analysis.

5.3.2 Grid Screening

Initial screen was performed in-house using the F20 microscope fitted with a CCD camera, which at the time had poorer signal-to-noise than a direct detector. Moreover, all images were collected manually in low-dose mode, which combined with difficulties in grid loading caused a low throughput and a shortage of data for analysis. Screening of grids later moved to the ABSL on Krios microscopes 1 and 2. This allowed for more rapid screening of grids and access to means for more rapid data collection.

Unfortunately, many of the screening images taken in-house during the early stages of the ABSL electron microscopy facility operation was lost as a result of file corruptions and selection of incorrect formats for saving, which impeded optimisation of grid conditions.

5.3.3 Data collection and processing

SMALP-solubilised protein was taken forward to cryo-EM analysis on the F20 microscope in Leeds with the assistance of Dr. Rebecca Thompson. 10, 20 and 50-fold dilutions were created and examined on the microscope. It was determined that 20-fold dilute samples were best for analysis (Figure 5.4). These grids were submitted to Diamond, where 3000 micrographs were taken on a Titan Krios fitted with a K2 direct electron detector.

The micrographs displayed a number of discrete particles, although there were signs of ethane ice contamination, likely as a result of errors in grid preparation or grid storage. This may have been a result of low salt concentrations causing SMA polymer to stick together and to the his-tags of the proteins. Particle selection was carried out on a subset of 100 micrographs and class averaging was conducted by Shaun Rawson (Figure 5.5). No suitable classes could be produced however and no means of autopicking particles computationally could be determined. Given the poor quality of the resulting classes, particularly given the low signal-to-noise visible in the images, it did not seem justifiable to further process the data.

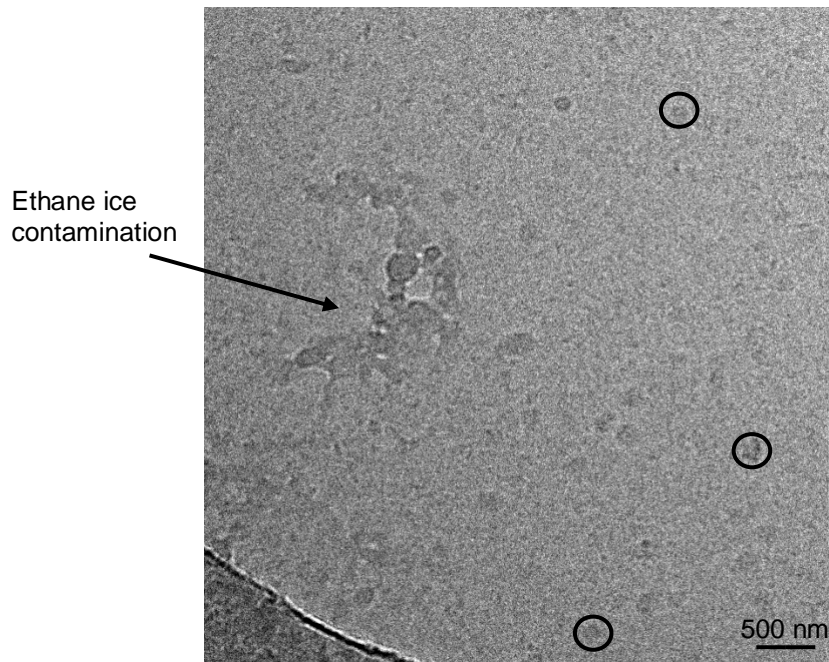


Figure 5.4 – Representative image of micrographs taken of SMA-solubilised sample screened at the Diamond Synchrotron electron microscopy facility. Grid screening and micrograph collection was conducted on Titan Krios electron microscopes. Examples of possible protein particles have been circled in black. The quality of sample on the grid was poor, with ethane and non-vitreous water ice contamination, as annotated.

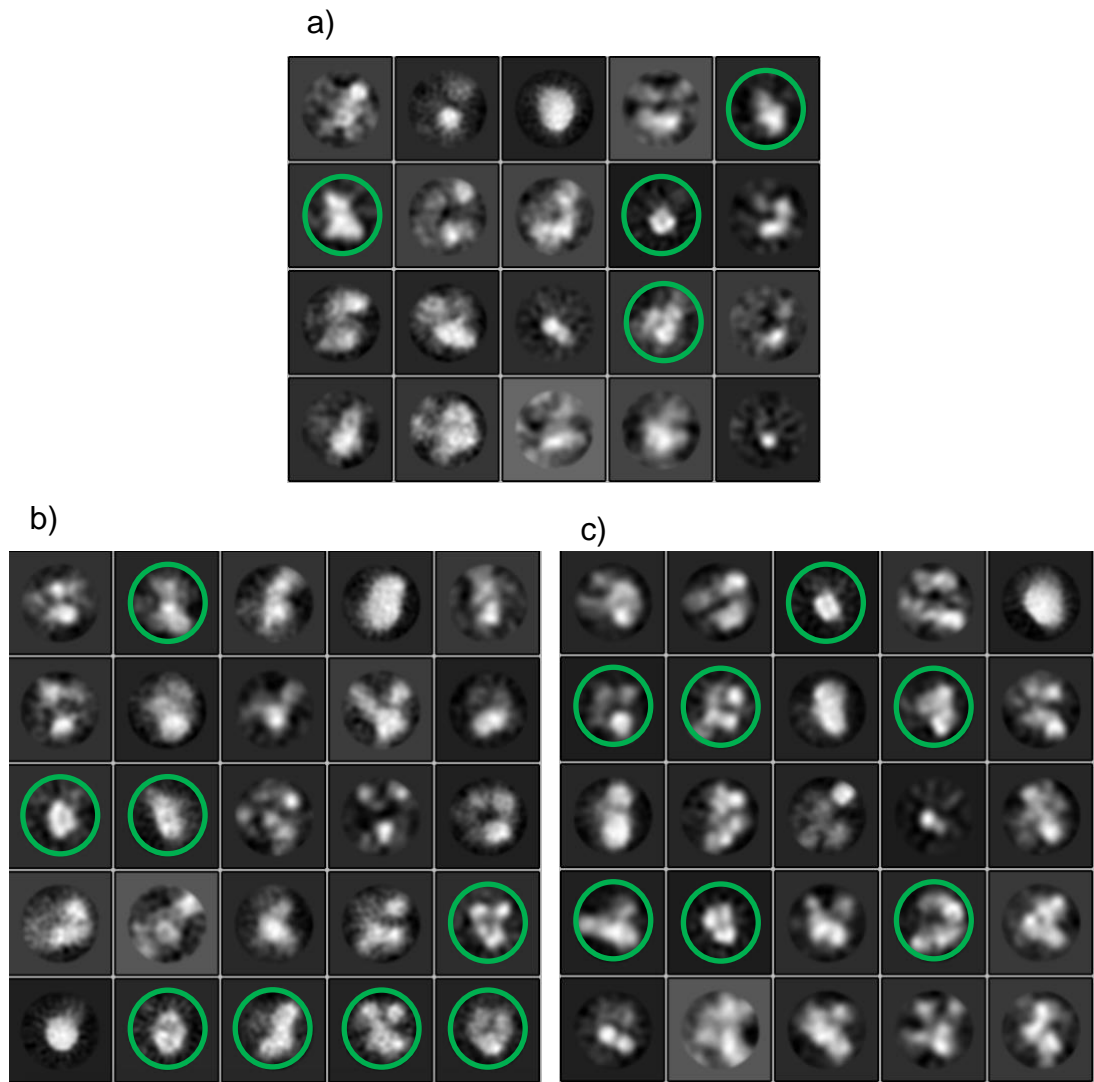


Figure 5.5 – Classes generated with (a) and without a reference model (b and c) from autopicked cryo-EM data of SMA-solubilised sample. Class averages which display more defined shape have been outlined in green.

Classes generated without a reference model (a) do not show any features of note. Classes generated with homology model used as reference (b and c) show slightly more consistency, with some potential, however these were in the minority, indicating that the dataset was not of sufficient quality to justify further processing.

5.4 Negative stain EM of K_v1.1 co-incubation with α -DTX

A number of EM studies have used small molecule inhibitors to stabilise membrane protein complexes. In addition to being more stable it can also inform on small molecule binding. Therefore, to try and improve the quality of the resulting reconstruction, K_v1.1 was studied in the presence of α -DTX.

K_v1.1-TY10 was recovered from stably transfected HEK 293S GnTI⁻ cells grown in adherent culture. Protein recovery was carried out using DDM following the protocol detailed in section 2.3.2. The concentration of protein was determined to be 0.5 mg/ml through 260 nm absorbance using the DS11 nanodrop. α -DTX, supplied as a 1 μ M stock in PBS, was diluted to 10 nM through a 10x dilution into dialysis buffer. 27 μ l of K_v1.1 was applied to 3 μ l of 10 nM toxin to produce a final concentration of 1 nM. This was then taken forward to negative stain electron microscopy, with a 25-fold dilution tested, however the micrographs proved to have poor background, which was believed to have resulted from an excess of α -DTX in the solution, leading to issues with staining.

An alternative strategy was developed to remove excess α -DTX from the solution prior to staining. The concentration of α -DTX was reduced 10-fold and

excess toxin was removed through dialysis in 6-8 kDa cut-off GeBAflex tubes (Scienova); this cut-off limit was selected as it most closely matched the 7 kDa molecular weight of α -DTX (Tytgat et al. 1995). Dialysis was repeated 3 times, with samples recovered after each step. Each dialysis step lasted 10-15 minutes. The 3rd dialysis sample was tested first through negative stain electron microscopy of a 2-fold diluted sample (Figure 5.6).

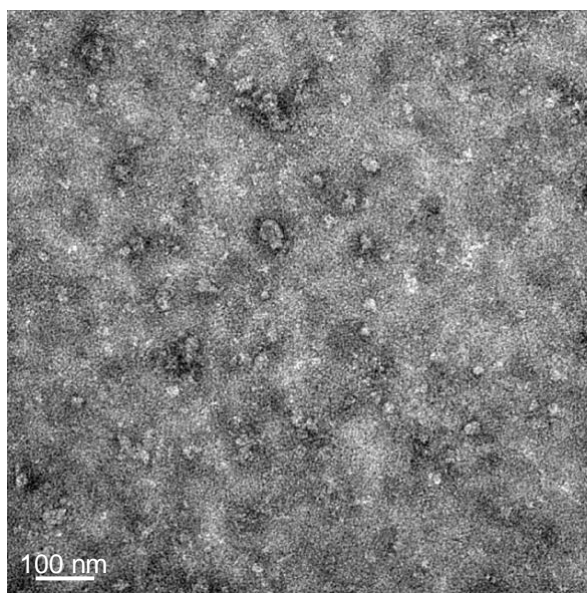


Figure 5.6 – Representative micrograph of DDM-solubilised $K_v1.1$ -TY10 co-incubated with α -DTX. The grid displays poor signal-to-noise with an inconsistent background. This is likely due to excessive quantities of toxin molecules, which due to its peptidic nature will also be stained by the uranyl acetate.

While the quality of the micrograph, shown in Figure 5.7, proved to be a substantial improvement over the initial attempt, the micrograph appeared to be over-populated. A further grid was created a 3-fold dilution of the sample to reduce the density of particles (Figure 5.7).

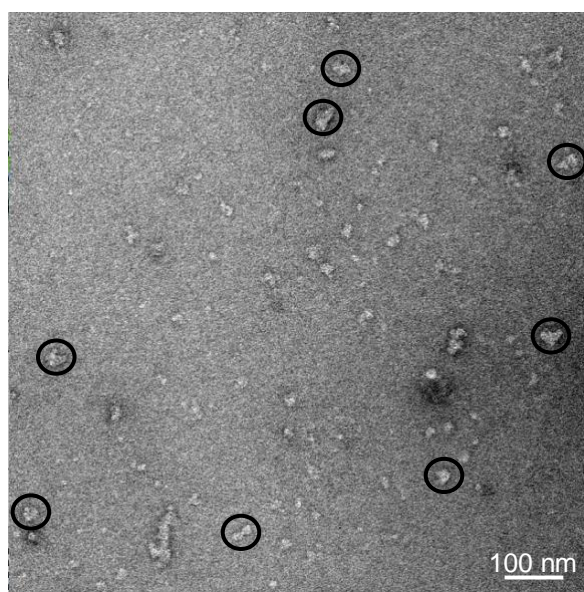


Figure 5.7 – *Representative micrograph of diluted Kv1.1-TY10 co-incubated with dendrotoxin- α . This grid displays improved background over Figure 5.7, with particles more easily discernible from the background. Examples of particles which display good contrast with the background, defined edges and sufficient distance from other particles have been outlined.*

The quality of the observed micrograph in Figure 5.8 images was deemed of high enough warrant the collection of a data series – in total, 132 micrograph images were collected for processing. This improvement is likely a result of dilution of the peptide toxin, resulting in lower staining of the grid. No class averages could be generated from the collected particles using EMAN2, with no distinct shapes identified in the processed data. This might have been the result of excessive background making the edges of particles more difficult to determine with consistency, leading to particles becoming more difficult to classify.

Two cryo-electron microscopy grids were generated using undiluted 0.5 mg/ml Kv1.1 using the Leica EM GP automatic plunge freezer. 2 further grids were also made using the 3rd dialysis sample used in the successful negative stain trial above. These grids were placed into storage in liquid nitrogen for later analysis. However, due to the poor quality in the previously analysed negative stain data and limited time remaining in the final year of the project, it was not deemed worthwhile to screen these grids.

6 Discussion

6.1 Expression of K_v proteins in HEK cell culture

6.1.1 Construct production

Sanger sequencing of the plasmids extracted from transformed bacterial cells confirmed that the desired modifications had been made in the cases of K_v1.1-EYFP-His₆, K_v1.1-TEV-EYFP-His₆ and K_v1.1-TY10. The native *KCNAB2* gene was also successfully cloned out of foetal brain cDNA and inserted into pcDNA3.1, with a modified KCNAB2-cMyc-His₆ plasmid made later on. The fluorescence observed following transfection with the EYFP-tagged K_v1.1 constructs confirmed that the constructs carried by plasmids had been expressed, however such a result only confirmed that the fluorescent tag had been expressed and correctly folded.

Later assessment of purified protein via CD spectroscopy indicated that the protein displayed a secondary structure profile matching that expected of K_v1.1-TY10, corroborating that the protein was correctly folded. Mass spectrometry also positively confirmed that the protein had been overexpressed in the transgenic cell line. Negative stain EM of extracted protein produced an electron potential map resembling the expected structure of K_v1.1, indicating that a tetrameric channel was formed. Together, these results strongly indicate that the constructs were expressed in a correctly folded state, with the tetrameric channel forming successfully at the membrane.

6.1.2 K_vβ2 co-expression

Attempts to generate a cell line for co-expression of K_v1.1 & K_vβ2 constructs were less successful than overexpression of K_v1.1 alone. Cells did not thrive long term in the presence of G-418, indicating that they either did not take up the plasmid, did not retain the plasmid for a long period, or suffered one or more fatal side-effects from uptake of the pcDNA3.1 plasmid. A repeat of transfection with G-418 concentrations reduced to 100 ng/μl, in line with results of the G-418 killing curve, did not improve viability of the cells.

Further work must be done to establish what factors are causing doubly transfected cells to die. Placing doubly transfected cells into medium without antibiotic, as a positive control, would be advisable. If cells continue to die in the absence of antibiotic, this would indicate that cells are suffering ill-effects from the presence of the second plasmid, with death occurring independently of the presence of G-418. If cells survive, this would indicate the neomycin resistance gene encoded by the plasmid had failed to express, in which case it may be advisable to transfer the *KCNAB2* gene out of the plasmid and into a new vector with functional antibiotic resistance.

6.1.3 Suspension culture of HEK cells

Experimental trials of suspension cultures for HEK 293S GnTI^r were able to identify a number of conditions in which cells would thrive and replicate. Initial difficulties in the culturing of cells in DMEM were corrected through the introduction of additional serum to the medium, indicating that the calcium ion content of 10% FBS medium is not high enough to promote excessive clumping of cells. The addition of 2.5% (w/v) primatone and 0.2% (w/v)

pluronic acid were unable to achieve the same effect, indicating that the issues experienced were not the result of apoptosis, nor shearing of the cells.

The cell culturing protocols developed during the course of this project provided reproducible methods for large scale culture of HEK cells. This was crucial for generating the quantity of protein required for structural study of the proteins. The ability to produce K_v1.1 in its native organism provided additional confidence in the quality of the protein going forward into subsequent steps.

The quantity of pellet recovered from suspension culture per unit volume of medium used was equivalent to the quantity produced by adherent cell culture. Given that suspension cell culture often required higher investment of time and resources to conduct, it may be more efficient to revert to large scale adherent protocols in order to develop large quantities of cells more effectively. These shortcomings could be addressed in future by testing growth and expression in other vessels for human cell culture, such as bioreactor bags, roller flasks or larger scale adherent culture flasks.

Initial challenges with cell growth and survival in DMEM during suspension culture were remedied by increasing the concentration of bovine serum in the medium from 1% (v/v) to 10% (v/v), in line media used in adherent cultures. Based on these results, it would be recommendable to begin suspension culture with related protein using serum concentrations at 10% (v/v).

Many recent methodology papers on suspension culture techniques proscribe the use of expensive serum-free commercial suspension media, such as FreeStyle 293 or EX-CELL, with DMEM recommended only as a supplement to either, rather than a primary medium (De Los Milagros Bassani Molinas et

al. 2014, Goehring et al. 2014, Büssow 2015). It would likely benefit the scientific community at large that more research papers be published describing more cost-effective suspension protocols based on DMEM. This should be tempered however, by stressing the need to experiment with different medium types to identify the best protocol for expressing each protein.

The recently published TRPC3 and TRPC6 channel structures both feature an alternative transfection regimen involving the viral BacMam vector for introduction of transgenic DNA to the host cell (Tang, Q. et al. 2018, Goehring et al. 2014). This approach may be worth adopting for experimentation, as short-term transfection in advance of harvesting might improve expression and cell viability by reducing stress on cells during early stages of culture.

6.2 Protein purification and characterisation of K_v proteins

6.2.1 Methods for primary purification

The small-scale expression trials conducted early in this project, in combination with fluorescence microscopy, were able to confirm the presence of transgenic $K_v1.1$ expression. Polyhistidine-tagged protein extracted by detergent and maleic acid polymers were each purified on both nickel and cobalt-charged IMAC resins, with cobalt displaying the highest retention of protein.

This result was unsurprising, as cobalt-based IMAC resins typically bind more broadly than nickel-based equivalents, leading to greater quantities of protein

in elution fractions, but ultimately less pure (Bornhorst and Falke 2000). As a result, effective secondary purification is essential in removing contaminants which follow the polyhistidine-tagged Kv1.1 through the process. However, the later difficulties experienced with TEV cleavage and SEC have rendered this approach less effective.

Based on the setbacks experienced with secondary purification, experimentation with primary purification techniques could be employed to try and achieve a purer sample than has so far been accomplished with IMAC. Use of antibody-based resins with specificity for polyhistidine, GFP/EFYP or against Kv1.1 itself could be employed against the constructs which have been created to date. Further constructs with tags specifically designed as antibody epitopes, such as FLAG and nanotag (nTag), could also be used by modifying the construct with further tags. However, resins charged with antibodies are typically significantly more expensive than IMAC resins, making this approach less cost-effective.

6.2.2 Methods for secondary purification

6.2.2.1 TEV cleavage and reverse purification

Identifying an efficient and cost-effective method for secondary purification of Kv1.1-TY10 was less straightforward than primary methods. Initial plans to reverse purify the protein on IMAC columns by removing the C-terminal tag using TEV digestion were hindered by an inability to reproduce the positive results observed in initial TEV cleavage trials. Successful digestion in initial trials may have been false positives caused by unfolding protein.

This may be due to the cleavage site being obscured by the flanking Kv1.1 monomer and EYFP. If this hypothesis is correct, the issue could be addressed by modifying the plasmid to add linker sequences ahead and behind the TEV cleavage site, limiting the chance of other domains obscuring the site. The early purification studies under which positive results for TEV cleavage were observed were not coupled with CD spectroscopy, thus it is unknown if the protein was fully folded in these earlier instances. If the TEV site is indeed being obscured by neighbouring domains, this could be addressed by modifying the Kv1.1-TY10 plasmid to extend the linker sequence both upstream and downstream of the cleavage site.

6.2.2.2 Size-exclusion chromatography

Applying SEC as a secondary purification step in the preparation of the protein did not supply any visible results in SDS-PAGE or UV spectroscopic analysis of samples. It is possible that the Superdex 200 column and/or Äkta rig being used might be responsible either for binding the protein non-specifically and retaining, or a result of protein denaturation and precipitation leading Kv1.1 eluting in earlier fractions off of the column. It is also possible that protein was diluted and became difficult to detect if the amount loaded onto the column was low in the first instance.

6.2.3 Protein characterisation

6.2.3.1 Mass spectrometry

Protein identification of both Kv1.1, as well as a series of prominent contaminant bands from primary IMAC purification provided some insights

into the purification products. Most of the contaminating bands corresponded to proteins involved in protein folding/translocation (such as Hsp70) or associated with DNA.

It should also be noted that Kv1.1 was prominently represented in fragments discovered in protein ID of band B3 (see Appendix 8.3.4). This is potentially significant, as the mass of this band is ~58 kDa, which corresponds to the expected mass of monomeric Kv1.1 following TEV cleavage. This points to the possibility that some of the product proteins might have lost their C-terminal tag, possibly through degradation or truncation of expression.

The presence of a fragment aligning with the sequence of Kv1.3 was initially greeted as an exciting development, as it was taken to point to the presence of heterotetrameric channels forming between Kv1.1-TY10 and Kv1.3 expressed endogenously by HEK 293S cells. However, this was tempered by the observation that only one fragment attributable to Kv1.3 was unique to it alone; all other fragments found in protein ID which aligned with KCNA3 also aligned with homologous regions of KCNA1, making it difficult to be certain how well represented Kv1.3 is represented in purified samples.

The later realisation that the detected deamination of what was initially identified as Q188 residue of Kv1.3 could be alternately explained as a misidentification of the E121 residue of Kv1.1 lead to the abandonment of this explanation. It is therefore thought highly unlikely that Kv1.3 is present in the purified protein samples that were screened.

6.2.3.2 Circular dichroism

The CD spectra of IMAC purified Kv1.1-TY10 indicated that the protein was folded and had a proportion of secondary structure expected for the protein, as well as included tags. The alignment of the predicted secondary structure content of the homology model with the results of CD analysis is compelling.

It is difficult to say with certainty how accurate analysed CD data is, however, particularly because the protein samples used could not be purified further by any secondary purification methods which were attempted. As a result, interference by contaminating species cannot be entirely ruled out. CD spectroscopy should therefore be repeated once a method for producing purer sample has been developed.

6.2.3.3 SEC-MALS

The results of SEC-MALS did not match up well with those that we anticipated from our predictions about the Kv1.1 complex. MALS is inherently limited to discrete complexes and cannot differentiate between proteins and the lipid belts that surround membrane-spanning regions, making the hydrodynamic radius a poor metric for determining the boundaries of the complex without supplementary data (Sahin and Roberts 2012).

More accurate estimations of the dimensions of the complex will require the application of other techniques. Small-angle neutron scattering (SANS) is a good candidate for approaching this topic, as it provides means of separately assessing the radius of different species, such as the proteins of the channel

complex as well as the lipids and detergent of the vesicular belt surrounding the membrane-spanning region.

6.3 Structural analysis of homotetrameric K_v1.1

6.3.1 Negative stain electron microscopy

The structure generated from particles observed on DDM-solubilised samples of K_v1.1-TY10 matched well with the homology model of the tetrameric K_v1.1 complex. The appearance of 4-fold symmetry in the model without the imposition of symmetry during processing was particularly encouraging. Based on this result, pursuit of a cryo-EM structure in DDM could produce materials suitable for publication in future.

Additionally, the successful generation of a structure from negative stain micrographs of SMA-solubilised protein provides further evidence that K_v1.1 is stably extracted by the polymer. This also constitutes a good avenue for further study, as a human membrane protein structure would be a novel result and a strong candidate for publication.

The inability to produce a structure from DIBMA-solubilised sample was in line with results observed in CD data indicating that the DIBMA polymer is substantially less optimal for extraction than DDM or SMA. The reduced stability of K_v1.1 in DIBMA is the likely cause of the difficulties in producing data of sufficient quality for development of a structure.

6.3.2 Cryo-electron microscopy

As negative stain analysis has displayed some promise, cryo-EM analysis of samples was the logical extension of those studies. Although higher resolution

cryo-EM has additional challenges in the production of grids, such as blotting and freezing conditions, the potential to generate higher resolution maps makes it an inviting technique.

A large number of cryo-EM grids were produced with a series of grid types across a series of blotting parameters, scaffold types and concentrations. However, screening and optimisation of procedures for improvement of datasets were hampered by early technical difficulties at the ABSL electron microscopy facility.

Although a large dataset was collected from SMA-solubilised materials at the Diamond electron microscopy facility, the quality of the grids and subsequent micrographs were not sufficient for the generation of a high-resolution map. Future efforts towards the development of cryo-EM datasets could be improved with new technologies, for example phase plates and direct spraying of samples to grids.

6.3.3 α -DTX co-incubated sample

The addition of α -DTX to protein samples resulted in grids with high quantities of background stain which were difficult to analyse. This was likely due to ineffective removal of excess toxin during post-incubation dialysis, as the high affinity of α -DTX for Kv1.1 would make shedding of toxin back into solution unlikely. Longer dialysis times would therefore be advisable to remove excess of α -DTX.

6.4 Final Comments

Membrane protein research is commonly affected by the particular challenges posed by their nature. The issues experienced with the cleavage of tags from Kv1.1, as well as interference from detergent, lipid and scaffold molecules with purification and characterisation of samples, while unfortunate was not unexpected. Difficulty with UV and visible light-based assays are a common issue with membrane protein research due to the overlap in the absorbance of proteins and lipids/detergent. The presence of large vesicular belts around the protein can obscure linker regions between domains and make cleavage sites inaccessible.

While this project has exhibited a number of significant challenges, much work has been done in the development of methods for expressing Kv1.1. The results of extraction studies in DDM, SMA and DIBMA and CD spectroscopy of the recovered proteins represents a novel investigative study comparing their properties. Data relating to SMA and DIBMA is currently in preparation for publication as part of a larger collaboration with Dr. Vincent Postis comparing the effectiveness of maleic acid polymers across a series of membrane proteins.

The comparison and evaluation of HEK cell culturing techniques conducted in the course of this project will provide a solid foundation for future expression of Kv1.1. A number of plasmids encoding both *KCNA1* and *KCNAB2* have been developed, which can be modified and experimented as necessary to improve the quality of expressed protein, as well as adjust the tags present on each protein to expand avenues for purification and characterisation.

Screening of cryo-EM grids under different blotting parameters and grid types should be continued now that the ABSL electron microscopy facility has become fully operational and initial issues with equipment and software have been addressed. Unfortunately, as much of the data was lost either to corruption or accidental loss in April 2017, much of the work involved will have to be repeated, however throughput of screening at the facility has now become much quicker, which will help with further efforts in data collection.

Based on the results of CD spectroscopy and negative stain cryo-EM, it is likely that the DIBMA is not suitable for effective extraction of Kv1.1 from membranes. While this is disappointing, particularly in light of current industrial interest in DIBMA, both DDM and SMA are capable of extracting the protein and maintaining sufficient stability across purification and grid preparation for negative stain EM structures to be elucidated. Based on this result, it would be advisable to favour these two means of extraction for the time being, however it is also worth exploring other extraction techniques, such as amphipols and nanodiscs (Rouck et al. 2017, Le Bon et al. 2018).

To conclude, the work conducted during the course of the project, as detailed in this thesis, provides a solid foundation for future studies on Kv1.1. The practical data on expression techniques for effective expression of Kv1.1 in human cells is also applicable to other projects focused on human membrane proteins and will be helpful in quickly establishing other projects on-site. Finally, the data on the application of DIBMA and SMA to human membrane proteins increases our overall understanding of the usefulness and applicability of these novel compounds to membrane protein preparation.

7 References

- Agar Scientific Ltd. (2018) *Lacey Carbon Films - Copper* [online] available from <<http://www.agarscientific.com/lacey-carbon-films>> [2 July 2018]
- Akkaladevi, N., Hinton-Chollet, L., Katayama, H., Mitchell, J., Szerszen, L., Mukherjee, S., Gogol, E.P., Pentelute, B.L., Collier, R.J., and Fisher, M.T. (2013) 'Assembly of Anthrax Toxin Pore: Lethal-Factor Complexes into Lipid Nanodiscs'. *Protein Science* **22** (4), 492–501
- Armstrong, C.M. and Bezanilla, F. (1973) 'Currents Related to Movement of the Gating Particles of the Sodium Channels'. *Nature* **242** (5398), 459–461
- Bai, X. chen, McMullan, G., and Scheres, S.H.W. (2015) 'How Cryo-EM Is Revolutionizing Structural Biology'. *Trends in Biochemical Sciences* **40** (1), 49–57
- Banerjee, A., Lee, A., Campbell, E., and MacKinnon, R. (2013) 'Structure of a Pore-Blocking Toxin in Complex with a Eukaryotic Voltage-Dependent K⁺ Channel'. *eLife* **2013** (2), 1–22
- Beekwilder, J.P., O'Leary, M.E., van Den Broek, L.P., van Kempen, G.T.H., Ypey, D.L., and van Den Berg, R.J. (2003) 'Kv1.1 Channels of Dorsal Root Ganglion Neurons Are Inhibited by n-Butyl-p-Aminobenzoate, a Promising Anesthetic for the Treatment of Chronic Pain.' in *The Journal of Pharmacology and Experimental Therapeutics* [online] vol. 304 (2). 531–8. available from <<http://www.ncbi.nlm.nih.gov/pubmed/12538804>>
- Beeton, C., Wulff, H., Standifer, N.E., Azam, P., Mullen, K.M., Pennington,

M.W., Kolski-Andreaco, A., Wei, E., Grino, A., Counts, D.R., Wang, P.H., LeeHealey, C.J., S. Andrews, B., Sankaranarayanan, A., Homerick, D., Roeck, W.W., Tehranzadeh, J., Stanhope, K.L., Zimin, P., Havel, P.J., Griffey, S., Knaus, H.-G., Nepom, G.T., Gutman, G.A., Calabresi, P.A., and Chandy, K.G. (2006) 'Kv1.3 Channels Are a Therapeutic Target for T Cell-Mediated Autoimmune Diseases'. *Proceedings of the National Academy of Sciences* **103** (46), 17414–17419

Bezanilla, F. (2000) 'The Voltage Sensor in Voltage-Dependent Ion Channels.' *Physiological reviews* **80** (2), 555–592

Le Bon, C., Marconnet, A., Masscheleyn, S., Popot, J.L., and Zoonens, M. (2018) 'Folding and Stabilizing Membrane Proteins in Amphipol A8-35'. in *Methods*. 95–105

Bornhorst, J.A. and Falke, J.J. (2000) 'Purification of Proteins Using Polyhistidine Affinity Tags.' *Methods in enzymology* **326**, 245–254

Burgess, S.A., Walker, M.L., Thirumurugan, K., Trinick, J., and Knight, P.J. (2004) 'Use of Negative Stain and Single-Particle Image Processing to Explore Dynamic Properties of Flexible Macromolecules'. *Journal of Structural Biology* **147** (3), 247–258

Büssow, K. (2015) 'Stable Mammalian Producer Cell Lines for Structural Biology'. *Current Opinion in Structural Biology* **32**, 81–90

Choi, J.H., Keum, K.C., and Lee, S.Y. (2006) 'Production of Recombinant Proteins by High Cell Density Culture of Escherichia Coli'. *Chemical Engineering Science* **14** (3), 98–105

- Clark, J.D. and Tempel, B.L. (1998) 'Hyperalgesia in Mice Lacking the Kv1.1 Potassium Channel Gene'. *Neuroscience Letters* **251** (2), 121–124
- Deivanayagabarathy, V., Mager, T., Apelbaum, A., Bothe, A., Merino, F., Hofnagel, O., Gatsogiannis, C., and Raunser, S. (2018) 'Electron Cryo-Microscopy Structure of the Canonical TRPC4 Ion Channel'. *eLife* **7**, e36615
- Dimroth, P., Kaim, G., and Matthey, U. (2000) 'Crucial Role of the Membrane Potential for ATP Synthesis BY F1F0 ATP Synthases'. *The Journal of Experimental Biology* (203), 51–59
- Dörr, J.M., Koorengevel, M.C., Schäfer, M., Prokofyev, A. V, Scheidelaar, S., van der Crujisen, E.A.W., Dafforn, T.R., Baldus, M., and Killian, J.A. (2014) 'Detergent-Free Isolation, Characterization, and Functional Reconstitution of a Tetrameric K⁺ Channel: The Power of Native Nanodiscs.' *Proceedings of the National Academy of Sciences of the United States of America* [online] **111** (52), 18607–12. available from <<http://www.pubmedcentral.nih.gov/articlerender.fcgi?artid=4284610&tool=pmcentrez&rendertype=abstract>>
- Doyle, D.A., Cabral, J.M., Pfuetzner, R.A., Kuo, A., Gulbis, J.M., Cohen, S.L., Chait, B.T., and MacKinnon, R. (1998) 'The Structure of the Potassium Channel: Molecular Basis of K⁺ Conduction and Selectivity.' *Science (New York, N.Y.)* **280** (5360), 69–77
- Earl, L.A., Falconieri, V., Milne, J.L.S., and Subramaniam, S. (2017) 'Cryo-EM: Beyond the Microscope'. *Current Opinion in Structural Biology* **46**,

Electron Microscopy Sciences (2018) *QUANTIFOIL® – Holey Carbon Grids for Cryo TEM* [online] available from <<https://www.emsdiasum.com/microscopy/technical/datasheet/quantifoil.aspx>> [2 July 2018]

Eschenfeldt, W.H., Maltseva, N., Stols, L., Donnelly, M.I., Gu, M., Nocek, B., Tan, K., Kim, Y., and Joachimiak, A. (2010) 'Cleavable C-Terminal His-Tag Vectors for Structure Determination'. *Journal of Structural and Functional Genomics* **11** (1), 31–39

Fekete, S., Beck, A., Veuthey, J.-L., and Guilleme, D. (2014) 'Theory and Practice of Size Exclusion Chromatography for the Analysis of Protein Aggregates'. *Journal of Pharmaceutical and Biomedical Analysis* **101**, 161–73

Frech, G.C., VanDongen, A.M.J., Schuster, G., Brown, A.M., and Joho, R.H. (1989) 'A Novel Potassium Channel with Delayed Rectifier Properties Isolated from Rat Brain by Expression Cloning'. *Nature*

Galeotti, N., Ghelardini, C., Papucci, L., Capaccioli, S., Quattrone, A., Morgagni, V.G.B., and Florence, I.- (1997) *An Antisense Oligonucleotide on the Mouse Shaker -like Potassium Channel Kv1 . 1 Gene Prevents Antinociception Induced by Morphine and Baclofen 1*. **281** (2), 941–949

Garrison, S.R., Weyer, A.D., Barabas, M.E., Beutler, B.A., and Stucky, C.L. (2014) 'A Gain-of-Function Voltage-Gated Sodium Channel 1.8 Mutation Drives Intense Hyperexcitability of A- and C-Fiber Neurons'. *Pain* **155** (5),

Gasteiger, E., Hoogland, C., Gattiker, A., Duvaud, S., Wilkins, M.R., Appel, R.D., and Bairoch, A. (2005) 'Protein Identification and Analysis Tools on the ExPASy Server'. in *The Proteomics Protocols Handbook*. 571–607

Ge, J., Li, W., Zhao, Q., Li, N., Chen, M., Zhi, P., Li, R., Gao, N., Xiao, B., and Yang, M. (2015) 'Architecture of the Mammalian Mechanosensitive Piezo1 Channel'. *Nature* **527** (7576), 64–69

Generon Ltd (n.d.) *N-Dodecyl-b-D-Maltopyranoside (DDM) - Anagrade Analytical - Purity* [online] available from <<https://www.generon.co.uk/maltosides-1834/n-dodecyl-b-d-maltopyranoside-ddm-237000196.html>> [10 July 2018]

Goehring, A., Lee, C.-H., Wang, K.H., Michel, J.C., Claxton, D.P., Bacongus, I., Althoff, T., Fischer, S., Garcia, K.C., and Gouaux, E. (2014) 'Screening and Large-Scale Expression of Membrane Proteins in Mammalian Cells for Structural Studies.' *Nature protocols* [online] **9** (11), 2574–85. available from <<http://dx.doi.org/10.1038/nprot.2014.173>>

Gohon, Y. and Popot, J.-L. (2003) 'Membrane Protein–surfactant Complexes'. *Current Opinion in Colloid & Interface Science* **8** (1), 8–15

González, C., Baez-Nieto, D., Valencia, I., Oyarzún, I., Rojas, P., Naranjo, D., and Latorre, R. (2012) 'K⁺ Channels: Function-Structural Overview'. *Comprehensive Physiology* **2** (3), 2087–2149

Gouaux, E. and Mackinnon, R. (2005) 'Principles of Selective Ion Transport in Channels and Pumps.' *Science (New York, N.Y.)* [online] **310** (5753),

1461–5. available from
<<http://science.sciencemag.org/content/310/5753/1461.abstract>>
<<http://www.ncbi.nlm.nih.gov/pubmed/16322449>>

Gulati, S., Jamshad, M., Knowles, T.J., Morrison, K.A., Downing, R., Cant, N., Collins, R., Koenderink, J.B., Ford, R.C., Overduin, M., Kerr, I.D., Dafforn, T.R., and Rothnie, A.J. (2014) 'Detergent-Free Purification of ABC (ATP-Binding-Cassette) Transporters'. *Biochemical Journal* [online] **461** (2), 269–278. available from
<<http://www.ncbi.nlm.nih.gov/pubmed/24758594>>
<<http://biochemj.org/lookup/doi/10.1042/BJ20131477>>

Gulbis, J.M., Mann, S., and MacKinnon, R. (1999) 'Structure of a Voltage-Dependent K⁺ Channel Beta Subunit'. *Cell* **97** (7), 943–952

Gulbis, J.M., Zhou, M., Mann, S., and MacKinnon, R. (2000) 'Structure of the Cytoplasmic Beta Subunit-T1 Assembly of Voltage-Dependent K⁺ Channels.' *Science* [online] **289** (5476), 123–7. available from
<<http://www.ncbi.nlm.nih.gov/pubmed/10884227>>

Hille, B. (2001) 'Ion Channel Excitable Membranes'. in *Sunderland Massachusetts USA*. Third Edit. ed. by Hille, B. Sunderland, Massachusetts U.S.A.: Sinauer Associates, Inc, 131–168

Hoshi, T., Zagotta, W.N., and Aldrich, R.W. (1990) 'Biophysical and Molecular Mechanisms of Shaker Potassium Channel Inactivation'. *Science* **250** (4980), 533–538

Humphries, E.S. a. and Dart, C. (2015) 'Neuronal and Cardiovascular

Potassium Channels as Therapeutic Drug Targets: Promise and Pitfalls'. *Journal of Biomolecular Screening* [online] **20** (9), 1055–1073. available from <<http://jbx.sagepub.com/cgi/doi/10.1177/1087057115601677>>

Ishikawa, K., Tanaka, M., Black, J. a, and Waxman, S.G. (1999) 'Changes in Expression of Voltage-Gated Potassium Channels in Dorsal Root Ganglion Neurons Following Axotomy.' *Muscle & nerve* **22** (April), 502–507

Jackson, W. (2005) 'Potassium Channels and Proliferation of Vascular Smooth Muscle Cells'. *Circulation Research* **97** (12), 1211–1212

Jan, L.Y. and Jan, Y.N. (2012) 'Voltage-Gated Potassium Channels and the Diversity of Electrical Signalling.' *The Journal of physiology* [online] **590** (Pt 11), 2591–2599. available from <<http://www.ncbi.nlm.nih.gov/pubmed/22431339>>

Janda, C.Y., Li, J., Oubridge, C., Hernandez, H., Robinson, C. V, and Nagai, K. (2010) 'Recognition of a Signal Peptide by the Signal Recognition Particle'. *Nature* **465** (7297), 507–10

Kelley, L.A., Mezulis, S., Yates, C.M., Wass, M.N., and Sternberg, M.J.E. (2015) 'The Phyre2 Web Portal for Protein Modeling, Prediction and Analysis'. *Nature Protocols* **10**, 845–858

Kelly, S.M., Jess, T.J., and Price, N.C. (2005) 'How to Study Proteins by Circular Dichroism'. *Biochimica et Biophysica Acta - Proteins and Proteomics* **1751** (2), 119–139

Kim, Y., Bigelow, L., Borovilos, M., Dementieva, I., Duggan, E., Eschenfeldt, 165

W., Hatzos, C., Joachimiak, G., Li, H., Maltseva, N., Mulligan, R., Quartey, P., Sather, A., Stols, L., Volkart, L., Wu, R., Zhou, M., and Joachimiak, A. (2008) 'High-Throughput Protein Purification for X-Ray Crystallography and NMR'. *Advances in Protein Chemistry and Structural Biology* **75**, 85–105

Kinoshita, M., Suzuki, K., Murata, M., and Matsumori, N. (2018) 'Evidence of Lipid Rafts Based on the Partition and Dynamic Behavior of Sphingomyelins'. *Chemistry and Physics of Lipids* [online] available from <<https://www.sciencedirect.com/science/article/pii/S0009308418300744>>

Kintzer, A.F. and Stroud, R.M. (2016) 'Structure, Inhibition and Regulation of Two-Pore Channel TPC1 from *Arabidopsis Thaliana*'. *Nature* **531**, 258–264

Klepsch, M.M., Persson, J.O., and De Gier, J.W.L. (2011) 'Consequences of the Overexpression of a Eukaryotic Membrane Protein, the Human KDEL Receptor, in *Escherichia Coli*'. *Journal of Molecular Biology* **407** (4), 532–542

Kota, J. and Ljungdahl, P.O. (2005) 'Specialized Membrane-Localized Chaperones Prevent Aggregation of Polytopic Proteins in the ER'. *Journal of Cell Biology* **168** (1), 79–88

Kruh, J. (1981) 'Effects of Sodium Butyrate, a New Pharmacological Agent, on Cells in Culture'. *Molecular and Cellular Biochemistry* **42** (2), 65–82

Lee, J., Shin, M.K., Ryu, D.K., Kim, S., and Ryu, W.S. (2010) 'Insertion and

Deletion Mutagenesis by Overlap Extension PCR'. *Methods in Molecular Biology* **634**, 137–146

Lewis, R., Asplin, K.E., Bruce, G., Dart, C., Mobasheri, A., and Barrett-Jolley, R. (2011) 'The Role of the Membrane Potential in Chondrocyte Volume Regulation'. *Journal of Cellular Physiology* **226**, 2979–2986

Lichtenberg, D., Ahyayauch, H., and Goñi, F.M. (2013) 'The Mechanism of Detergent Solubilization of Lipid Bilayers'. *Biophysical Journal* **105**, 298–299

Lin, C.Y., Huang, Z., Wen, W., Wu, A., Wang, C., and Niu, L. (2015) 'Enhancing Protein Expression in HEK-293 Cells by Lowering Culture Temperature'. *PLoS ONE* **10** (4), e0123562

Lobley, A., Whitmore, L., and Wallace, B.A. (2002) 'DICHROWEB: An Interactive Website for the Analysis of Protein Secondary Structure from Circular Dichroism Spectra'. *Bioinformatics* **18** (1), 211–212

Long, S.B., Campbell, E.B., and Mackinnon, R. (2005) 'Crystal Structure of a Mammalian Voltage-Dependent Shaker Family K⁺ Channel'. in *Science*. vol. 897 (August). 897–903

Long, S.B., Tao, X., Campbell, E.B., and MacKinnon, R. (2007) 'Atomic Structure of a Voltage-Dependent K⁺ Channel in a Lipid Membrane-like Environment.' *Nature* **450** (7168), 376–382

De Los Milagros Bassani Molinas, M., Beer, C., Hesse, F., Wirth, M., and Wagner, R. (2014) 'Optimizing the Transient Transfection Process of HEK-293 Suspension Cells for Protein Production by Nucleotide Ratio

Monitoring'. *Cytotechnology* **66** (3), 493–514

Lu, P., Bai, X.C., Ma, D., Xie, T., Yan, C., Sun, L., Yang, G., Zhao, Y., Zhou, R., Scheres, S.H., and Shi, Y. (2014) 'Three-Dimensional Structure of Human Gamma-Secretase'. *Nature* **512** (7513), 166–170

Lund, S., Orłowski, S., de Foresta, B., Champeil, P., le Maire, M., and Mølle, J. (1989) 'Detergent Structure and Associated Lipid as Determinants in the Stabilization of Solubilized Ca²⁺-ATPase from Sarcoplasmic Reticulum'. *The Journal of Biological Chemistry* **264** (9), 4907–4915

Maibaum, L., Dinner, A.R., and Chandler, D. (2004) 'Micelle Formation and the Hydrophobic Effect'. *The Journal of Physical Chemistry B* **108** (21), 6778–6781

McPherson, A. and Gavira, J.A. (2014) 'Introduction to Protein Crystallization'. *Acta Crystallographica Section F Structural Biology Communications* **34** (3), 254–265

Medical Research Council (2014) *Outputs, Outcomes and Impact of MRC Research: 2013/14 Report* [online] available from <<https://mrc.ukri.org/publications/browse/outputs-outcomes-and-impact-of-mrc-research-2013-14/>> [21 December 2018]

Van Meer, G., Voelker, D.R., and Feigenson, G.W. (2008) 'Membrane Lipids: Where They Are and How They Behave'. *Nature Reviews Molecular Cell Biology* **9** (2), 112–124

Nurani, G., Radford, M., Charalambous, K., O'Reilly, A.O., Cronin, N.B., Haque, S., and Wallace, B.A. (2008) 'Tetrameric Bacterial Sodium

Channels: Characterization of Structure, Stability, and Drug Binding'.
Biochemistry **47**, 8114–8121

Oluwole, A.O., Danielczak, B., Meister, A., Babalola, J.O., Vargas, C., and Keller, S. (2017a) 'Solubilization of Membrane Proteins into Functional Lipid-Bilayer Nanodiscs Using a Diisobutylene/Maleic Acid Copolymer'.
Angewandte Chemie - International Edition **56** (7), 1919–1924

Oluwole, A.O., Klingler, J., Danielczak, B., Babalola, J.O., Vargas, C., Pabst, G., and Keller, S. (2017b) 'Formation of Lipid-Bilayer Nanodiscs by Diisobutylene/Maleic Acid (DIBMA) Copolymer'. *Langmuir* **33** (50), 14378–14388

Ostroumov, S., Jasaitis, A., and Samuilov, V. (1979) 'Electrochemical Proton Gradient across the Membranes of Photophosphorylating Bacteria'.
Biomembranes **10**, 209–233

Pettersen, E.F., Goddard, T.D., Huang, C.C., Couch, G.S., Greenblatt, D.M., Meng, E.C., and Ferrin, T.E. (2004) 'UCSF Chimera - A Visualization System for Exploratory Research and Analysis'. *Journal of Computational Chemistry* **25**, 1605–1612

Popot, J.L. and Engelman, D.M. (2000) 'Helical Membrane Protein Folding, Stability, and Evolution'. *Annual Review of Biochemistry* **69**, 881–922

Porath, J. (1992) 'Immobilized Metal Ion Affinity Chromatography'. *Protein Expression and Purification* **11**, 17–31

Postis, V., Rawson, S., Mitchell, J.K., Lee, S.C., Parslow, R.A., Dafforn, T.R., Baldwin, S.A., and Muench, S.P. (2015) 'The Use of SMALPs as a Novel

Membrane Protein Scaffold for Structure Study by Negative Stain Electron Microscopy'. *Biochimica et Biophysica Acta - Biomembranes* [online] **1848** (2), 496–501. available from <<http://dx.doi.org/10.1016/j.bbamem.2014.10.018>>

Postis, V.G., Rawlings, A.E., Lesiuk, A., and Baldwin, S.A. (2013) 'Use of Escherichia Coli for the Production and Purification of Membrane Proteins'. in *Ion Channels*. 33–54

Protein Data Bank (2018) *PDB Statistics: Growth of Structures from 3DEM Experiments Released per Year* [online] available from <<https://www.rcsb.org/stats/growth/em>> [30 May 2018]

Protein Data Bank in Europe (2018) *EMStats: Release Trends for EMDB Entries* [online] available from <https://www.ebi.ac.uk/pdbe/emdb/statistics_releases.html/> [30 May 2018]

Quantifoil Micro Tools GmbH. (2015a) *QUANTIFOIL - Carbon Support Films* [online] available from <<http://www.quantifoil.com/index.php?name=carbon>> [2 July 2018]

Quantifoil Micro Tools GmbH. (2015b) *QUANTIFOIL - Quantifoil Holey Carbon* [online] available from <<http://www.quantifoil.com/index.php?name=circular>> [2 July 2018]

Rabu, C. and High, S. (2007) 'Membrane Protein Chaperones: A New Twist in the Tail?' in *Current Biology*. R472–R274

Rawson, S., Davies, S., Lippiat, J.D., and Muench, S.P. (2016) 'The Changing

Landscape of Membrane Protein Structural Biology through Developments in Electron Microscopy'. *Molecular Membrane Biology* **33** (1–2), 12–22

Rhodes, K.J., Monaghan, M.M., Barrezueta, N.X., Nawoschik, S., Bekele-Arcuri, Z., Matos, M.F., Nakahira, K., Schechter, L.E., and Trimmer, J.S. (1996) 'Voltage-Gated K⁺ Channel Beta Subunits: Expression and Distribution of Kv Beta 1 and Kv Beta 2 in Adult Rat Brain.' *The Journal of neuroscience : the official journal of the Society for Neuroscience* **16** (16), 4846–4860

Rouck, J.E., Krapf, J.E., Roy, J., Huff, H.C., and Das, A. (2017) 'Recent Advances in Nanodisc Technology for Membrane Protein Studies (2012–2017)'. in *FEBS Letters*. 2057–2088

Sahin, E. and Roberts, C.J. (2012) 'Characterising Protein/Detergent Complexes by Triple-Detection Size-Exclusion Chromatography'. in *Therapeutic Proteins*. ed. by V., V. and J., C. Humana Press, Totowa, NJ: Springer Science+Business Media, LLC, 403–423

Scheres, S.H.W. (2012) 'RELION: Implementation of a Bayesian Approach to Cryo-EM Structure Determination'. *Journal of Structural Biology* **180** (3), 519–530

Schlaeger, E.J. (1996) 'The Protein Hydrolysate, Primatone RL, Is a Cost-Effective Multiple Growth Promoter of Mammalian Cell Culture in Serum-Containing and Serum-Free Media and Displays Anti-Apoptosis Properties'. *Journal of Immunological Methods* **194** (2), 191–199

- Seddon, A.M., Curnow, P., and Booth, P.J. (2004) 'Membrane Proteins, Lipids and Detergents: Not Just a Soap Opera'. *Biochimica et Biophysica Acta - Biomembranes* **1666** (1–2), 105–117
- Sievers, F., Wilm, A., Dineen, D., Gibson, T.J., Karplus, K., Li, W., Lopez, R., McWilliam, H., Remmert, M., Söding, J., Thompson, J.D., and Higgins, D.G. (2011) 'Fast, Scalable Generation of High-Quality Protein Multiple Sequence Alignments Using Clustal Omega'. *Molecular Systems Biology* **7**, 539
- Stühmer, W., Ruppersberg, J.P., Schröter, K.H., Sakmann, B., Stocker, M., Giese, K.P., Penschke, a, Baumann, a, and Pongs, O. (1989) 'Molecular Basis of Functional Diversity of Voltage-Gated Potassium Channels in Mammalian Brain.' *The EMBO journal* **8** (1), 3235–3244
- Tang, G., Peng, L., Baldwin, P.R., Mann, D.S., Jiang, W., Rees, I., and Ludtke, S.J. (2007) 'EMAN2: An Extensible Image Processing Suite for Electron Microscopy'. *Journal of Structural Biology* **157** (1), 38–46
- Tang, Q., Guo, W., Zheng, L., Wu, J., Liu, M., Zhou, X., Zhang, X., and Chen, L. (2018) 'Structure of the Receptor-Activated Human TRPC6 and TRPC3 Ion Channels'. *Cell Research* **28** (7), 746–755
- Tempel, B.L., Papazian, D.M., Schwarz, T.L., Jan, Y.N., and Jan, L.Y. (1987) 'Sequence of a Probable Potassium Channel Component Encoded at Shaker Locus of Drosophila'. *Science* **237** (4816), 770–775
- Thériault, O. and Chahine, M. (2014) 'Correlation of the Electrophysiological Profiles and Sodium Channel Transcripts of Individual Rat Dorsal Root

Ganglia Neurons'. *Frontiers in Cellular Neuroscience* **285**

Thompson, R.F., Walker, M., Siebert, C.A., Muench, S.P., and Ranson, N.A.

(2016) 'An Introduction to Sample Preparation and Imaging by Cryo-Electron Microscopy for Structural Biology'. *Methods* **100**, 3–15

Tytgat, J., Debont, T., Carmeliet, E., and Daenens, P. (1995) 'The α -Dendrotoxin Footprint on a Mammalian Potassium Channel'. *Journal of Biological Chemistry* **20**, 24776–24781

Urh, M., Simpson, D., and Zhao, K. (2009) 'Affinity Chromatography: General Methods.' *Methods in enzymology* **463**, 417–438

Vacher, H., Mohapatra, D.P., and Trimmer, J.S. (2008) 'Localization and Targeting of Voltage-Dependent Ion Channels in Mammalian Central Neurons'. *Physiological Reviews* **88** (4), 1407–1447

Vanaken, T., Foxall-Vanaken, S., Castleman, S., and Ferguson-Miller, S. (1986) 'Alkyl Glycoside Detergents: Synthesis and Applications to the Study of Membrane Proteins'. *Methods in Enzymology* **125**, 27–35

Wagner, S., Bader, M.L., Drew, D., and de Gier, J.-W. (2006) 'Rationalizing Membrane Protein Overexpression'. *Trends in Biotechnology* **24** (8), 364–371

Waterhouse, A.M., Procter, J.B., Martin, D.M.A., Clamp, M., and Barton, G.J. (2009) 'Jalview Version 2-A Multiple Sequence Alignment Editor and Analysis Workbench'. *Bioinformatics* **25**, 1189–1191

Whitmore, L. and Wallace, B.A. (2004) 'DICHROWEB, an Online Server for

Protein Secondary Structure Analyses from Circular Dichroism Spectroscopic Data'. *Nucleic Acids Research* **32** (Web Server issue), W668–673

Whitmore, L. and Wallace, B.A. (2008) 'Protein Secondary Structure Analyses from Circular Dichroism Spectroscopy: Methods and Reference Databases'. *Biopolymers* **89** (5), 392–400

Wolkers, W.F., Balasubramanian, S.K., Ongstad, E.L., Zec, H.C., and Bischof, J.C. (2007) 'Effects of Freezing on Membranes and Proteins in LNCaP Prostate Tumor Cells'. *Biochimica et Biophysica Acta - Biomembranes* **1768**, 728–736

Wu, J., Yan, Z., Li, Z., Yan, C., Lu, S., Dong, M., and Yan, N. (2015) 'Structure of the Voltage-Gated Calcium Channel Cav1.1 Complex'. *Science* [online] **350** (6267), 2395–2395. available from <<http://www.ncbi.nlm.nih.gov/pubmed/26680202>>

Yan, Z., Bai, X.C., Yan, C., Wu, J., Li, Z., Xie, T., Peng, W., Yin, C.C., Li, X., Scheres, S.H.W., Shi, Y., and Yan, N. (2015) 'Structure of the Rabbit Ryanodine Receptor RyR1 at Near-Atomic Resolution'. *Nature* **517** (7532), 50–55

Zagotta, W.N., Hoshi, T., and Aldrich, R.W. (1990) 'Restoration of Inactivation in Mutants of Shaker Potassium Channels by a Peptide Derived from ShB'. *Science* **250** (4980), 568–571

Zhang, L., Tong, H., Garewal, M., and Ren, G. (2013) 'Optimized Negative-Staining Electron Microscopy for Lipoprotein Studies'. *Biochimica et*

Zhou, Y., Morais-Cabral, J.H., Kaufman, A., and MacKinnon, R. (2001)
'Chemistry of Ion Coordination and Hydration Revealed by a K⁺ Channel-
Fab Complex at 2.0 Å Resolution.' *Nature* [online] **414** (6859), 43–48.
available from <<http://www.ncbi.nlm.nih.gov/pubmed/11689936>>

8 Appendix

8.1 Maps of plasmids used during project

8.1.1 pcDNA6

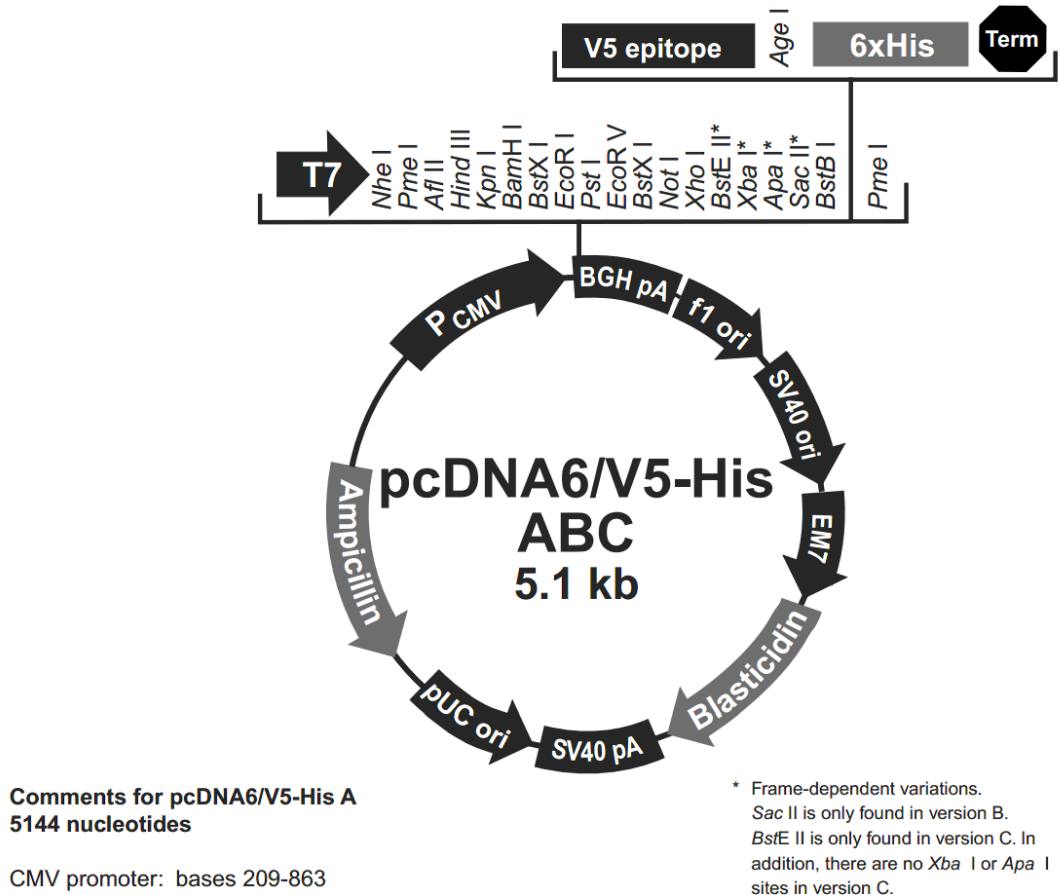


Figure 8.1 – Map of pcDNA6 plasmid.

8.1.2 pcDNA3.1

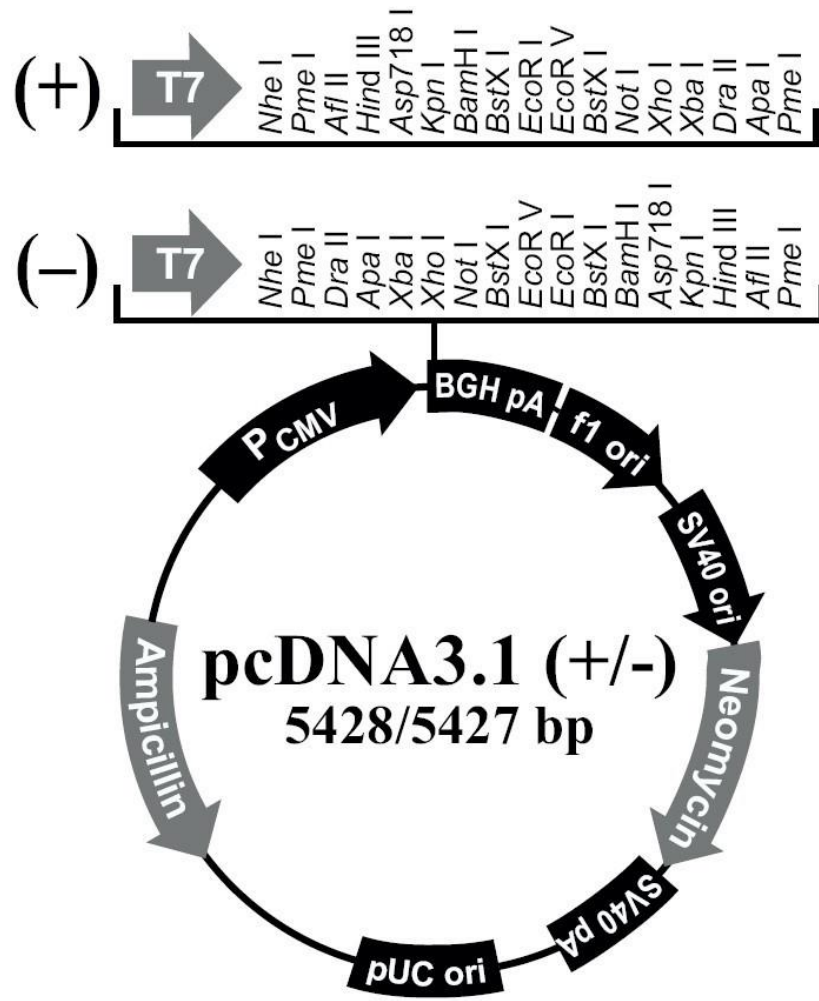


Figure 8.2 – Map of pcDNA3.1 plasmid.

8.1.3 pJET1.2

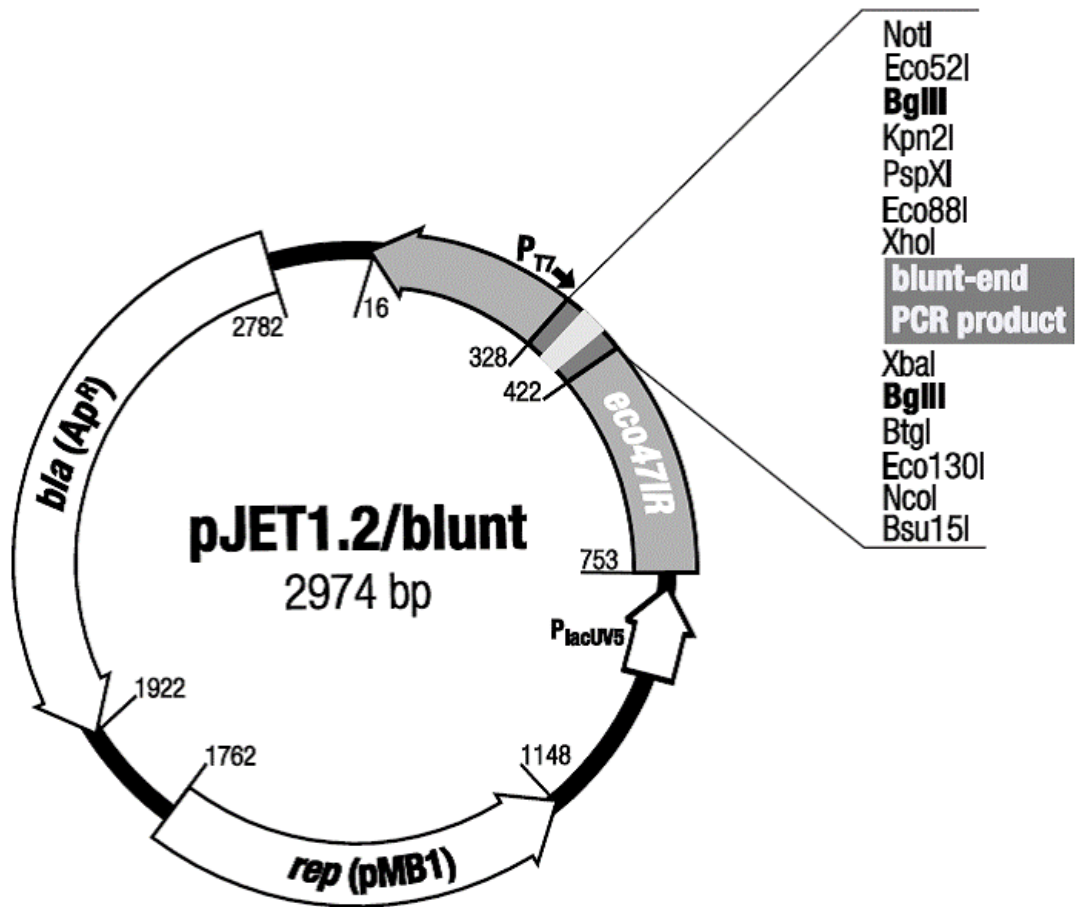


Figure 8.3 – Map of pJET1.2 plasmid.

8.2 Mass spectrometry data

8.2.1 A1 band

Accession code	-10lgP	Coverage (%)	Number of Peptides	Number of Unique Peptides	PTM	Avg. Mass	Description
Q969P6 (TOP1M_HUMAN)	47.65	2	1	1	Y	69872	DNA topoisomerase I, mitochondrial, <i>Homo sapiens</i>
O94986 (CE152_HUMAN)	23.92	0	1	1	N	195625	Centrosomal protein of 152 kDa, <i>Homo sapiens</i>
A7E2Y1 (MYH7B_HUMAN)	21.78	1	1	1	Y	221386	Myosin-7B, <i>Homo sapiens</i>

Table 8.1 – Table of protein fragments identified through mass spectrometry in band A1 (Figure 4.8).

8.2.2 B1 band

Accession code	-10lgP	Coverage (%)	Number of Peptides	Number of Unique Peptides	PTM	Avg. Mass	Description
Q09470 (KCNA1_HUMAN)	337.59	54	45	31	Y	56466	Potassium voltage-gated channel subfamily A member 1, <i>Homo sapiens</i>
P35908 (K22E_HUMAN)	228.2	26	13	8	Y	65433	Keratin, type II cytoskeletal 2 epidermal, <i>Homo sapiens</i>
P22001 (KCNA3_HUMAN)	222.76	16	15	1	Y	63842	Potassium voltage-gated channel subfamily A member 3, <i>Homo sapiens</i>
P13645 (K1C10_HUMAN)	220.57	27	18	15	N	58827	Keratin, type I cytoskeletal 10, <i>Homo sapiens</i>
P04264 (K2C1_HUMAN)	203.6	20	14	9	Y	66039	Keratin, type II cytoskeletal 1, <i>Homo sapiens</i>
P35527 (K1C9_HUMAN)	141.45	12	6	6	N	62064	Keratin, type I cytoskeletal 9, <i>Homo sapiens</i>
Q01546 (K22O_HUMAN)	92.07	5	4	1	Y	65841	Keratin, type II cytoskeletal 2 oral, <i>Homo sapiens</i>
P02533 (K1C14_HUMAN)	89.24	7	4	1	N	51562	Keratin, type I cytoskeletal 14, <i>Homo sapiens</i>
P08779 (K1C16_HUMAN)	89.24	7	4	1	N	51268	Keratin, type I cytoskeletal 16, <i>Homo sapiens</i>
P07477 (TRY1_HUMAN)	47.15	4	1	1	Y	26558	Trypsin-1, <i>Homo sapiens</i>
P81605 (DCD_HUMAN)	28.05	10	1	1	N	11284	Dermcidin, <i>Homo sapiens</i>
P78357 (CNTP1_HUMAN)	21.17	0	1	1	Y	156266	Contactin-associated protein 1, <i>Homo sapiens</i>

Table 8.2 – Table of protein fragments identified through mass spectrometry in band B1 (Figure 4.8).

8.2.3 B2 band

Accession code	-10lgP	Coverage (%)	Number of Peptides	Number of Unique Peptides	PTM	Avg. Mass	Description
P0DMV8 (HS71A_HUMAN)	314.74	46	24	16	Y	70052	Heat shock 70 kDa protein 1A, <i>Homo sapiens</i>
P0DMV9 (HS71B_HUMAN)	314.74	46	24	16	Y	70052	Heat shock 70 kDa protein 1B, <i>Homo sapiens</i>
P11142 (HSP7C_HUMAN)	209.09	18	11	4	Y	70898	Heat shock cognate 71 kDa protein, <i>Homo sapiens</i>
Q09470 (KCNA1_HUMAN)	183.66	27	10	6	Y	56466	Potassium voltage-gated channel subfamily A member 1, <i>Homo sapiens</i>
P35908 (K22E_HUMAN)	133.17	10	6	4	N	65433	Keratin, type II cytoskeletal 2 epidermal, <i>Homo sapiens</i>
P13645 (K1C10_HUMAN)	128.81	13	7	6	N	58827	Keratin, type I cytoskeletal 10, <i>Homo sapiens</i>
P35527 (K1C9_HUMAN)	128.06	9	5	4	N	62064	Keratin, type I cytoskeletal 9, <i>Homo sapiens</i>
Q07065 (CKAP4_HUMAN)	117.9	11	5	5	N	66023	Cytoskeleton-associated protein 4, <i>Homo sapiens</i>
P04264 (K2C1_HUMAN)	116.09	10	6	4	N	66039	Keratin, type II cytoskeletal 1, <i>Homo sapiens</i>
P38646 (GRP75_HUMAN)	110.01	10	5	4	N	73681	Stress-70 protein, mitochondrial, <i>Homo sapiens</i>
P22001 (KCNA3_HUMAN)	107.71	7	5	1	Y	63842	Potassium voltage-gated channel subfamily A member 3, <i>Homo sapiens</i>
P0DMV8 (HS71A_HUMAN)	314.74	46	24	16	Y	70052	Heat shock 70 kDa protein 1A, <i>Homo sapiens</i>

Table 8.3 – Table of protein fragments identified through mass spectrometry in band B2 (Figure 4.8).

8.2.4 B3 band

Accession code	-10lgP	Coverage (%)	Number of Peptides	Number of Unique Peptides	PTM	Avg. Mass	Description
Q09470 (KCNA1_HUMAN)	181.82	25	10	6	Y	56466	Potassium voltage-gated channel subfamily A member 1, <i>Homo sapiens</i>
P13645 (K1C10_HUMAN)	142.78	16	7	7	Y	58827	Keratin, type I cytoskeletal 10, <i>Homo sapiens</i>
P04264 (K2C1_HUMAN)	142.02	10	6	3	N	66039	Keratin, type II cytoskeletal 1, <i>Homo sapiens</i>
P07437 (TBB5_HUMAN)	136.94	18	7	2	Y	49671	Tubulin beta chain, <i>Homo sapiens</i>
P35908 (K22E_HUMAN)	134.08	10	6	2	Y	65433	Keratin, type II cytoskeletal 2 epidermal, <i>Homo sapiens</i>
P68371 (TBB4B_HUMAN)	130.2	15	6	1	Y	49831	Tubulin beta-4B chain, <i>Homo sapiens</i>
P06576 (ATPB_HUMAN)	113.15	10	4	4	Y	56560	ATP synthase subunit beta, mitochondrial, <i>Homo sapiens</i>
Q9BQE3 (TBA1C_HUMAN)	107.87	15	5	5	N	49895	Tubulin alpha-1C chain, <i>Homo sapiens</i>
P22001 (KCNA3_HUMAN)	94.02	7	5	1	Y	63842	Potassium voltage-gated channel subfamily A member 3, <i>Homo sapiens</i>
Q8IUJ8 (MINA_HUMAN)	56.81	5	2	2	N	52800	Bifunctional lysine-specific demethylase and histidyl-hydroxylase MINA, <i>Homo sapiens</i>

Table 8.4 – Table of protein fragments identified through mass spectrometry in band B3 (Figure 4.8).

8.2.5 B4 band

Accession code	-10lgP	Coverage (%)	Number of Peptides	Number of Unique Peptides	PTM	Avg. Mass	Description
P04264 (K2C1_HUMAN)	166.21	15	9	8	N	66039	Keratin, type II cytoskeletal 1, <i>Homo sapiens</i>
P13645 (K1C10_HUMAN)	162.57	20	9	9	Y	58827	Keratin, type I cytoskeletal 10, <i>Homo sapiens</i>
P35527 (K1C9_HUMAN)	153.62	16	7	7	Y	62064	Keratin, type I cytoskeletal 9, <i>Homo sapiens</i>
P35908 (K22E_HUMAN)	100.46	6	3	2	N	65433	Keratin, type II cytoskeletal 2, epidermal, <i>Homo sapiens</i>
Q92504 (S39A7_HUMAN)	96.85	3	2	2	N	50118	Zinc transporter SLC39A7, <i>Homo sapiens</i>
P39656 (OST48_HUMAN)	81.61	7	3	3	N	50801	Dolichyl-diphosphooligosaccharide--protein glycosyltransferase 48 kDa subunit, <i>Homo sapiens</i>
P13647 (K2C5_HUMAN)	71.67	4	2	1	N	62378	Keratin, type II cytoskeletal 5, <i>Homo sapiens</i>
P81605 (DCD_HUMAN)	41.26	10	1	1	N	11284	Dermcidin, <i>Homo sapiens</i>
P07477 (TRY1_HUMAN)	37.77	4	1	1	Y	26558	Trypsin-1, <i>Homo sapiens</i>

Table 8.5 – Table of protein fragments identified through mass spectrometry in band B4 (Figure 4.8).

8.2.6 B5 band

Accession code	-10lgP	Coverage (%)	Number of Peptides	Number of Unique Peptides	PTM	Avg. Mass	Description
P04264 (K2C1_HUMAN)	154.79	11	7	5	Y	66039	Keratin, type II cytoskeletal 1, <i>Homo sapiens</i>
P35527 (K1C9_HUMAN)	148.54	13	7	7	Y	62064	Keratin, type I cytoskeletal 9, <i>Homo sapiens</i>
P35908 (K22E_HUMAN)	132.76	11	5	3	N	65433	Keratin, type II cytoskeletal 2 epidermal, <i>Homo sapiens</i>
P13645 (K1C10_HUMAN)	132.18	11	4	4	Y	58827	Keratin, type I cytoskeletal 10, <i>Homo sapiens</i>
P21796 (VDAC1_HUMAN)	122.55	15	3	3	Y	30773	Voltage-dependent anion-selective channel protein 1, <i>Homo sapiens</i>
P45880 (VDAC2_HUMAN)	90.68	10	2	2	N	31567	Voltage-dependent anion-selective channel protein 2, <i>Homo sapiens</i>
P04259 (K2C6B_HUMAN)	71.04	3	2	0	N	60067	Keratin, type II cytoskeletal 6B, <i>Homo sapiens</i>

Table 8.6 – Table of protein fragments identified through mass spectrometry in band B5 (Figure 4.8).